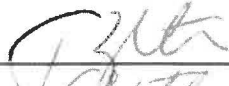
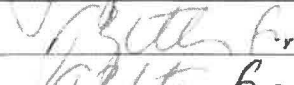





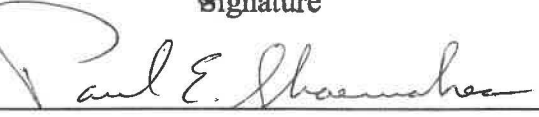


**SANDIA NATIONAL LABORATORIES
WASTE ISOLATION PILOT PLANT**

**SUMMARY REPORT FOR THE 2019 COMPLIANCE
RECERTIFICATION APPLICATION PERFORMANCE
ASSESSMENT (CRA-2019 PA)**

REVISION 0

Author:	Todd R. Zeitler		11/22/2019
Author:	James Bethune		11/22/2019
Author:	Sarah Brunell		11/22/2019
Author:	Dwayne Kicker		11/22/2019
Author:	Jennifer Long		11/22/2019
	Print	Signature	Date
Technical Reviewer:	Chris Camphouse		11/22/2019
	Print	Signature	Date
QA Reviewer:	Shelly Nielsen		11-22-19
	Print	Signature	Date
Management Reviewer:	Paul Shoemaker		11/22/2019
	Print	Signature	Date

ERMS #571376

NOVEMBER, 2019

WIPP:4.2.1:PA:QA-L:571155

Information Only

This page intentionally left blank.

TABLE OF CONTENTS

EXECUTIVE SUMMARY	XI
1.0 INTRODUCTION.....	13
1.1 Changes Since the CRA-2014 PA	14
1.1.1 Approach to Abandonment of Panel Closures in the South and No Waste in Panel 9	15
1.1.2 Additional Shaft and Associated Drifts.....	21
1.1.3 Brine Radiolysis as Part of Gas Generation Process Model	22
1.1.4 Refinement to the Probability of Encountering Pressurized Brine	23
1.1.5 Refinement to the Corrosion Rates of Steel	24
1.1.6 Refinement to the Effective Shear Strength of WIPP Waste	25
1.1.7 Refinement to Colloid Enhancement Parameters.....	25
1.1.8 Refinement to Hydromagnesite Conversion Rate	26
1.1.9 Removal of Iron Sulfidation Reactions	26
1.1.10 Correction to Length of Northernmost Panel Closure Representation.....	27
1.1.11 Updates to Drilling Rate and Plugging Pattern Parameters	28
1.1.12 Updates to WIPP Waste Inventory Parameters	29
1.1.13 Updates to Radionuclide Solubilities	32
1.1.14 Update to BH_OPEN:RELP_MOD Parameter	34
1.1.15 New Materials to Define Properties in DRZ Surrounding OPS, EXP, and Panel Closure Areas	35
1.1.16 Hardware and Computational Code Updates	38
2.0 CONCEPTUAL APPROACH FOR THE CRA-2019 PA.....	39
3.0 ANALYSIS METHODOLOGY	41
3.1 CRA19 Analysis	41
3.1.1 Inventory Analysis	41
3.1.2 PA Calculations.....	42
3.1.3 FEPs Analysis.....	42
3.2 CRA19_CL Analysis	42
4.0 RUN CONTROL.....	43
5.0 RESULTS	45
5.1 Inventory Screening Analysis.....	45
5.2 Sampling of Uncertain Parameters	46

5.3	Radionuclide Concentrations for Solid Releases	46
5.3.1	Overall Activity	47
5.3.2	Activity on a Waste Stream Basis	48
5.3.3	Average CH Waste Activity Concentration	50
5.4	Mobilized Radionuclide Concentrations.....	50
5.4.1	Total Mobile Concentration Limits	51
5.4.2	Instantaneous Mobile Concentrations	54
5.5	Salado Flow Results.....	55
5.5.1	Repository Representation in BRAGFLO.....	56
5.5.2	Modeling Scenarios	59
5.5.3	Gas Generation	59
5.5.4	Pressure	65
5.5.5	Brine Saturation.....	75
5.5.6	Brine and Gas Flows	87
5.6	Cuttings, Cavings, and Spallings Results	97
5.6.1	Modeling Scenarios	98
5.6.2	Cuttings Area Results	98
5.6.3	Cavings Area Results	98
5.6.4	Spallings Volume Results	99
5.7	Direct Brine Release Volume Results.....	102
5.7.1	Repository Representation in BRAGFLO.....	103
5.7.2	Modeling Scenarios	104
5.7.3	Initial Conditions for DBRs	104
5.7.4	DBR Volumes	108
5.8	Salado Transport Results	112
5.8.1	Repository Representation and Modeling Scenarios.....	112
5.8.2	Transport Results for an Undisturbed Repository.....	113
5.8.3	Transport Results for a Disturbed Repository.....	113
5.9	Normalized Releases.....	115
5.9.1	Cuttings and Cavings Normalized Releases.....	115
5.9.2	Spallings Normalized Releases	116
5.9.3	Normalized Direct Brine Releases	117
5.9.4	Normalized Culebra Transport Releases	118
5.9.5	Total Normalized Releases.....	119
5.10	Sensitivity of Releases to Uncertain Parameters	122
5.11	FEPs Analysis.....	123

5.11.1 Overall Results	124
5.11.2 Updated Screening Decision	124
5.11.3 Updated Screening Arguments.....	124
6.0 SUMMARY	125
7.0 REFERENCES.....	127
APPENDIX A. RESULTS OF CRA19_CL ANALYSIS	135
A.1 Background.....	135
A.2 Differences Between CRA19 and CRA19_CL Analyses.....	136
A.3 Waste Area Pressures.....	137
A.4 Waste Area Saturations.....	139
A.5 Gas Generation and Brine and Gas Flows	141
A.6 Normalized Releases.....	143
A.6.1 Cuttings and Cavings Normalized Releases.....	143
A.6.2 Spallings Normalized Releases	144
A.6.3 Normalized Direct Brine Releases	145
A.6.4 Normalized Culebra Transport Releases	146
A.6.5 Total Normalized Releases.....	148
A.7 Summary.....	149

LIST OF TABLES

Table 1 – Open Panel Closure Properties for CRA19	16
Table 2 – Material Properties Used for Operations, Experimental, and Panel Closure Areas from 0 to 10,000 yr in CRA14, CRA19, and CRA19_CL Analyses.....	19
Table 3 – BRAGFLO Grid Cell X- and Z-Dimensions for Shaft Representation (CRA14 and CRA19).....	21
Table 4 – BRAGFLO Grid Dimensions for Experimental Area (CRA14 and CRA19)	21
Table 5 – Radionuclide Radiolysis and Decay Parameters for CRA19.....	23
Table 6 – GLOBAL:PBRINE Distribution for CRA19.....	24
Table 7 – Iron Corrosion Parameters for CRA19	25
Table 8 – BOREHOLE:TAUFAIL Update for CRA19	25
Table 9 – Colloid Enhancement Parameters for CRA19	26
Table 10 – WAS_AREA:HYMAGCON Update for CRA19.....	26

Table 11 – Iron Sulfidation Stoichiometric Coefficient Parameter Updates for CRA19	27
Table 12 – BRAGFLO Grid Cell X-Dimensions for Northernmost Panel Closure Representation (CRA14 and CRA19).....	27
Table 13 – Drilling Rate and Plugging Pattern Parameters (CRA14 and CRA19)	28
Table 14 – Inventory Parameter Updates for CRA19.....	29
Table 15 – Solubility Parameter Updates for CRA19	33
Table 16 – BH_OPEN:RELP_MOD Parameter Value for CRA19.....	35
Table 17 – DRZ_OE_0 and DRZ_OE_1 Parameter Values for CRA19.....	36
Table 18 – DRZ_PC_0 and DRZ_PC_1 Parameter Values for CRA19.....	37
Table 19 – CAVITY_5 Parameter Values for CRA19	38
Table 20 – WIPP PA Codes Used for CRA19.....	44
Table 21 – BRAGFLO Modeling Scenarios.....	59
Table 22 – Gas Generation Statistics on Overall Means for CRA14 and CRA19	63
Table 23 – Pressure Statistics on Overall Means for CRA14 and CRA19.....	73
Table 24 – Brine Saturation Statistics on Overall Means for CRA14 and CRA19	85
Table 25 – Brine Flow Statistics on Overall Means for CRA14 and CRA19	94
Table 26 – PA intrusion Scenarios Used in Calculating Direct Solids Releases.....	98
Table 27 – Summary of Spallings Volumes by Scenario	101
Table 28 – Summary of Spallings Volumes by Intrusion Location.....	102
Table 29 – S2-DBR Mean Initial Conditions, Lower and Middle Locations.....	105
Table 30 – DBR Volume Summary.....	109
Table 31 – Statistics on the Overall Mean for Total Normalized Releases	122
Table 32 – Comparison of Total Releases at Compliance Points for CRA14, CRA19 and CRA19_CL Analyses.....	148

LIST OF FIGURES

Figure 1 – Total (CH and RH) Repository Waste Activity	47
Figure 2 – Dominant Waste Isotopes from Closure to 10,000 Years Post-Closure	48
Figure 3 – Waste Stream Concentration Complementary Cumulative Distribution at Closure (Top) and 10,000 Years Post-Closure (Bottom).....	49
Figure 4 – Spallings Concentration from Closure to 10,000 Years Post-Closure	50
Figure 5 – Log10 of Total Mobilization Potential for Base Elements, Castile Brine, All Conditions.....	52

Figure 6 – Log10 of Total Mobilization Potential for Base Elements, Castile Brine, by Brine Redox Condition53

Figure 7 – Mean Mobilized Concentrations vs Time, Castile Brine55

Figure 8 – Generic CRA-2014 PA BRAGFLO Grid with Modeled Area Descriptions57

Figure 9 – Generic CRA-2019 PA BRAGFLO Grid with Modeled Area Descriptions58

Figure 10 – Gas Generation from Corrosion and Biodegradation, Scenario S1-BF61

Figure 11 – Gas Generation from Corrosion and Biodegradation, Scenario S2-BF61

Figure 12 – CRA19 Moles of Gas Generated by All Sources, Scenario S1-BF.....62

Figure 13 – CRA19 Moles of Gas Generated by All Sources, Scenario S2-BF.....62

Figure 14 – Pressure Means for the Experimental Area, Scenario S1-BF.....66

Figure 15 – Pressure Means for the Experimental Area, Scenario S2-BF.....67

Figure 16 – Pressure Means for the Operations Area, Scenario S1-BF.....67

Figure 17 – Pressure Means for the Operations Area, Scenario S2-BF.....68

Figure 18 – Pressure Means for the North Rest-of-Repository, Scenario S1-BF68

Figure 19 – Pressure Means for the North Rest-of-Repository, Scenario S2-BF69

Figure 20 – Pressure Means for the North Rest-of-Repository, Scenario S4-BF69

Figure 21 – Pressure Means for the South Rest-of-Repository, Scenario S1-BF70

Figure 22 – Pressure Means for the South Rest-of-Repository, Scenario S2-BF70

Figure 23 – Pressure Means for the South Rest-of-Repository, Scenario S4-BF.....71

Figure 24 – Pressure Means for the Waste Panel, Scenario S1-BF71

Figure 25 – Pressure Means for the Waste Panel, Scenario S2-BF72

Figure 26 – Pressure Means for the Waste Panel, Scenario S4-BF72

Figure 27 – Brine Saturation Means for the Experimental Area, Scenario S1-BF.....77

Figure 28 – Brine Saturation Means for the Experimental Area, Scenario S2-BF.....77

Figure 29 – Brine Saturation Means for the Operations Area, Scenario S1-BF.....78

Figure 30 – Brine Saturation Means for the Operations Area, Scenario S2-BF.....78

Figure 31 – Brine Saturation Means for the North Rest-of-Repository, Scenario S1-BF79

Figure 32 – Brine Saturation Means for the North Rest-of-Repository, Scenario S2-BF79

Figure 33 – Brine Saturation Means for the North Rest-of-Repository, Scenario S4-BF80

Figure 34 – Brine Saturation Means for the South Rest-of-Repository, Scenario S1-BF80

Figure 35 – Brine Saturation Means for the South Rest-of-Repository, Scenario S2-BF81

Figure 36 – Brine Saturation Means for the South Rest-of-Repository, Scenario S4-BF81

Figure 37 – Brine Saturation Means for the Waste Panel, Scenario S1-BF82

Figure 38 – Brine Saturation Means for the Waste Panel, Scenario S2-BF82

Figure 39 – Brine Saturation Means for the Waste Panel, Scenario S4-BF83

Figure 40 – Brine Flow Means into Repository, Scenario S1-BF89

Figure 41 – Brine Flow Means into Repository, Scenario S2-BF89

Figure 42 – Brine Flow Means into Experimental Area, Scenario S1-BF90

Figure 43 – Brine Flow Means up the Shaft, Scenario S1-BF.....90

Figure 44 – Brine Flow Means up the Shaft, Scenario S2-BF.....91

Figure 45 – Brine Flow Means up the Shaft, Scenario S4-BF.....91

Figure 46 – Brine Flow Means up the Borehole, Scenario S2-BF92

Figure 47 – Brine Flow Means up the Borehole, Scenario S4-BF92

Figure 48 – Gas Flow Means out of South Rest-of-Repository (South to North) Across the Panel
 Closure Plane, Scenario S2-BF.....93

Figure 49 – Gas Flow Means out of North Rest-of-Repository (South to North) Across the Panel
 Closure Plane, Scenario S2-BF.....93

Figure 50 – Cumulative Frequency of Cavings Areas.....99

Figure 51 – Cumulative Frequency of Spallings Volumes.....100

Figure 52 – CRA-2019 PA DBR Grid with Simulated Intrusion Locations103

Figure 53 – S2-DBR Brine Pressure, All Lower and Middle Intrusions106

Figure 54 – S2-DBR Brine Saturation, All Lower and Middle Intrusions107

Figure 55 – Release Volume Frequency, All Intrusions.....110

Figure 56 – Release Volume Boxplots, All Nonzero Events.....110

Figure 57 – S2-DBR Release Volumes, All Intrusions111

Figure 58 – Cumulative Radionuclide Discharge Up Borehole at 10000 Years114

Figure 59– Cumulative Brine Discharge Up Borehole at 10000 Years.....114

Figure 60 –Overall Mean for Cuttings and Cavings Normalized Releases with Confidence Limits
116

Figure 61 –Overall Mean for Normalized Spallings Releases with Confidence Limits.....117

Figure 62 – Overall Mean for Normalized Direct Brine Releases with Confidence Limits.....118

Figure 63 –Overall Means for Transport Releases from the Culebra with Confidence Limits...119

Figure 64 – Replicate 1 Total Normalized Releases.....120

Figure 65 – Replicate 2 Total Normalized Releases.....120

Figure 66 – Replicate 3 Total Normalized Releases.....121

Figure 67 – Comparison of Overall Means for Release Components	121
Figure 68 – Overall Mean for Total Normalized Releases with Confidence Limits	122
Figure 69 – Waste Panel Integrated Function Average Brine Pressures	138
Figure 70 – South Rest-of-Repository Integrated Function Average Brine Pressures	138
Figure 71 – North Rest-of-Repository Integrated Function Average Brine Pressures	139
Figure 72 – Waste Panel Integrated Function Average Brine Saturations	140
Figure 73 – South Rest-of-Repository Integrated Function Average Brine Saturations	140
Figure 74 – North Rest-of-Repository Integrated Function Average Brine Saturations	141
Figure 75 – Total Waste Areas Integrated Function Average Gas Generation from All Sources	142
Figure 76 – Repository Waste Areas Integrated Function Average Brine Inflow.....	142
Figure 77 – North Rest-of-Repository Integrated Function Average Gas Flow (South to North) Across the Northernmost Panel Closure Plane	143
Figure 78 – Mean Cuttings and Cavings Release CCDFs Across Replicates for the CRA14, CRA19, and CRA19_CL Analyses.....	144
Figure 79 – Mean Spallings Release CCDFs Across Replicates for the CRA14, CRA19, and CRA19_CL Analyses.....	145
Figure 80 – Mean Direct Brine Release CCDFs Across Replicates for the CRA14, CRA19, and CRA19_CL Analyses.....	146
Figure 81 – Mean Release to Culebra CCDFs Across Replicates for the CRA14, CRA19, and CRA19_CL Analyses.....	147
Figure 82 – Mean Release from Culebra CCDFs Across Replicates for the CRA14, CRA19, and CRA19_CL Analyses.....	147
Figure 83 – Mean Total Release CCDFs Across Replicates for the CRA14, CRA19, and CRA19_CL Analyses.....	148

This page intentionally left blank.

Executive Summary

The Land Withdrawal Act requires that the U.S. Department of Energy (DOE) apply for recertification of the Waste Isolation Pilot Plant (WIPP) every five years following the initial 1999 receipt of waste. The 2019 Compliance Recertification Application (CRA-2019) is the fourth WIPP recertification application submitted for approval by the U.S. Environmental Protection Agency. A performance assessment (PA) has been executed by Sandia National Laboratories in support of the DOE submittal of the CRA-2019. Results found in the CRA-2019 PA (CRA19 analysis) are compared to those obtained in the 2014 Compliance Recertification Application (CRA-2014) PA (CRA14 analysis) in order to assess repository performance in terms of the current regulatory baseline. This report documents a summary of the CRA-2019 PA results. Changes incorporated into the CRA-2019 PA included repository planned changes, parameter updates, and refinements to PA implementation, including the following:

- Inclusion of an approach to accommodate the operational decisions to not emplace panel closures in Panels 3, 4, 5, and 6 and to not emplace waste in Panel 9.
- Inclusion of an approach to accommodate an additional shaft connecting the repository to the surface, as well as an additional mined region in the repository north end to accommodate drifts that lead to the new shaft.
- Refinement of the gas generation process model to include brine radiolysis.
- An update to the probability that a drilling intrusion into a repository excavated region will intersect the Castile brine reservoir modeled in BRAGFLO.
- Refinement to the corrosion rates of steel under humid and inundated conditions.
- Refinement to the effective shear strength of WIPP waste.
- Refinement to colloid enhancement parameters associated with actinide mobilization.
- Refinement to the hydromagnesite to magnesite conversion rate.
- Removal of two chemical reactions associated with iron sulfidation.
- Correction to the length of the northernmost panel closure in the BRAGFLO grid.
- Updates to drilling rate and plugging pattern parameters.
- Updates to WIPP waste inventory parameters.
- Updates to radionuclide solubilities and their associated uncertainty.
- An update to the BH_OPEN:RELP_MOD parameter.
- Introduction of new materials to define properties in some disturbed rock zone areas.
- Hardware and computational code updates.

Total normalized releases for the CRA19 analysis are increased at all probabilities compared to those from the CRA14 analysis. Releases from each release mechanism have also increased at all probabilities. Cuttings and cavings releases continue to dominate total releases at high probabilities and direct brine releases continue to dominate total releases at low probabilities. Total normalized releases continue to remain below regulatory limits. As a result, the CRA-2019 PA demonstrates that the WIPP remains in compliance with the containment requirements of 40 CFR Part 191.

This page intentionally left blank.

1.0 INTRODUCTION

The Waste Isolation Pilot Plant (WIPP), located in southeastern New Mexico, has been developed by the U.S. Department of Energy (DOE) for the geologic (deep underground) disposal of transuranic (TRU) waste. Containment of TRU waste at the WIPP is regulated by the U.S. Environmental Protection Agency (EPA) according to the regulations set forth in Title 40 of the Code of Federal Regulations (CFR), Part 191. The DOE demonstrates compliance with the containment requirements according to the Certification Criteria in Title 40 CFR Part 194 by means of performance assessment (PA) calculations performed by Sandia National Laboratories (SNL). WIPP PA calculations estimate the probability and consequence of potential radionuclide releases from the repository to the accessible environment for a regulatory period of 10,000 years after facility closure. The models used in PA are maintained and updated with new information as part of an ongoing process. Improved information regarding important WIPP features, events, and processes typically results in refinements and modifications to PA models and the parameters used in them. Planned changes to the repository and/or the components therein also result in updates to WIPP PA models. WIPP PA models are used to support the repository recertification process that occurs at five-year intervals following the receipt of the first waste shipment at the site in 1999.

PA calculations were included in the 1996 Compliance Certification Application (CCA) (U.S. DOE 1996), and in a subsequent Performance Assessment Verification Test (PAVT) (MacKinnon and Freeze 1997a, 1997b and 1997c). Based in part on the CCA and PAVT PA calculations, the EPA certified that the WIPP met the regulatory containment criteria. The facility was approved for disposal of transuranic waste in May 1998 (U.S. EPA 1998). PA calculations were an integral part of the 2004 Compliance Recertification Application (CRA-2004) (U.S. DOE 2004). During their review of the CRA-2004, the EPA requested an additional PA calculation, referred to as the CRA-2004 Performance Assessment Baseline Calculation (PABC) (Leigh et al. 2005), be conducted with modified assumptions and parameter values (Cotsworth 2005). Following review of the CRA-2004 and the CRA-2004 PABC, the EPA recertified the WIPP in March 2006 (U.S. EPA 2006).

PA calculations were completed for the second WIPP recertification and documented in the 2009 Compliance Recertification Application (CRA-2009). The CRA-2009 PA resulted from continued review of the CRA-2004 PABC, including a number of technical changes and corrections, as well as updates to parameters and improvements to the PA computer codes (Clayton et al. 2008). To incorporate additional information which was received after the CRA-2009 PA was completed, but before the submittal of the CRA-2009, the EPA requested an additional PA calculation, referred to as the 2009 Compliance Recertification Application Performance Assessment Baseline Calculation (PABC-2009) (Clayton et al. 2010), be undertaken which included updated information (Cotsworth 2009). Following the completion and submission of the PABC-2009, the WIPP was recertified in 2010 (U.S. EPA 2010).

PA calculations were completed for the third WIPP recertification and documented in the 2014 Compliance Recertification Application (CRA-2014). Following the completion and submission of the CRA-2014, the WIPP was recertified in 2017 (U.S. EPA 2017).

The Land Withdrawal Act (U.S. Congress 1992) requires that the DOE apply for WIPP recertification every five years following the initial 1999 waste shipment. The 2019 Compliance Recertification Application (CRA-2019) is the fourth WIPP recertification application submitted by the DOE for EPA approval. The PA executed by SNL in support of the CRA-2019 is detailed in AP-181 (Zeitler 2019). The CRA-2019 PA includes repository planned changes, parameter updates, and refinements to PA implementation. Results found in the CRA-2019 PA are compared to those obtained in the CRA-2014 in order to assess repository performance in terms of the current regulatory baseline. This document comprises the summary report of the CRA-2019 PA, which includes the results of the CRA19 analysis, as well as the supplemental CRA19_CL sensitivity study (Appendix A).

1.1 Changes Since the CRA-2014 PA

Several changes were incorporated in the CRA-2019 PA relative to the CRA-2014 PA that potentially impact parameter sensitivity analysis results. The analysis plan for the CRA-2019 PA calculations (AP-181) outlines the 16 categories of changes since the CRA-2014 PA (Zeitler 2019a) that were incorporated into the CRA-2019 PA calculations. The changes are:

- Inclusion of an approach to accommodate the operational decisions to not emplace panel closures in Panels 3, 4, 5, and 6 and to not emplace waste in Panel 9.
- Inclusion of an approach to accommodate an additional shaft connecting the repository to the surface, as well as an additional mined region in the repository north end to accommodate drifts that lead to the new shaft.
- Refinement of the gas generation process model to include brine radiolysis.
- An update to the probability that a drilling intrusion into a repository excavated region will intersect the Castile brine reservoir modeled in BRAGFLO.
- Refinement to the corrosion rates of steel under humid and inundated conditions.
- Refinement to the effective shear strength of WIPP waste.
- Refinement to colloid enhancement parameters associated with actinide mobilization.
- Refinement to the hydromagnesite to magnesite conversion rate.
- Removal of two chemical reactions associated with iron sulfidation.
- Correction to the length of the northernmost panel closure representation in the BRAGFLO grid.
- Updates to drilling rate and plugging pattern parameters.
- Updates to WIPP waste inventory parameters.
- Updates to radionuclide solubilities and their associated uncertainty.
- An update to the BH_OPEN:RELP_MOD parameter.
- Introduction of new materials to define properties in some disturbed rock zone areas.

- Hardware and computational code updates.

Changes listed above are discussed in more detail in the sections that follow. In parameter tables, the (-) designation is used to signify that the parameter is unitless.

1.1.1 Approach to Abandonment of Panel Closures in the South and No Waste in Panel 9

In February 2014, the WIPP repository was closed and later reopened on a limited basis, which resulted in maintenance delays in the repository. The DOE has proposed an operational policy change at WIPP as a result of the severe ground control issues caused by the maintenance delays. The policy change prohibits personnel access to (with the ultimate goal of withdrawal from) the area in the WIPP underground designated as equivalent Panel 9 (U.S. DOE 2016). With that change, the planned implementation of run-of-mine salt panel closures (ROMPCS) in Panels 3, 4, 5, and 6 would no longer be possible. Also, waste emplacement in the area designated as Panel 9 would no longer be possible. In response to the operational changes, the DOE requested that SNL undertake calculations and analyses to determine the impacts of the proposed changes to the repository configuration on the long-term performance of the facility (U.S. DOE 2017). The approach to modeling the impacts of the operational changes and the results of the Abandonment of Panel Closures in South End of Repository (APCS) analysis are described in Zeitler et al. (2017). This same approach was taken for CRA-2019 PA calculations and is described briefly below.

Panel closures are represented in PA calculations in the computational grids used by the BRAGFLO code, one grid for Salado flow calculations (“BRAGFLO grid”) and one for direct brine release (DBR) calculations (“DBR grid”). In the BRAGFLO grid representation, there are three waste areas: (1) the “waste panel” (WP) represents waste emplaced in Panel 5; (2) the “south rest-of-repository” (SROR) represents waste emplaced in Panels 3, 4, 6, and 9; and (3) the “north rest-of-repository” (NROR) represents waste emplaced in Panels 1, 2, 7, 8, and 10. There are also three panel closure areas (PCS): the “southernmost” PCS representation is between the WP and SROR, the “middle” PCS representation is between the SROR and NROR, and the “northernmost” PCS representation is between the NROR and operations (OPS) area.

1.1.1.1 Properties of Open Panel Closures

In CRA-2014 PA calculations, there were two areas in the BRAGFLO grid that were modeled as “open,” the OPS and EXP areas. There is no plan to backfill those areas, so they are assumed to close “naturally” following closure of the WIPP. Although the closure of the OPS/EXP areas is expected to occur gradually over time, in PA calculations, constant porosity and permeability over 10,000 years have been assumed (SNL 1996). In the APCS analysis, material properties for abandoned panel closure areas (i.e., panel closures for Panels 3-6 in the DBR grid and the southernmost panel closure in the BRAGFLO grid) were changed to be those used for the OPS/EXP areas and given a new material name, PCS_NO (Table 1). This change is justified in that it was shown to be conservative with respect to releases, and that the properties used for the OPS/EXP areas are the only analogues for open areas used in WIPP PA. Additionally, the DRZ above and below the abandoned panel closure areas retained the properties applied to the DRZ

above and below the waste areas and operations and experimental areas (i.e., DRZ_PCS is not invoked at 200 years) (Table 2). For the ROMPCS panel closure areas, the same properties used in the CRA-2014 PA were applied.

For the CRA-2019 PA, the parameterization of the abandoned panel closures and associated DRZ areas was the same as that used in the APCS analysis for the computational grids used in BRAGFLO and BRAGFLO_DBR calculations. The parameter values summarized in Table 1 and Table 2 already existed in the Performance Assessment Parameter Database (PAPDB) prior to the CRA-2019 PA and were therefore carried forward for CRA-2019 PA calculations.

Table 1 – Open Panel Closure Properties for CRA19

Material	Property	Description	Units	Value
PCS_NO	CAP_MOD	Model number, capillary pressure model	(-)	1
PCS_NO	COMP_RCK	Bulk Compressibility	Pa ⁻¹	0
PCS_NO	KPT	Flag for Permeability Determined Threshold	(-)	0
PCS_NO	PCT_A	Threshold Pressure Linear Parameter	Pa	0
PCS_NO	PCT_EXP	Threshold pressure exponential parameter	(-)	0
PCS_NO	PC_MAX	Maximum allowable capillary pressure	Pa	1.0E8
PCS_NO	PORE_DIS	Brooks-Corey pore distribution parameter	(-)	0.7
PCS_NO	POROSITY	Effective porosity	(-)	0.18
PCS_NO	PO_MIN	Minimum brine pressure for capillary model KPC=3	Pa	101325
PCS_NO	PRESSURE	Brine far-field pore pressure	Pa	101325
PCS_NO	PRMX_LOG	Log of intrinsic permeability, X-direction	log(m ²)	-11
PCS_NO	PRMY_LOG	Log of intrinsic permeability, Y-direction	log(m ²)	-11
PCS_NO	PRMZ_LOG	Log of intrinsic permeability, Z-direction	log(m ²)	-11
PCS_NO	RELP_MOD	Model number, relative permeability model	(-)	11
PCS_NO	SAT_IBRN	Initial Brine Saturation	(-)	0
PCS_NO	SAT_RBRN	Residual Brine Saturation	(-)	0
PCS_NO	SAT_RGAS	Residual Gas Saturation	(-)	0

1.1.1.2 Redefinition of Panel Adjacency in CCDFGF

An additional piece of the APCS approach is that of “panel reneighboring” in CCDFGF calculations. Some conservativity with respect to releases is built into the APCS approach as a result of the reconsideration of panel adjacencies following intrusions (Zeitler and Day (2017) and Zeitler et al. (2017)). Panel neighbor relationships were modified to correspond to the degree of separation by panel closures instead of merely spatial proximity. The modification is

consistent with the definition that panels having one or fewer panel closures between them are considered neighbors. The approach is consistent with the use of panel closures in both the BRAGFLO and BRAGFLO_DBR grids and the definitions of SROR and NROR. The panel neighboring scheme followed in the APCS analysis was carried forward for CRA-2019 PA calculations.

1.1.1.3 Removal of Waste from Panel 9

The APCS approach also considered the removal of waste from Panel 9 and relocation of waste to a new panel somewhere north of Panel 8, outside of the current repository configuration. In the APCS analysis, it was shown to be appropriately conservative with respect to releases to continue to model waste within the existing Panel 9 in lieu of adding new waste panel(s) to the north (Zeitler et al. 2017). The conservatism was attributed to the 1-degree (south) dip in the Salado formation, which results in increased brine accumulation due to gravity drainage, increased hydrostatic pressure, and increased gas generation due to corrosion (enabled by the increased availability of brine) at the deeper/south portion of the repository. Previous PA analyses consistently show increasing brine saturations and pressures in the repository when moving from the north to the south. Thus, continuing to model the same mass of waste as if it is located in Panel 9 results in somewhat larger DBR and spallings releases compared to if the same mass was relocated to an arbitrary location further north. In the APCS analysis, this conservatism was greatly enhanced due to the abandonment of panel closures between Panels 3, 4, 5, 6, and 9, which effectively equilibrates the brine pressures and saturations in Panels 3, 4, 5, 6, and 9. The APCS analysis also showed that the potential non-conservative condition of not considering DBRs from both the empty Panel 9 and the hypothetical Panel 9 replacement is more than covered by the conservative assumptions of the panel neighbor redefinitions. For CRA-2019 PA calculations, it was considered to be appropriately conservative with respect to releases to continue to model waste within the existing Panel 9 in lieu of adding new waste panel(s) to the north.

1.1.1.4 Supplemental Calculation for CRA-2019 PA

In the APCS analysis (Zeitler et al. 2017), the decision to use “open” area properties for the abandoned panel closures was shown to substantially increase estimated releases over the CRA14_SEN4 (Zeitler and Day 2016) baseline case due to increased communication between the WP and SROR areas. The increased communication was due to the substitution of an “open” area for the southernmost panel closure area in the BRAGFLO representation, which allowed for greater brine pressures and saturations in the SROR following Castile intrusions, as there was no longer a significant barrier to equilibration with the WP. The saturations resulting from the flooding of Panels 3, 4, 6, and 9 with Castile brine from the borehole in Panel 5 through the abandoned panel closure led to increased gas generation and associated brine pressures in these areas. These conditions contributed to increases in calculated direct brine releases (DBRs) and releases to/from the Culebra and increased pressures led to increased spallings releases.

In discussions between the DOE and EPA subsequent to the APCS analysis, the EPA questioned whether, due to uncertainty in the timing of closure of open areas in the repository (i.e., when the material properties of the open areas might approach the properties of intact halite), the approach

to model “open” areas of the repository, including abandoned panel closure areas, as permanently “open” could potentially underpredict releases. As an example, the EPA noted that for the CRA14_SEN3 sensitivity study (Day and Zeitler 2016), in which ROMPCS, OPS, and EXP two-phase flow properties were changed to more closely resemble intact halite (e.g., decreased porosity and permeability), estimated total releases increased over the baseline CRA-2014 PA case. However, the assumption made in the APCS analysis of no panel closure emplacement in the south end of the repository, which allowed greater communication among the panels in the south, is what drove releases higher for that analysis. Therefore, an effort to reduce porosity and permeability in all open areas would also serve to return the abandoned panel closure area to having a similar role to that prior to the APCS analysis (i.e., reducing communication among the panels in the south). Reducing the communication between the WP and SROR areas was expected to result in lower brine pressures and saturations in the SROR following Castile intrusions (and thus lower calculated releases) compared to a baseline case that considers an “open” abandoned closure area representation (e.g., the APCS case).

It was expected that the reduction in releases due to the reduction in communication between the WP and SROR areas (as observed for the APCS analysis) would not be less than the nominal increase in releases observed for reduced open area flow properties that limit gas flow to the north and increase pressures by reducing available void space to accommodate gas generation (as observed for the CRA14_SEN3 analysis). Because the APCS and CRA14_SEN3 analyses were based on different baselines (CRA14_SEN4 and CRA-2014 PA, respectively), a direct comparison of releases for an “open vs. closed” comparison had not been made prior to the CRA-2019 PA. In order to show the impact of the assumed long-term behavior of open areas (i.e., resulting in “open” or “closed” OPS, EXP, and abandoned closure areas), a supplemental calculation was performed as part of the CRA-2019 PA.

In this supplemental calculation (CRA19_CL analysis), the only differences from the baseline case (CRA19 analysis) were the properties assigned to three areas (the OPS, EXP, and abandoned panel closure areas) and assignment of the panel neighbor relationships to be consistent with the isolation of panels in the south end of the repository (i.e., reassignment to “pre-APCS” relationships to be consistent with the basis described in Section 1.1.1.2). For the CRA19_CL analysis, OPS, EXP, and abandoned panel closure (southernmost panel closure) areas had two-phase flow parameters equivalent to those specified for intact halite in order to facilitate modeling the impact of the assumption that rapid closure of open areas results in those areas having material properties more like the low porosity and low permeability Salado formation. Because these parameter values already existed in the PAPDB, no new parameter values were specified for the CRA19_CL analysis. Results of the CRA19_CL analysis are presented in Appendix A.

Table 2 – Material Properties Used for Operations, Experimental, and Panel Closure Areas from 0 to 10,000 yr in CRA14, CRA19, and CRA19_CL Analyses

Model Area	CRA14	CRA19	CRA19_CL
Northernmost and Middle Panel Closure Areas	PCS_T1 (0-100 yr), PCS_T2 (100-200 yr), PCS_T3 (200-10,000 yr)	PCS_T1 (0-100 yr), PCS_T2 (100-200 yr), PCS_T3 (200-10,000 yr)	PCS_T1 (0-100 yr), PCS_T2 (100-200 yr), PCS_T3 (200-10,000 yr)
Southernmost Panel Closure Area	PCS_T1 (0-100 yr), PCS_T2 (100-200 yr), PCS_T3 (200-10,000 yr)	PCS_NO	S_HALITE
Operations Area	OPS_AREA	OPS_AREA	S_HALITE
Experimental Area	EXP_AREA	EXP_AREA	S_HALITE

This page intentionally left blank.

1.1.2 Additional Shaft and Associated Drifts

In the wake of the 2014 radiological release event at the WIPP site, a modified ventilation system is planned that will provide sufficient airflow necessary for the resumption of increased-rate disposal operations in the future. The primary components of the modified ventilation system are an additional shaft in the north end of the repository and associated drifts to connect the additional shaft to the experimental area of the repository.

There are four shafts currently located in the repository north end, namely a salt handling shaft, an exhaust shaft, a waste shaft, and an air intake shaft. In WIPP PA, these shafts are combined into a single shaft that captures the combined impacts of all of them. The additional, planned shaft will be combined with the four existing shafts in the CRA-2019 PA. Additionally, mined volume in the repository north end will be modified in the repository representation so as to include the additional drifts created to access the new shaft. A similar approach was employed for the SHFT14 analysis that accompanied a planned change notice (PCN) submitted to the EPA in 2017 (Camphouse 2014). That analysis showed minimum impact to the long-term repository performance from representing the additional shaft and drifts. The shaft and drift dimensions assumed for the SHFT14 analysis were based on a preliminary design, while the dimensions assumed for the CRA-2019 PA are based on a more recent design. Updated model dimensions for the shaft and experimental area representations to be used in the BRAGFLO Salado grid were derived by Zeitler (2019b) and are summarized below in Table 3 and Table 4.

Table 3 – BRAGFLO Grid Cell X- and Z-Dimensions for Shaft Representation (CRA14 and CRA19)

Analysis	X-Dimension (m)	Z-Dimension (m)	Area (m ²)	Length (m)	Volume (m ³)
CRA14	10	9.5	95	658.56	62563
CRA19	12.6933	12.0586	153.06	658.56	100802

Table 4 – BRAGFLO Grid Dimensions for Experimental Area (CRA14 and CRA19)

Analysis	One-Cell Dimension			Full Dimension			Volume (m ³)
	X-Dim (m)	Y-Dim (m)	Z-Dim (m)	X-Dim (m)	Y-Dim (m)	Z-Dim (m)	
CRA14	361.65	1.32	51.68 ^a	723.3	3.96	51.68 ^a	148011
CRA19	361.65	1.32	67.05	723.3	3.96	67.05	192053

^a – Three EXP cells in the CRA-2014 PA had a z-dimension of 51.68 m and three had z-dimension of 51.67 m.

1.1.3 Brine Radiolysis as Part of Gas Generation Process Model

A recent evaluation has identified a need to include radiolytic gas generation in WIPP PA (Day 2019a). Therefore brine radiolysis was included in the CRA-2019 PA as part of the gas generation process model. The FEPs screening analysis performed for the CRA-2019 PA confirmed the decision to include the impact of brine radiolysis on gas generation in the repository (Kirkes 2019a). The implementation and associated assumptions are described in detail in Day (2019a) and parameterization implications are summarized below.

The total radiolytic H₂ generation rate is due to contributions from one or more decaying radionuclides in the waste area. The hydrogen generation rate due to radiolysis of radionuclides in solution and due to a fractional contribution from the wetted solid form of the radionuclides is dependent upon the following variables:

GDEPFAC = energy deposition probability for wetted solid radionuclides [-]

DECAYNRG = disintegration energy of radionuclide [MeV]

GH2AVG = average “G” value for H₂ [molecule/eV]

SRADO2 = stoichiometric coefficient for O₂ from radiolysis [mol O₂/mol H₂]

An inventory assessment as part of the CRA-2019 PA (Kicker 2019a) has determined which radionuclides are to be considered to participate in radiolysis based on the relative amount of decay heats compared to the overall inventory heat production (i.e., ²⁴¹Am, ²³⁸Pu, ²³⁹Pu, ²⁴⁰Pu, and ²⁴²Pu). For those selected radionuclides, new DECAYNRG parameters (Table 5) were implemented in CRA-2019 PA to support the radiolysis and decay calculations. The source for the GLOBAL:GH2AVG parameter is an experimentally-derived value from Reed et al. (1993). Justifications for the GLOBAL:GDEPFAC and GLOBAL:SRADO2 parameter recommendations are provided by Day (2019a).

Table 5 – Radionuclide Radiolysis and Decay Parameters for CRA19

Material	Property	Description	Units	Value
AM241	DECAYNRG	Radionuclide disintegration energy	MeV	5.6379
PU238				5.593
PU239				5.2442
PU240				5.2559
PU242				4.9855
GLOBAL	GH2AVG	Average G-value for H ₂	molecules/eV	0.014
GLOBAL	GDEPFAC	Energy deposition probability for wetted solid radionuclides	(-)	Uniform Distribution from [0 - 0.5]
GLOBAL	SRADO2	Stoichiometric coefficient for O ₂ from radiolysis	mol O ₂ /mol H ₂	0

1.1.4 Refinement to the Probability of Encountering Pressurized Brine

The WIPP PA parameter GLOBAL:PBRINE (hereafter PBRINE) is used to specify the probability that a drilling intrusion into the excavated region of the repository encounters a region of pressurized brine below the repository. Development of the distribution for PBRINE used prior to the CRA-2014 PA was the result of an analysis of TDEM data (Rechard et al. 1991, Peake 1998). A framework that provided a quantitative argument for refinement of the PBRINE parameter was developed for the CRA-2014 PA (Kirchner et al. 2012). The refinement of PBRINE resulted from a re-examination of the TDEM data while also including a greatly expanded set of drilling data for locations adjacent to the WIPP site than were available when the original analysis was performed in 1998. The EPA has since created a revised distribution for the PBRINE parameter based on a reexamination of the original TDEM data and recommended its use in the CRA-2019 PA. The resulting cumulative distribution for PBRINE is described in detail in U.S. EPA (2017b) and summarized in Zeitler (2019c) (Table 6). The DOE agreed to use of the U.S. EPA-identified distribution in the CRA-2019 PA. The EPA previously directed this distribution for use by the DOE as part of the CRA14_SEN4 sensitivity study (Zeitler and Day 2016) and the distribution thus already existed in the PAPDB as version 4 of the PBRINE parameter.

Table 6 – GLOBAL:PBRINE Distribution for CRA19

Material	Property	Description	Units	Value
GLOBAL	PBRINE	Prob. that Drilling Intrusion In Excavated Area Encounters Pressurized Brine	(-)	Cum. distribution as summarized in U.S. EPA (2017b) and Zeitler (2019c)

1.1.5 Refinement to the Corrosion Rates of Steel

The interaction of steel in the WIPP with repository brines will result in the formation of H₂ gas due to anoxic corrosion of the metal. Two steel corrosion rates were updated for the CRA-2019 PA, STEEL:CORRMCO₂ (hereafter CORRMCO₂) and STEEL:HUMCORR (hereafter HUMCORR).

For the CRA-2014 PA, experimental results from Roselle (2013) were used to determine an updated parameter distribution for CORRMCO₂, which represents the anoxic steel corrosion rate for brine-inundated steel in the absence of microbially produced CO₂. Subsequent to the submittal of the CRA-2014, the EPA requested that the DOE reconsider the subset of the Roselle data to be included in the CORRMCO₂ distribution. As a result, a new, cumulative distribution for CORRMCO₂ was developed (Zeitler and Hansen 2015a). Later, in their technical support document (TSD) on chemistry-related issues, the EPA recommended an adjustment of the Zeitler and Hansen (2015a) distribution for the CRA-2019 PA via an increase by a factor of two (U.S. EPA 2017c) and the DOE has agreed to the adjustment by a factor of two to accommodate the potential for enhanced corrosion at elevated pressures. The resulting cumulative distribution for CORRMCO₂ is described in detail in Zeitler (2018a) and was used in the CRA-2019 PA (Table 7).

For the CRA-2014 PA, experimental results from Roselle (2013) were used to determine that HUMCORR, which represents the humid corrosion rate of steel should maintain a value of zero. Subsequent to the submittal of the CRA-2014, the EPA requested that the DOE reconsider the subset of the Roselle data to be used for development of the STEEL:HUMCORR parameter. As a result, a cumulative distribution for HUMCORR was developed (Zeitler and Hansen 2015b) and later revised based on an updated estimate of the CO₂ level expected in the repository, which itself is recalculated each time the thermodynamic database is revised (Zeitler and Hansen 2015c). In order to avoid recalculation of the HUMCORR distribution each time the thermodynamic database is revised in the future, a CO₂ level that is expected to bound future predicted CO₂ levels was selected and used to again revise the HUMCORR distribution (Zeitler 2018b). The cumulative distribution described in Zeitler (2018b) was in the CRA-2019 PA (Table 7).

Table 7 – Iron Corrosion Parameters for CRA19

Material	Property	Description	Units	Value
STEEL	CORRMCO2	Inundated corrosion rate for steel without CO2 present	m/s	Cum. distribution as summarized in Zeitler (2018a)
STEEL	HUMCORR	Humid corrosion rate for steel	m/s	Cum. distribution as summarized in Zeitler (2018b)

1.1.6 Refinement to the Effective Shear Strength of WIPP Waste

WIPP PA includes scenarios in which human intrusion results in a borehole intersecting the repository. During the intrusion, drilling mud flowing up the borehole will apply a hydrodynamic shear stress on the borehole wall. Erosion of the wall material can occur if this stress is high enough, resulting in a release of radionuclides being carried up the borehole with the drilling mud. The WIPP PA parameter BOREHOLE:TAUFAIL (hereafter TAUFAIL) is used to represent the effective shear strength for erosion of WIPP waste.

For the CRA-2014 PA, experimental results from Herrick et al. (2012) were used to determine an updated parameter distribution for TAUFAIL (Herrick 2013). Subsequent to the submittal of the CRA-2014, the EPA requested that the DOE reconsider the subset of the Herrick data to be included in the TAUFAIL distribution, including lowering the lower bound of the distribution. The resulting cumulative distribution for TAUFAIL is described in U.S. EPA (2017d) and summarized in Zeitler (2019c). The DOE agreed to its use in the CRA-2019 PA. The EPA previously directed this distribution for use by the DOE as part of the CRA14_SEN4 sensitivity study (Zeitler and Day 2016) and the distribution thus already existed in the PAPDB as version 7 of the TAUFAIL parameter.

Table 8 – BOREHOLE:TAUFAIL Update for CRA19

Material	Property	Description	Units	Value
BOREHOLE	TAUFAIL	Effective shear strength for erosion	Pa	Uniform distribution from [1.60 - 77]

1.1.7 Refinement to Colloid Enhancement Parameters

Based on new laboratory and literature data since the CRA-2014 PA, new parameter recommendations have been made to colloid enhancement parameters used to calculate mobilized radionuclide concentrations (Reed et al. 2019 and Mariner 2019). Colloid enhancement parameter updates incorporated into the CRA-2019 PA are summarized in Table 9.

Table 9 – Colloid Enhancement Parameters for CRA19

Material	Property	Description	Units	Value
PHUMOX3	PHUMSIM	Proportionality Constant, Humic Colloids, Salado Brine	(-)	0.2
PHUMOX4				0.01
PHUMOX3	PHUMCIM	Proportionality Constant, Humic Colloids, Castile Brine	(-)	0.2
PHUMOX4				0.01
AM	CAPMIC	Maximum Concentration of Actinide on Microbe Colloids	moles/L	2.3E-9
NP, PU, TH, U				3.8E-8
AM	PROPMIC	Moles of Actinide Mobilized on Microbe Colloids per Moles Dissolved	(-)	0.03
NP, PU, TH, U				0.21
AM	CONCINT	Actinide Concentration with Mobile Actinide Intrinsic Colloids	moles/L	9.5E-9
NP, PU, TH				4.3E-8
U				1.4E-6

1.1.8 Refinement to Hydromagnesite Conversion Rate

For the CRA-2014 PA, the reaction of hydromagnesite to form magnesite was included along with an associated reaction rate, parameterized as WAS_AREA:HYMAGCON (hereafter HYMAGCON), derived by Clayton (2013). Subsequent to the submittal of the CRA-2014, the EPA requested that the DOE revise the distribution for HYMAGCON. A revised distribution was provided to the EPA by the DOE, but the EPA recommended a different distribution for the CRA-2019 PA (U.S. EPA 2017c). The uniform distribution used for HYMAGCON in the CRA-2019 PA is described in U.S. EPA (2017c) and summarized in Zeitler (2019c) (Table 10). The DOE agreed to its use in the CRA-2019 PA.

Table 10 – WAS_AREA:HYMAGCON Update for CRA19

Material	Property	Description	Units	Value
WAS_AREA	HYMAGCON	Rate of conversion of hydromagnesite to magnesite	mol kg ⁻¹ sec ⁻¹	Uniform distribution from [0 – 3.4E-10)

1.1.9 Removal of Iron Sulfidation Reactions

For the CRA-2014 PA, the sulfidation reactions with iron and iron hydroxide were included as part of the repository brine and gas production/consumption calculations. Subsequent to the submittal of the CRA-2014, the EPA requested that the DOE remove these chemical reactions from WIPP PA by setting the appropriate stoichiometric coefficients (i.e., REFCON:STCO_31, REFCON:STCO_32, REFCON:STCO_35, REFCON:STCO_36, REFCON:STCO_43, and REFCON:STCO_46) to zero. The request to remove iron sulfidation reactions from WIPP PA

and the impact to WIPP PA parameters for the CRA-2019 PA is described in U.S. EPA (2017c) and summarized in Zeitler (2019c). The EPA previously directed the definition of zero values for these stoichiometric coefficients for use by the DOE as part of the CRA14_SEN4 sensitivity study (Zeitler and Day 2016) and thus these values already existed in the PAPDB as version 2 of the respective parameters (Table 11). The DOE agreed to their use in the CRA-2019 PA.

Table 11 – Iron Sulfidation Stoichiometric Coefficient Parameter Updates for CRA19

Material	Properties	Description	Units	Value
REFCON	STCO_31, STCO_32, STCO_35, STCO_36, STCO_43, STCO_46	FeOH ₂ and metallic Fe sulfidation stoichiometric coefficients	(-)	0

1.1.10 Correction to Length of Northernmost Panel Closure Representation

Three separate panel closure areas are modeled in BRAGFLO. The “northernmost” panel closure area separates the operations area from the “north rest of repository” (NROR) waste area, the “middle” panel closure separates the NROR from the “south rest of repository” (SROR), and the “southernmost” panel closure separates the SROR from the waste panel.

As part of the DOE/EPA completeness determination discussions for CRA-2014, an error in the length of the northernmost panel closure was identified by the DOE—the northernmost panel closure in the BRAGFLO grid should represent the length of two panel closures. This is done to represent the combined blockage corresponding to the set of panel closures directly north of Panel 10 and the set of closures between the operations and experimental areas. Thus, the northernmost panel closure should have been 200 ft. (60.96 m) long, rather than 100 ft. (30.48 m) long, as had been used in the BRAGFLO model for the CRA-2014 PA (U.S. DOE 2015). A PA calculation was done to examine the impact of doubling the length of the northernmost panel closure and negligible changes to the pressures and saturations in the waste areas were found (Zeitler 2015). The correction to the BRAGFLO grid was made for the CRA-2019 PA via changes in grid cell x-dimensions for the two columns of cells that contain the representation of the northernmost panel closures (Table 12).

Table 12 – BRAGFLO Grid Cell X-Dimensions for Northernmost Panel Closure Representation (CRA14 and CRA19)

Analysis	One-Cell Length (m)	Full Length (m)
CRA14	15.24	30.48
CRA19	30.48	60.96

1.1.11 Updates to Drilling Rate and Plugging Pattern Parameters

WIPP regulations require that current drilling practices be assumed for future inadvertent intrusions. The DOE continues to survey drilling activity in the Delaware Basin in accordance with the criteria established in 40 CFR 194.33. Local well operators are surveyed annually to provide the WIPP project with information on drilling practices, Castile brine encounters, etc. Survey results through September 2018 are documented in the 2018 Delaware Basin Monitoring Annual Report (DBMAR) (U.S. DOE 2018).

Drilling parameters were updated for the CRA-2019 PA to include information assembled through September 2018. The 2018 DBMAR indicates a drilling rate of 99.0 boreholes per km² over 10,000 years, resulting in a value for WIPP PA parameter GLOBAL:LAMBAD of 9.90×10^{-3} boreholes per km² per year for the CRA-2019 PA, a notable increase to the value of 6.73×10^{-3} specified for this parameter in the CRA-2014 PA.

Borehole plugging pattern parameters were also updated based on data contained in the 2018 DBMAR. The DBMAR reports six types of plugging patterns (summarized in Table 9 of the DBMAR), which have historically been translated into three unique plugging patterns for PA purposes. This same translation scheme (i.e., type VI is the same as a full plug, types II and IV are the same as a two-plug, and types I, III, and V are the same as a three-plug configuration) was used for the parameterization of the GLOBAL:ONEPLG, GLOBAL:TWOPLG, and GLOBAL:THREEPLG parameters for the CRA-2019 PA (see SNL (2010) for a description of the use of the plugging pattern parameters in WIPP PA).

Although the translation scheme remains the same as for the CRA-2014 PA, the DOE made a change to the physical area over which plugging pattern data were collected. The DBMAR states that the new dataset “more accurately represents plugging techniques and activities used in the vicinity of the WIPP and is consistent with the provisions of 40 CFR 194.33(c)(1) and the future states assumptions of 40 CFR 194.25” (U.S. DOE 2018). As a result, the plugging pattern dataset is somewhat different than in previous versions of the DBMAR. Because of the substantial and potentially impactful changes of the drilling parameters, comparison values from the CRA-2014 PA are also presented in Table 13.

Table 13 – Drilling Rate and Plugging Pattern Parameters (CRA14 and CRA19)

Material	Property	Description	Units	CRA14 Value	CRA19 Value
GLOBAL	LAMBAD	Drilling rate per unit area	km ⁻² yr ⁻¹	6.73×10^{-3}	9.90×10^{-3}
GLOBAL	ONEPLG	Probability of having Plug Pattern 1 (full plug)	(-)	0.04	0.403
GLOBAL	TWOPLG	Probability of having Plug Pattern 2	(-)	0.594	0.331
GLOBAL	THREEPLG	Probability of having Plug Pattern 3	(-)	0.366	0.266

1.1.12 Updates to WIPP Waste Inventory Parameters

The Performance Assessment Inventory Report (PAIR) - 2018 (Van Soest 2018) was released on December 20, 2018. The PAIR-2018 contains updated estimates to the radionuclide content and waste material parameters, scaled to a full repository, based on inventory information collected up to December 31, 2017. In order to incorporate this update to the inventory into the CRA-2019 PA, the parameters for the initial radionuclide, chemical component and waste material inventories were updated. In addition, parameters which are calculated based on the initial radionuclide inventories, such as the Waste Unit Factor (WUF) and the initial lumped radionuclide inventories, were updated as well. Inventory parameters that were updated in the CRA-2019 PA are listed in Table 14.¹ Along with the parameter updates shown in Table 14, the analysis of the radionuclides that dominate potential releases were also updated (Kicker 2019a).

Table 14 – Inventory Parameter Updates for CRA19

Material	Property	Description	Value
AM241	INVCHD	WIPP-Scale Initial Radionuclide Inventory (CH=contact-handled; RH=remote-handled) (in Curies)	1.13E+06
AM241	INVRHD		1.30E+04
AM243	INVCHD		2.24E+01
AM243	INVRHD		4.12E+02
CF252	INVCHD		5.07E-01
CF252	INVRHD		1.76E+00
CM243	INVCHD		2.54E+00
CM243	INVRHD		3.61E+01
CM244	INVCHD		6.19E+03
CM244	INVRHD		3.32E+04
CM245	INVCHD		2.97E+00
CM245	INVRHD		2.15E+01
CM248	INVCHD		4.63E-01
CM248	INVRHD		1.31E+00
CS137	INVCHD		6.16E+02
CS137	INVRHD		2.50E+05
NP237	INVCHD		2.75E+01
NP237	INVRHD		6.96E+00
PA231	INVCHD		1.59E+01

¹ The SM147:INVCHD and SM147:INVRHD parameters, which represent initial inventories of the ¹⁴⁷Sm radionuclide in CH and RH waste, respectively, are new for the CRA-2019 PA. The ¹⁴⁷Sm radionuclide inventory with time continues to be calculated in the PANEL code, but an initial inventory of ¹⁴⁷Sm had not been previously defined.

Summary Report for the 2019 Compliance Recertification Application Performance
 Assessment (CRA-2019 PA)
 Rev. 0, ERMS 571376

PA231	INVRHD	1.04E-03
PB210	INVCHD	9.79E-01
PB210	INVRHD	1.45E+01
PM147	INVCHD	4.40E-01
PM147	INVRHD	2.54E+01
PU238	INVCHD	9.42E+05
PU238	INVRHD	2.25E+04
PU239	INVCHD	8.70E+05
PU239	INVRHD	4.22E+03
PU240	INVCHD	3.16E+05
PU240	INVRHD	3.16E+03
PU241	INVCHD	1.82E+06
PU241	INVRHD	4.53E+04
PU242	INVCHD	1.48E+02
PU242	INVRHD	1.59E+01
PU244	INVCHD	5.80E-03
PU244	INVRHD	2.82E-02
RA226	INVCHD	1.78E+00
RA226	INVRHD	1.85E+01
RA228	INVCHD	9.03E-02
RA228	INVRHD	4.55E-02
SM147	INVCHD	1.23E-09
SM147	INVRHD	9.40E-08
SR90	INVCHD	8.18E+02
SR90	INVRHD	1.96E+05
TH229	INVCHD	3.80E-01
TH229	INVRHD	8.74E-01
TH230	INVCHD	3.98E-01
TH230	INVRHD	2.26E+00
TH232	INVCHD	9.60E-02
TH232	INVRHD	2.26E-02
U233	INVCHD	1.10E+02
U233	INVRHD	1.72E+01
U234	INVCHD	4.77E+02

Summary Report for the 2019 Compliance Recertification Application Performance
 Assessment (CRA-2019 PA)
 Rev. 0, ERMS 571376

U234	INVRHD		9.70E+00
U235	INVCHD		4.56E+00
U235	INVRHD		1.85E+00
U236	INVCHD		4.24E-01
U236	INVRHD		2.53E-01
U238	INVCHD		3.92E+01
U238	INVRHD		3.13E+00
AM241L	INVCHD		WIPP-Scale Initial Lumped Radionuclide Inventory (CH=contact-handled; RH=remote-handled) (in Curies)
AM241L	INVRHD	1.45E+04	
TH230L	INVCHD	7.78E-01	
TH230L	INVRHD	3.13E+00	
PU238L	INVCHD	9.42E+05	
PU238L	INVRHD	2.25E+04	
U234L	INVCHD	5.86E+02	
U234L	INVRHD	2.69E+01	
PU239L	INVCHD	1.19E+06	
PU239L	INVRHD	7.63E+03	
BOREHOLE	WUF	Waste Unit Factor	3.30
NITRATE	QINIT	WIPP-Scale Amount of Nitrate (in moles)	2.72E+07
SULFATE	QINIT	WIPP-Scale Amount of Sulfate (in moles)	4.73E+06
WAS_AREA	IRONCHW	Mass of iron-based material in CH waste (in kg)	1.41E+07
WAS_AREA	IRONRHW	Mass of iron-based material in RH waste (in kg)	1.33E+06
WAS_AREA	IRNCCHW	Mass of iron containers, CH waste (in kg)	3.12E+07
WAS_AREA	IRNCRHW	Mass of iron containers, RH waste (in kg)	1.65E+07
WAS_AREA	CELLCHW	Mass of cellulose in CH waste (in kg)	4.10E+06
WAS_AREA	CELLRHW	Mass of cellulose in RH waste (in kg)	1.70E+05
WAS_AREA	CELCCHW	Mass of cellulose in CH waste container materials (in kg)	1.47E+06
WAS_AREA	CELCRHW	Mass of cellulose in RH waste container materials (in kg)	0.00E+00
WAS_AREA	CELECHW	Mass of cellulose in CH waste emplacement materials (in kg)	2.24E+05

WAS_AREA	CELERHW	Mass of cellulose in RH waste emplacement materials (in kg)	0.00E+00
WAS_AREA	PLASCHW	Mass of plastics in CH waste (in kg)	5.32E+06
WAS_AREA	PLASRHW	Mass of plastics in RH waste (in kg)	4.14E+05
WAS_AREA	PLSCCHW	Mass of plastic liners, CH waste (in kg)	2.83E+06
WAS_AREA	PLSCRHW	Mass of plastic liners, RH waste (in kg)	4.68E+05
WAS_AREA	PLSECHW	Mass of plastic in CH waste emplacement materials (in kg)	1.55E+06
WAS_AREA	PLSERHW	Mass of plastic in RH waste emplacement materials (in kg)	0.00E+00
WAS_AREA	RUBBCHW	Mass of rubber in CH waste (in kg)	1.09E+06
WAS_AREA	RUBBRHW	Mass of rubber in RH waste (in kg)	5.12E+04
WAS_AREA	RUBCCHW	Mass of rubber in CH waste container materials (in kg)	7.28E+04
WAS_AREA	RUBCRHW	Mass of rubber in RH waste container materials (in kg)	5.73E+03
WAS_AREA	RUBECHW	Mass of rubber in CH waste emplacement materials (in kg)	4.79E+03
WAS_AREA	RUBERHW	Mass of rubber in RH waste emplacement materials (in kg)	0.00E+00

The PAIR-2018 also includes information on the volume and radionuclide content for each waste stream. This information was used to generate the probability of encountering a waste stream and the normalized release as a function of time for each contact-handled (CH) and remote-handled (RH) waste stream for cuttings and cavings releases. Waste stream information was stored in the input files for WIPP PA code EPAUNI. These input files were updated in the CRA-2019 PA to reflect the most current waste stream information.

1.1.13 Updates to Radionuclide Solubilities

The solubilities of actinide elements are influenced by the chemical components of the waste. With the release of the PAIR-2018 (Van Soest 2018), updated information on the amount of various chemical components in the waste was available. To incorporate this updated information, parameters used to represent actinide solubilities were updated in the CRA-2019 PA. Additionally, uncertainty ranges and probability distributions for actinide solubilities were recalculated based on experimental results that have been published in the literature since the CRA-2014 PA, as well as the discussions between the DOE and EPA. Details of the development of radionuclide solubilities and their associated uncertainty for the CRA-2019 PA are contained in AP-153 (Brush et al. 2012) and were expanded upon in the baseline solubility analysis report generated for CRA-2019 (Domski and Sisk-Scott 2019) Baseline solubility

parameters for the CRA-2019 PA are summarized in Domski (2019a). Table 15 lists solubility parameters that were updated in the CRA-2019 PA.

Table 15 – Solubility Parameter Updates for CRA19

Material	Property	Description	Value
SOLMOD3	SOLSOH	Oxidation state III model, solubility in the minimum volume of Salado brine (in mol/L)	1.63E-07
	SOLSOH2	Oxidation state III model, solubility in 2 × the minimum volume of Salado brine (in mol/L)	1.58E-07
	SOLSOH3	Oxidation state III model, solubility in 3 × the minimum volume of Salado brine (in mol/L)	1.56E-07
	SOLSOH4	Oxidation state III model, solubility in 4 × the minimum volume of Salado brine (in mol/L)	1.55E-07
	SOLSOH5	Oxidation state III model, solubility in 5 × the minimum volume of Salado brine (in mol/L)	1.54E-07
	SOLCOH	Oxidation state III model, solubility in the minimum volume of Castile brine (in mol/L)	1.78E-07
	SOLCOH2	Oxidation state III model, solubility in 2 × the minimum volume of Castile brine (in mol/L)	1.63E-07
	SOLCOH3	Oxidation state III model, solubility in 3 × the minimum volume of Castile brine (in mol/L)	1.58E-07
	SOLCOH4	Oxidation state III model, solubility in 4 × the minimum volume of Castile brine (in mol/L)	1.54E-07
	SOLCOH5	Oxidation state III model, solubility in 5 × the minimum volume of Castile brine (in mol/L)	1.52E-07
SOLMOD4	SOLSOH	Oxidation state IV model, solubility in the minimum volume of Salado brine (in mol/L)	5.45E-08
	SOLSOH2	Oxidation state IV model, solubility in 2 × the minimum volume of Salado brine (in mol/L)	5.45E-08
	SOLSOH3	Oxidation state IV model, solubility in 3 × the minimum volume of Salado brine (in mol/L)	5.45E-08
	SOLSOH4	Oxidation state IV model, solubility in 4 × the minimum volume of Salado brine (in mol/L)	5.45E-08
	SOLSOH5	Oxidation state IV model, solubility in 5 × the minimum volume of Salado brine (in mol/L)	5.45E-08
	SOLCOH	Oxidation state IV model, solubility in the minimum volume of Castile brine (in mol/L)	5.44E-08

	SOLCOH2	Oxidation state IV model, solubility in 2 × the minimum volume of Castile brine (in mol/L)	5.44E-08
	SOLCOH3	Oxidation state IV model, solubility in 3 × the minimum volume of Castile brine (in mol/L)	5.44E-08
	SOLCOH4	Oxidation state IV model, solubility in 4 × the minimum volume of Castile brine (in mol/L)	5.44E-08
	SOLCOH5	Oxidation state IV model, solubility in 5 × the minimum volume of Castile brine (in mol/L)	5.44E-08
SOLMOD5	SOLSOH	Oxidation state V model, solubility in the minimum volume of Salado brine (in mol/L)	4.02E-07
	SOLSOH2	Oxidation state V model, solubility in 2 × the minimum volume of Salado brine (in mol/L)	2.83E-07
	SOLSOH3	Oxidation state V model, solubility in 3 × the minimum volume of Salado brine (in mol/L)	2.42E-07
	SOLSOH4	Oxidation state V model, solubility in 4 × the minimum volume of Salado brine (in mol/L)	2.21E-07
	SOLSOH5	Oxidation state V model, solubility in 5 × the minimum volume of Salado brine (in mol/L)	2.09E-07
	SOLCOH	Oxidation state V model, solubility in the minimum volume of Castile brine (in mol/L)	1.20E-06
	SOLCOH2	Oxidation state V model, solubility in 2 × the minimum volume of Castile brine (in mol/L)	7.27E-07
	SOLCOH3	Oxidation state V model, solubility in 3 × the minimum volume of Castile brine (in mol/L)	5.52E-07
	SOLCOH4	Oxidation state V model, solubility in 4 × the minimum volume of Castile brine (in mol/L)	4.61E-07
	SOLCOH5	Oxidation state V model, solubility in 5 × the minimum volume of Castile brine (in mol/L)	4.05E-07
SOLMOD3, SOLMOD4	SOLVAR	Actinide Solubility Uncertainties (unitless)	Cum. distributions summarized in Domski (2019a)

1.1.14 Update to BH_OPEN:RELP_MOD Parameter

A minor error in the BRAGFLO code related to the calculation of capillary pressure was discovered, as detailed in software problem report (SPR) 18-002, and determined to have an insignificant effect on repository performance results (Day 2018). It was noted that one of the SPR 18-002 corrections also prompted the necessity to revise a BRAGFLO input parameter for

the relative permeability and capillary pressure function that is used to model an open borehole (BH_OPEN:RELP_MOD). The RELP_MOD parameter was revised from 5 (the value used in the CRA-2014 PA) to 11 for the CRA-2019 PA to resolve the issue where the code correction resulted in a positive capillary pressure within the open borehole under RELP_MOD=5, which is both physically unrealistic and numerically unstable. The use of RELP_MOD = 11 for the BH_OPEN material is consistent with the relative permeability and (zero) capillary pressure implemented for other “open” repository areas such as the operations and experimental areas.

Table 16 – BH_OPEN:RELP_MOD Parameter Value for CRA19

Material	Property	Description	Units	Value
BH_OPEN	RELP_MOD	Model number, relative permeability model	(-)	11

1.1.15 New Materials to Define Properties in DRZ Surrounding OPS, EXP, and Panel Closure Areas

As part of their review of the CRA-2014, the EPA directed multiple sensitivity studies that investigated impacts of parameter changes to the OPS, EXP, and panel closure areas and their associated disturbed-rock zones (DRZs), while leaving the DRZ surrounding the waste panel unchanged. To facilitate those analyses, new material names were used that introduced flexibility in specifying material properties independently across areas for which material properties in the CRA-2014 PA were identical. The flexibility of managing material properties by using these new material names was preserved in the CRA-2019 PA. This subsection describes the new materials (DRZ_OE_0, DRZ_OE_1, DRZ_PC_1, DRZ_PC_0, and CAVITY_5) and the sources for the associated property values that already exist in the PAPDB due to their use in the sensitivity studies. To be clear, while material names representing these areas of the BRAGFLO grid have changed since the CRA-2014 PA, properties for those areas have not changed (one exception is the DRZ surrounding the abandoned southernmost panel closure area, which will have DRZ_0 and DRZ_1 properties (Section 1.1.1.1)).

In the CRA-2014 PA, the DRZ surrounding the waste, OPS, and EXP areas were given identical properties in BRAGFLO calculations via the DRZ_0 and DRZ_1 materials. In the CRA14_SEN2 study (Day 2016), to isolate the parameter modifications for the DRZ surrounding the OPS and EXP areas, the new materials DRZ_OE_0 and DRZ_OE_1 were introduced to represent the DRZ surrounding only the OPS and EXP areas in the -5 to 0 y and 0 to 10,000 y timeframes, respectively (the DRZ_0 and DRZ_1 materials continued to represent the DRZ surrounding the waste areas). In the CRA14_SEN4 sensitivity study (Zeitler and Day 2016), the properties of the DRZ surrounding the OPS and EXP areas were not changed from the CRA-2014 PA values, but the flexibility of isolating potential changes to the DRZ surrounding the OPS and EXP areas was preserved by maintaining the DRZ_OE_0 and DRZ_OE_1 materials and assigning values used in the CRA-2014 PA for the DRZ_0 and DRZ_1 materials, respectively.

For the CRA-2019 PA, the DRZ_OE_0 and DRZ_OE_1 materials will be used with parameter values equal to those used in the CRA-2014 PA for the DRZ_0 and DRZ_1 materials,

respectively. Because the DRZ_OE_0 and DRZ_OE_1 materials did not exist for the CRA-2014 PA, the CRA-2019 PA used the values defined in the sensitivity studies, as described above and summarized in Table 17.

Table 17 – DRZ_OE_0 and DRZ_OE_1 Parameter Values for CRA19

Material	Material for which Property Values are Equivalent (CRA-2014 and CRA-2019)	Properties	Analysis from which Defined Property Values Were Used
DRZ_OE_0	DRZ_0	KPT, PC_MAX, PO_MIN, PORE_DIS, RELP_MOD	CRA14_SEN2
DRZ_OE_0	DRZ_0	CAP_MOD, COMP_RCK, PCT_A, PCT_EXP, POROSITY, PRMX_LOG, PRMY_LOG, PRMZ_LOG, SAT_IBRN, SAT_RBRN, SAT_RGAS	CRA14_SEN4
DRZ_OE_1	DRZ_1	KPT, PC_MAX, PO_MIN, PORE_DIS, RELP_MOD	CRA14_SEN2
DRZ_OE_1	DRZ_1	CAP_MOD, COMP_RCK, PCT_A, PCT_EXP, POROSITY, PRMX_LOG, PRMY_LOG, PRMZ_LOG, SAT_IBRN, SAT_RBRN, SAT_RGAS	CRA14_SEN4

In the CRA14_SEN3 study (Day and Zeitler 2016), to isolate the parameter modifications for the DRZ surrounding the panel closure areas, the new materials DRZ_PC_0 and DRZ_PC_1 were introduced that represented the DRZ surrounding panel closure areas in the -5 to 0 y and 0 to 10,000 y timeframes, respectively. In the CRA14_SEN4 sensitivity study (Zeitler and Day 2016), the properties of the DRZ surrounding the panel closure areas were not changed from the CRA-2014 PA values, but the flexibility of isolating potential changes to the DRZ surrounding the panel closure areas was preserved by maintaining the DRZ_PC_0 and DRZ_PC_1 materials and assigning values used in the CRA-2014 PA for the DRZ_0 and DRZ_1 materials, respectively (one caveat is that the DRZ_PC_1 material properties were only used for the 0 to 200 y timeframe, while the DRZ_PCS material properties were used for the 200 to 10,000 y timeframe, as in the CRA-2014 PA).

For the CRA-2019 PA, the DRZ_PC_0 and DRZ_PC_1 (0 to 200 y timeframe) materials were used with parameter values equal to those used in the CRA-2014 PA for the DRZ_0 and DRZ_1 materials, respectively. Because the DRZ_PC_0 and DRZ_PC_1 materials did not exist for the CRA-2014 PA, the CRA-2019 PA used the values defined in the sensitivity studies, as described above and summarized in Table 18.

Table 18 – DRZ_PC_0 and DRZ_PC_1 Parameter Values for CRA19

Material	Material for which Property Values are Equivalent (CRA14 and CRA19)	Properties	Analysis from which Defined Property Values Were Used
DRZ_PC_0	DRZ_0 (-5 to 0 y)	KPT, PC_MAX, PO_MIN, PORE_DIS, RELP_MOD	CRA14_SEN3
DRZ_PC_0	DRZ_0 (-5 to 0 y)	CAP_MOD, COMP_RCK, PCT_A, PCT_EXP, POROSITY, PRMX_LOG, PRMY_LOG, PRMZ_LOG, SAT_IBRN, SAT_RBRN, SAT_RGAS	CRA14_SEN4
DRZ_PC_1	DRZ_1 (0 to 200 y)	KPT, PC_MAX, PO_MIN, PORE_DIS, RELP_MOD	CRA14_SEN3
DRZ_PC_1	DRZ_1 (0 to 200 y)	CAP_MOD, COMP_RCK, PCT_A, PCT_EXP, POROSITY, PRMX_LOG, PRMY_LOG, PRMZ_LOG, SAT_IBRN, SAT_RBRN, SAT_RGAS	CRA14_SEN4

The CRA14_SEN3 sensitivity study (Day and Zeitler 2016) investigated changes to panel closure properties. For the CRA-2014 PA, the panel closure system was, along with the shaft area, part of the CAVITY_4 material used in the -5 to 0 y time frame, but was separated from CAVITY_4 for the CRA14_SEN3 analysis. The startup material used for the panel closure system was a new material, CAVITY_5, and that material was used for the CRA-2019 PA, in order to preserve flexibility in assigning startup material properties to panel closure areas independently of the shaft area. For the CRA14_SEN3 analysis, the CAVITY_4 and CAVITY_5 materials had different property values, but for the CRA-2019, the property values for these two materials were identical. Because the CAVITY_5 material did not exist for the CRA-2014 PA, the CRA-2019 PA used the values defined in the sensitivity studies, as described above and summarized in Table 19.

Table 19 – CAVITY_5 Parameter Values for CRA19

Material	Material for which Property Values are Equivalent (CRA-2014 and CRA-2019)	Properties	Analysis from which Defined Property Values Were Used
CAVITY_5	CAVITY_4	KPT, PC_MAX, PO_MIN, PORE_DIS, PRESSURE	CRA14_SEN3
CAVITY_5	CAVITY_4	CAP_MOD, COMP_RCK, PCT_A, PCT_EXP, POROSITY, PRMX_LOG, PRMY_LOG, PRMZ_LOG, RELP_MOD, SAT_IBRN, SAT_RBRN, SAT_RGAS	CRA14_SEN4

1.1.16 Hardware and Computational Code Updates

Calculations for the CRA-2014 PA were performed on the WIPP PA Alpha Cluster, which consisted of HP AlphaServer hardware running the OpenVMS operating system (Long 2013). WIPP PA codes were later migrated to the WIPP PA Solaris Cluster, which consists of Intel hardware running the Solaris operating system (Kirchner 2012, Kirchner et al. 2014, Kirchner et al. 2015). The migration process consisted of recompilation, retesting, and requalification of codes, as well as rerunning of the CRA-2009 PABC and CRA-2014 PA calculations for verification. Subsequent to the migration of codes to the Solaris system, additional code changes have been made and documented to account for bug fixes, added functionality, and the addition of two codes to the Software Baseline that were previously qualified and used under Nuclear Waste Management Procedure NP 9-1: Analyses (SCREEN_NUTS and CCDFVECTORSTATS). The CRA-2019 PA was run on the WIPP PA Solaris Cluster using code versions listed in Section 4.0.

2.0 CONCEPTUAL APPROACH FOR THE CRA-2019 PA

The CRA-2019 PA analysis is to be used to demonstrate compliance with the containment requirements according to the Certification Criteria in Title 40 CFR paragraph 194. PA calculations were executed that included changes occurring since the CRA-2014 PA, and results of these calculations are compared to CRA-2014 PA results.¹ As regulatory compliance impacts are assessed via a direct comparison to the CRA-2014 PA, the CRA-2019 PA is designed to reproduce the CRA-2014 PA implementation where possible. The CRA-2019 PA has examined all aspects of repository performance that are potentially impacted by changes occurring since the CRA-2014 PA.

The approach used for the CRA-2019 PA was similar to that used for the CRA-2014 PA (Camphouse 2013). The CRA-2019 PA included an analysis of the Features, Events and Processes (FEPs) that may or may not have bearing on the performance of the repository. The FEPs have been screened to determine which FEPs should be accounted for in the PA. These “retained” FEPs have been formulated into scenarios that were modeled. Scenarios have been modeled using conceptual models that represent the physical and chemical processes of the repository. The conceptual models have been implemented through a series of computer simulations and associated parameters that describe the natural and engineered components of the disposal system (e.g., site characteristics, waste forms, waste quantities, and engineered features). The results of the simulations quantify the magnitude and probability of potential releases of radioactive materials from the disposal system to the accessible environment over the 10,000-year regulatory period. The FEPs analysis also provided assurance that the initial FEPs screening performed prior to CRA-2019 PA calculations remained valid following the completion of CRA-2019 PA calculations.

The following section details how the CRA-2019 PA was implemented with particular attention given to how the CRA-2019 PA implementation differed from that of the CRA-2014 PA.

¹ CRA-2014 PA calculations were performed on the WIPP PA computing cluster running a VMS operating system. WIPP PA codes have since been migrated to a cluster running a Solaris operating system (Kirchner 2012, Kirchner et al. 2014, Kirchner et al. 2015). As part of the migration effort, CRA-2014 PA calculations were rerun on the Solaris system with results saved in the official results database (PA_Results) as Revision 0 (Kirchner et al. 2014). After correcting an error that existed in the version of the DRSPALL code used in the original CRA-2014 PA calculations, CRA-2014 PA calculations were again rerun on Solaris and the results were saved as Revision 1 (spallings releases had increased, but total releases were not substantially changed) (Kirchner et al. 2015). Also, as part of the migration effort, an updated version of the CCDFGF code (version 7.02) was migrated to the Solaris system and the CRA-2014 PA (Rev. 1) results were used as input to updated CRA-2014 calculations, the results of which were saved as Revision 2 (no releases were substantially different from the Rev. 1 results) (Kirchner et al. 2015). The baseline for comparison of CRA-2019 PA results will be the CRA-2014 PA results as calculated on the new WIPP PA Solaris system with the correction to the DRSPALL results and updated version of CCDFGF (i.e., CRA-2014, Rev. 2).

This page intentionally left blank.

3.0 ANALYSIS METHODOLOGY

The aim of the CRA-2019 PA is to quantify regulatory compliance impacts associated with changes made since the CRA-2014 PA. Impacts have been determined by a direct comparison of CRA-2019 PA and CRA-2014 PA results. As seen in Section 1.1, changes incorporated into the CRA-2019 PA include planned changes as well as parameter and implementation changes. The approach taken in the CRA-2019 PA was to assess the combined impact when all of these changes are included in the PA. As discussed in Section 1.1.1.4, a supplemental calculation has investigated the hypothesis that representing open areas of the repository (i.e., “open” panel closure, experimental, and operations areas) as having been closed from early times will lead to lower estimated releases from the repository. The primary CRA-2019 PA calculation (CRA19 analysis) and supplemental calculation (CRA19_CL analysis) are now discussed.

3.1 CRA19 Analysis

The first and primary analysis considered in the CRA-2019 PA is used to compare the changes made relative to the CRA-2014 PA. The name given to this analysis was CRA19. All of the changes described in Section 1.1, apart from those discussed in Section 1.1.1.4 relative to the supplemental calculation, were included in the CRA19 calculation. Three replicates were executed for the CRA19 analysis, with results compared to those obtained in the CRA-2014 PA (see Footnote 1 on page 39). The CRA19 analysis is the defining analysis associated with the CRA-2019 PA and the analysis to be used to ascertain regulatory compliance.

3.1.1 Inventory Analysis

A radionuclide screening analysis was included as part of the CRA-2019 PA to screen radionuclides to be included in PA calculations. The radionuclide inventory provided in the Performance Assessment Inventory Report (PAIR) – 2018 (Van Soest 2018), which contains updated estimates to the radionuclide content and waste material parameters using inventory information collected up to December 31, 2017, was the basis for the radionuclide screening analysis.

The PAIR-2018 contains inventory data for 195 radioisotopes. Many of these radioisotopes have low concentrations or are short lived and would not impact releases calculated by PA simulations. Additionally, PA calculations involve a suite of computationally intensive codes, and tracking all 195 radioisotopes is not practical. Therefore, the number of isotopes modeled in the PA codes was screened to reduce the number of isotopes while still capturing the dominant releases.

For the first time, the radionuclide screening analysis was also used to determine which radionuclides would participate in radiolysis based on the relative amount of decay heats compared to the overall inventory heat production. This was done due to the inclusion of brine radiolysis as a part of the gas generation model implemented in the BRAGFLO code.

3.1.2 PA Calculations

The CRA19 analysis was performed as planned in AP-181 (Zeitler 2019a). Documentation of computational code execution and file management is described in detail in Long (2019).

3.1.3 FEPs Analysis

A FEPs screening analysis began prior to performing PA calculations, but concluded subsequent to PA calculations. This approach was different than in prior CRA calculations due to the recognition that the screening of the criticality FEP would require an analysis based on current PA calculations. Thus, the CRA19 calculation results must be available prior to concluding the FEPs analysis.

3.2 CRA19_CL Analysis

With the results of the CRA19 analysis in hand, the material property changes described in Section 1.1.1.4 were added to the set of baseline changes implemented in the CRA19 analysis so that the impact of the early, “tight” closure of the OPS, EXP, and panel closure areas could be determined. The addition of these changes, and their potential impact on regulatory compliance, was captured in the CRA19_CL (for CRA-2019 CLOsure) analysis. Thus, the CRA19_CL analysis incorporated all changes included in case CRA19 as well as refinements to material properties in the OPS, EXP, and open panel closure areas.

Three replicates were executed for the CRA19_CL analysis and impacts of the changes described in Section 1.1.1.4 were assessed via a direct comparison of CRA19_CL results to CRA19 results. Documentation of computational code execution and file management is described in Long (2019). Results of the CRA19_CL analysis are described in Appendix A.

4.0 RUN CONTROL

A full description of the run control for the CRA19 analysis and CRA19_CL sensitivity study, including names and locations of input and output files, can be found in Long (2019). As outlined in AP-181 (Zeitler 2019a), in cases where comparisons were made to the CRA-2014 PA results, the CRA14 (Rev. 2) results from the Solaris migration integration tests were used (Kirchner et al. 2014, Kirchner et al. 2015). A summary of the computational code execution and file management for the CRA-2019 PA is provided below.

Two analyses were run in fulfillment of AP-181: CRA19 (the principal analysis and the one used to support compliance calculations) and CRA19_CL (a supplemental analysis focused on the impact of the timing of closure of open areas on PA results). The codes used for each analysis were identical and were retrieved from their respective CVS (Code Versioning System) repositories on the Solaris system.

Input files were prepared by individual analysts and the run control coordinator prepared run scripts. The CRA-2019 was performed using qualified code versions on the WIPP PA Solaris cluster (Table 20). The WIPP PA Solaris cluster consists of one head node (SAN) that distributes jobs to 20 other nodes. As described in AP-181, the DRSPALL, PRESECOTP2D, and SECOTP2D codes were not run for the CRA-2019 PA, but the results of previous runs were used. Two new codes were run for the CRA-2019 PA: SCREEN_NUTS and CCDFVECTORSTATS. The STEPWISE code was run for the CRA19 analysis, but not the CRA19_CL analysis.

Calculations performed on the WIPP PA Solaris Cluster used the WIPP PA Parameter Database (PAPDB) ParamDB as the source for parameter values. The results of the LHS sampling and CCDFGF release calculations were written to the WIPP PA Results Database PA_Results. Input and output files for the CRA19 analysis are found in /nfs/data/CVSLIB/WIPP_ANALYSES/CRA19 and input and output files for the CRA19_CL analysis are found in /nfs/data/CVSLIB/WIPP_ANALYSES/CRA19_CL.

Table 20 – WIPP PA Codes Used for CRA19

Code	Version	Executable ¹	Build Date
ALGEBRACDB	2.36	algebracdb	9/11/12
BRAGFLO	7.00	bragflo	8/14/18
CCDFGF	7.03	ccdfgf	5/3/17
CCDFVECTORSTATS	1.01	ccdfvectorstats	3/20/18
CUTTINGS_S	6.03	cuttings_s	1/15/13
EPAUNI	1.19	epauni	9/12/16
GENMESH	6.10	genmesh	1/12/15
ICSET	2.23	icset	9/11/12
LHS	2.44	lhs	6/2/15
MATSET	9.24	matset	10/11/16
NUTS	2.07	nuts	2/22/19
PANEL	5.00	panel	2/18/19
POSTBRAG	4.02	postbrag	1/10/13
POSTLHS	4.11	postlhs	6/2/16
PREBRAG	9.00	prebrag	8/16/18
PRECCDFGF	2.01	preccdfgf	9/9/13
PRELHS	2.44	prelhs	10/11/16
RELATE	1.45	relate	9/11/12
SCREEN_NUTS	1.02	screen_nuts	2/7/18
STEPWISE	2.22	stepwise	7/2/13
SUMMARIZE	3.02	summarize	10/31/12

¹ Executables are located in \$CVSLIB/WIPP_CODES/PA_CODES/CODE/Build/Solaris

5.0 RESULTS

Results from the various analysis reports outlined in Zeitler (2019a) are summarized below.

5.1 Inventory Screening Analysis

A radionuclide screening analysis was performed prior to PA calculations to document the basis for screening radionuclides to be included in PA calculations (Kicker 2019a). Based on the inventory information provided in the PAIR – 2018 (which provides radionuclide activities on a waste stream basis, with the total waste volume assumed to be equal to the legislated capacity of the repository) (Van Soest 2018), the analysis assessed the sufficiency of using the same radionuclides as in the CRA-2014 PA for calculations done using the PANEL, NUTS, and CCDFGF codes. It was concluded that it was appropriate to use the same lists of radionuclides as were used in the CRA-2014 PA for these three codes.

For the PANEL code, the following 30 radionuclides, which account for 99.96% of the total inventory in EPA Units at the time of repository closure¹, were used in decay calculations for determining brine concentrations ultimately used in calculating direct brine releases: ²⁴¹Am, ²⁴³Am, ²⁵²Cf, ²⁴³Cm, ²⁴⁴Cm, ²⁴⁵Cm, ²⁴⁸Cm, ¹³⁷Cs, ²³⁷Np, ²³¹Pa, ²¹⁰Pb, ¹⁴⁷Pm, ²³⁸Pu, ²³⁹Pu, ²⁴⁰Pu, ²⁴¹Pu, ²⁴²Pu, ²⁴⁴Pu, ²²⁶Ra, ²²⁸Ra, ¹⁴⁷Sm, ⁹⁰Sr, ²²⁹Th, ²³⁰Th, ²³²Th, ²³³U, ²³⁴U, ²³⁵U, ²³⁶U and ²³⁸U. Of these 30 radionuclides, 26 (²¹⁰Pb, ²²⁶Ra, ²²⁸Ra, and ¹⁴⁷Sm being excluded) were used in actinide mobilization calculations.

For the NUTS code, the following 10 radionuclides, which account for 98.61% of the total inventory in EPA Units at the time of repository closure¹, were used in calculating releases to the Culebra: ²⁴¹Am, ²³⁸Pu, ²³⁹Pu, ²⁴⁰Pu, ²⁴¹Pu, ²⁴²Pu, ²²⁹Th, ²³⁰Th, ²³³U and ²³⁴U.

For the CCDFGF code, the following 10 radionuclides, which account for 99.94% of the EPA Units at the time of repository closure, were used in calculating cuttings, cavings, and spillings releases: ²⁴¹Am, ²⁴⁴Cm, ¹³⁷Cs, ²³⁸Pu, ²³⁹Pu, ²⁴⁰Pu, ²⁴¹Pu, ⁹⁰Sr, ²³³U, and ²³⁴U. In total, 45 of the 195 radionuclides from the PAIR – 2018 inventory were included in CRA-2019 PA calculations.

The analysis also provided a list of PA inventory-related parameters that were used in CRA-2019 PA calculations and it produced inventory input files for use in the EPAUNI code. For example, the “waste unit factor” (WUF) was calculated to be 3.30, based on the total activity of the 17 alpha-emitting transuranic radionuclides with half-lives greater than 20 years in the inventory at repository closure (assumed to take place in 2033). The WUF is an impactful parameter, as it is used to normalize radionuclide activities in Curies into potential releases in “EPA Units.” Due in part to this normalization factor, the total number of EPA units of TRU waste assumed to be in the repository at closure has stayed approximately the same (decreased from 10,197 (Kicker 2019b) to 10,140 EPA Units) from the CRA-2014 PA inventory, despite an increase in initial activity of 69% (3.63E+06 to 6.14E+06 Ci) (Kicker 2019a).

¹ The EPA-unit composition of contaminated brine may be different from that of the overall total inventory (Sarathi 2019d).

Additionally, it was determined that the inventories of five radionuclides (^{241}Am , ^{238}Pu , ^{239}Pu , ^{240}Pu , and ^{242}Pu) should be included in brine radiolysis calculations due to their contributions to decay heat. Those five radionuclides account for more than 96% of the decay heat at closure and over 99% at 100 years post-closure and beyond.

5.2 Sampling of Uncertain Parameters

The LHS code was used to generate 100 vectors of sampled parameter values for each of three replicates for the CRA19 analysis of the CRA-2019 PA (Zeitler 2019d). A unique random number seed was assigned to each of the three replicates. These seed values were identical to those used in the CRA14 analysis. Sixty-four parameters were sampled for the CRA19 analysis, including two new parameters (also, one parameter from the CRA14 analysis was not sampled). Updated distributions were sampled for six additional parameters. All 300 sets of sampled parameters were written to the WIPP PA Results Database (PA_Results) for use by other WIPP PA codes. Details of the values of uncertain and certain parameters used for CRA19 calculations are found in Kim and Feng (2019).

Correlations were assigned to two pairs of variables (S_HALITE:PRMX_LOG and S_HALITE:COMP_RCK, as well as CASTILER:PRMX_LOG and CASTILER:COMP_RCK) and applied during the LHS sampling process. The LHS results were additionally influenced by an enforcement of a conditional relationship between three pairs of parameters: WAS_AREA:GRATMICH and WAS_AREA:GRATMICI, PCS_T3: POROSITY and PCS_T2: POROSITY, and PCS_T2: POROSITY and PCS_T1:POROSITY.

The resulting sampled data had the expected correlation structure and the values fell within the expected ranges (Zeitler 2019d). The distributions of sampled values matched the expected cumulative distribution functions (CDFs).

5.3 Radionuclide Concentrations for Solid Releases

Activity concentrations are calculated on a waste stream basis over time by the EPAUNI code for later use by the CCDFGF code as radionuclide concentrations for the solids released during a drilling intrusion via the mechanisms of cuttings, cavings, and spallings. For cuttings and cavings releases, waste streams are selected with a probability based on the waste type (contact-handled (CH) or remote-handled (RH)) and waste stream volume, with the associated release volume assigned the activity concentration of the selected waste stream at the time of intrusion. For spallings releases, the average CH waste activity concentration at the time of intrusion is assigned to the release volume. The change included in the CRA-2019 PA that was observed to most substantially affect radionuclide concentrations for solid releases as compared to the CRA-2014 PA was:

- Updates to WIPP waste inventory parameters (including waste stream activities and volumes).

Overall, the primary results of changes for the CRA-2019 PA in comparison to the CRA-2014 PA baseline are some increases and decreases in waste concentration on a waste stream basis, but

a similar total repository waste activity. Additional details of the EPAUNI calculations and results described by Kicker (2019b) are given in subsections below.

5.3.1 Overall Activity

The overall activity over time in Ci is consistently higher for the CRA-2019 PA due to the increased inventory of the long-lived ^{239}Pu radionuclide ($5.74\text{E}+05$ vs. $8.74\text{E}+05$ initial Ci for the CRA-2014 PA and CRA-2019 PA, respectively). However, the activity in EPA units at closure is similar due to the normalization methodology described in Section 5.1 and remains similar with time (Figure 1 (Figure 5a from Kicker 2019b)). Activity in EPA units over time is plotted in Figure 2 (Figure 7a from Kicker 2019b) for the dominant radionuclides used in the CRA14 and CRA19 analyses. For the most dominant radionuclides, there are not substantial differences between the two analyses. Thus, on average, the increased ^{239}Pu inventory does not impact solids releases much for CRA19 calculations.

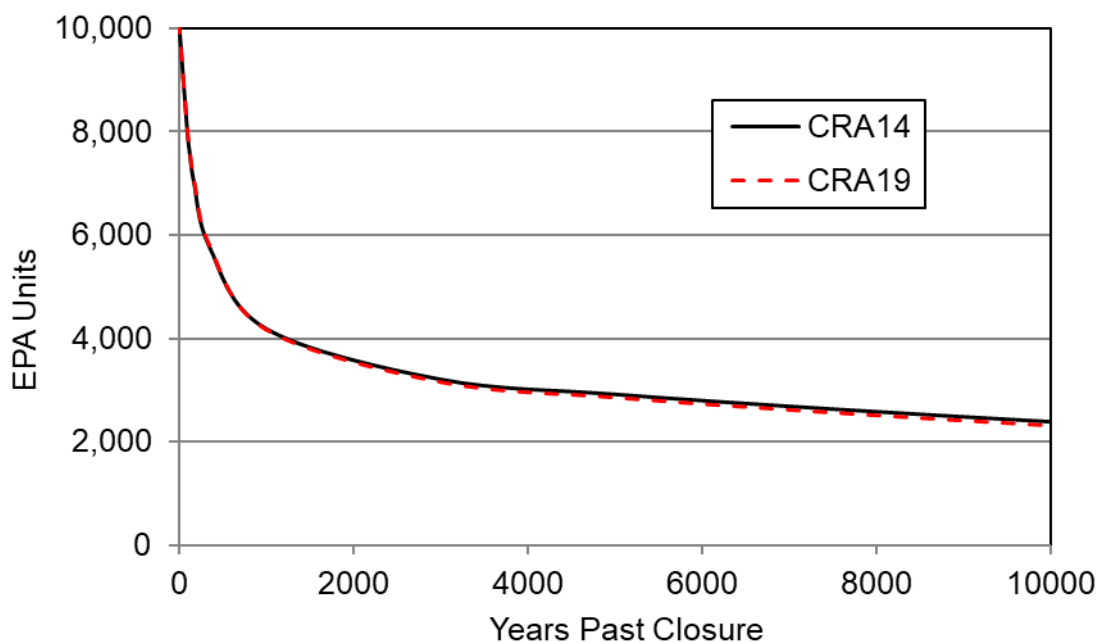


Figure 1 – Total (CH and RH) Repository Waste Activity

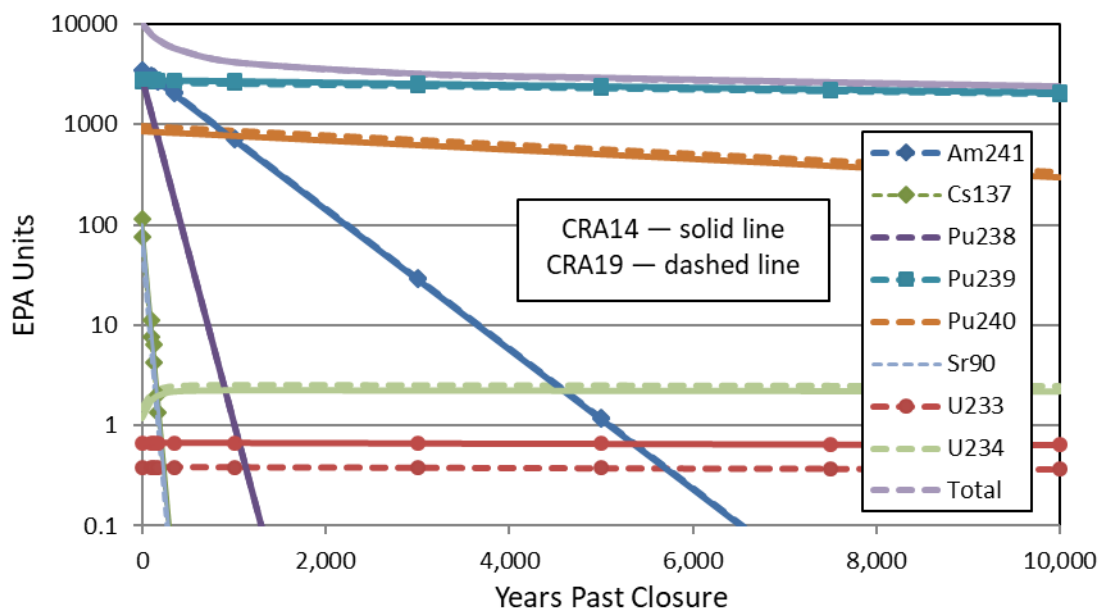


Figure 2 – Dominant Waste Isotopes from Closure to 10,000 Years Post-Closure

5.3.2 Activity on a Waste Stream Basis

For the CRA-2019 PA, 607 CH and RH waste streams were included in the inventory, compared to 528 in the CRA-2014 PA. Radionuclide concentrations for CH and RH waste streams are plotted in Figure 3 (Kicker 2019b) based on probability of intersection in a drilling intrusion (Figure 2b and Figure 4 from Kicker 2019b, redrawn on the same scale). For the CRA-2019 PA, increased activity concentration (in terms of probability of intersection) is observed for about 31% of the total waste volume at closure and varies with time (due to the decay of different radionuclides in each waste streams) down to about 20% at 10,000 years post-closure. These concentration changes are applicable to cuttings and cavings releases, since they are presented on a waste stream basis.

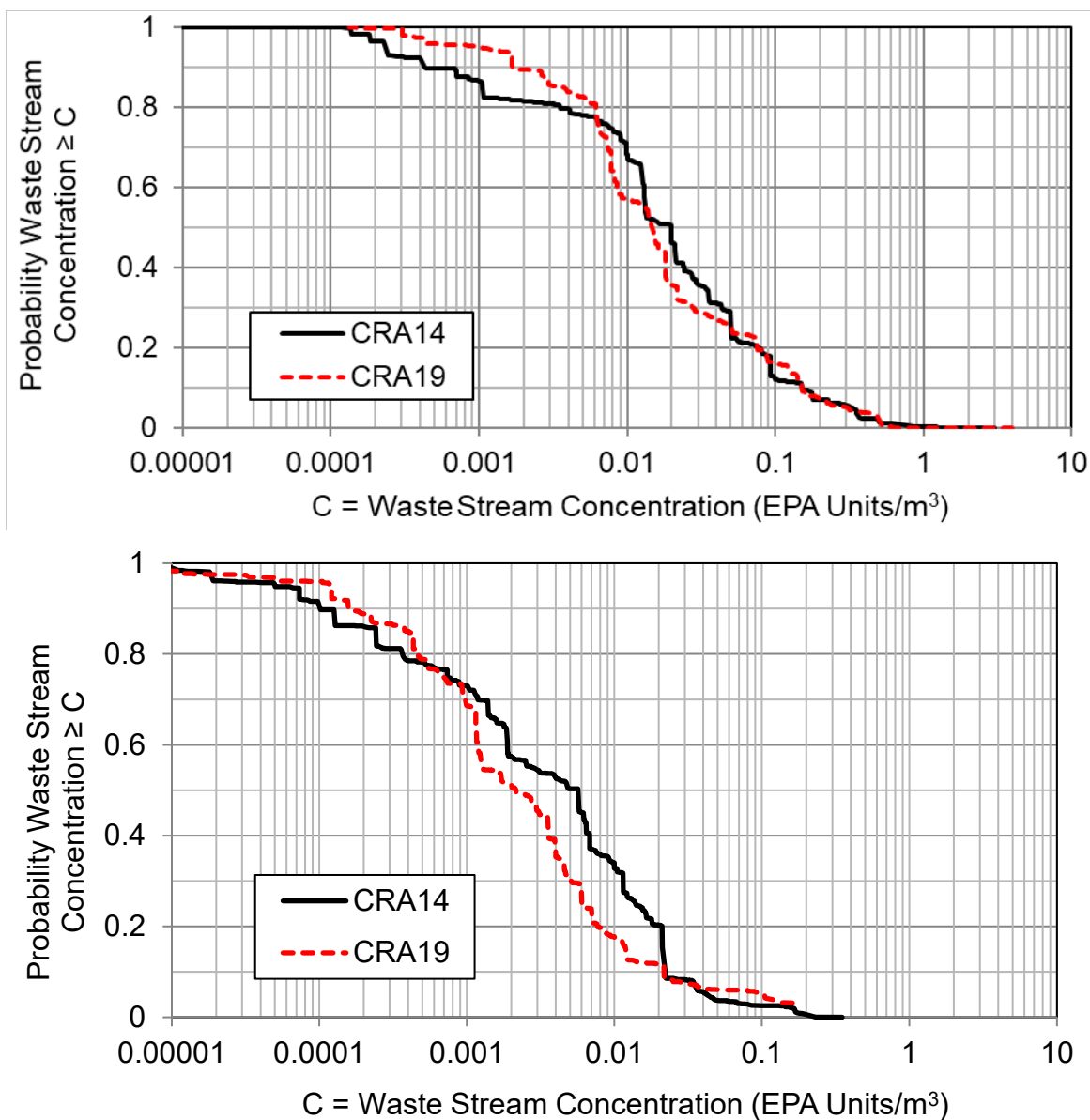


Figure 3 – Waste Stream Concentration Complementary Cumulative Distribution at Closure (Top) and 10,000 Years Post-Closure (Bottom)

One of the new waste streams, SR-KAC-PuOx, comprises about 29% of the total number of EPA units at the time of repository closure, the largest of all waste streams in these terms by over 20%. At 10,000 years post-closure, this waste stream accounts for about 42% of the total number of EPA units. This waste stream comprises about 3.5% of the waste stream volume (the 7th highest waste stream volume). Due to the relatively large volume, it does not have one of the highest waste stream concentrations at closure, but due to the large amount of the long-lived radionuclide ²³⁹Pu in that waste stream, it has the highest waste stream concentration at 10,000 years post-closure.

5.3.3 Average CH Waste Activity Concentration

The average CH waste activity concentration is calculated as part of CCDFGF calculations and is based on activities from CH waste streams. It varies with time due to radionuclide decay. It is used in PA calculations as the activity concentration applied to spallings releases. The average CH waste activity concentration for the CRA19 analysis is similar to that for the CRA14 analysis (Figure 4 (Figure 8 from Kicker 2019c)).

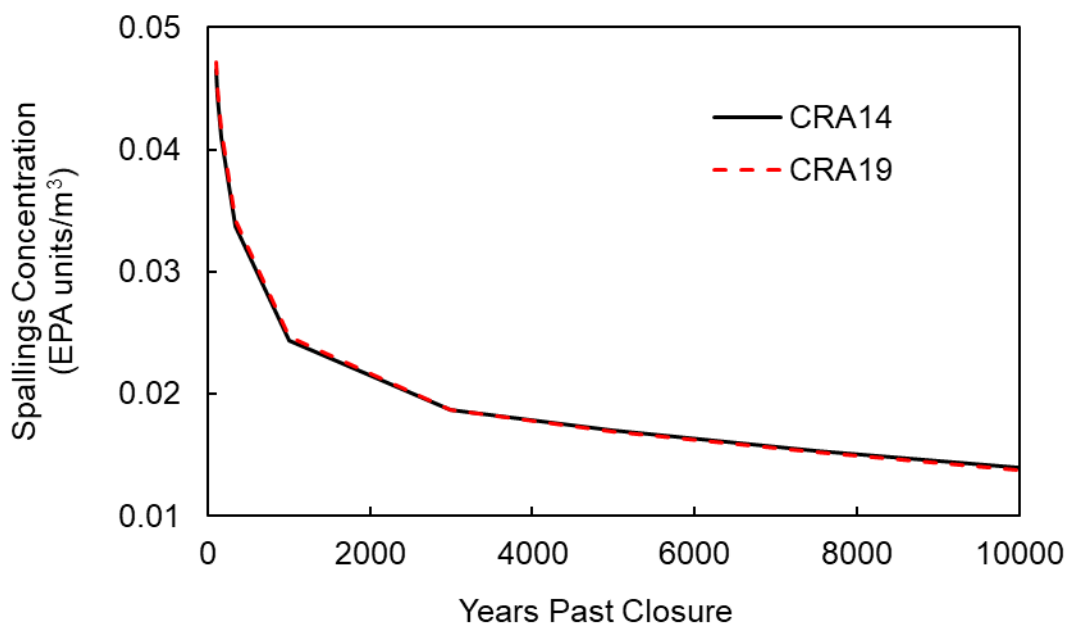


Figure 4 – Spallings Concentration from Closure to 10,000 Years Post-Closure

5.4 Mobilized Radionuclide Concentrations

The actinide mobilization sub-model underlies both the Direct Brine Release and long-term/Culebra release models as it determines the mobile concentration limits of radionuclides in contaminated brine. The actinide mobilization sub-model also computes the instantaneous mobile concentrations of radionuclides in contaminated brine contained in the waste panels as a function of time. This information is combined with the DBR (brine) volumes to calculate DBR (radionuclide) releases.

The conceptualization and general implementation of the actinide mobilization and Salado transport sub-models remain essentially unchanged from the CRA-2014. However, some minor changes have been implemented: 1) the microbial colloid enhancement equation has been updated to correct for the changed basis of the CAPMIC parameter (Sarathi 2019a); 2) isotopes of Cf, Pm, and Pa are now included in mobilization calculations; and 3) the number of panels over which mass balance calculations are performed has changed from one to five in order to account for the potential for up to five interconnected waste panels due to the lack of panel

closures in Panels 3, 4, 5, and 6. Additional details on these changes can be found in Sarathi (2019a), Sarathi (2019b), and Sarathi (2019c).

Changes included in the CRA-2019 PA that were observed to most substantially affect mobilized radionuclide concentrations as compared to the CRA-2014 PA are:

- Updates to WIPP waste inventory parameters.
- Updates to radionuclide solubilities and their associated uncertainty.
- Refinement to colloid enhancement parameters associated with actinide mobilization.

Parameter updates are discussed in Sections 1.1.7 and 1.1.13. Most significantly, the An(III) baseline solubility values decreased substantially, the An(III) solubility uncertainty distribution values increased, and the An(IV) solubility uncertainty distribution values decreased. As a result, the Am(III), Pu(III), and especially Pu(IV) median and mean concentrations decreased, and total mobile radioactivity concentrations decreased overall. The reduction in Pu mobile concentrations reduces late-time concentrations in particular since little ²⁴¹Am remains in the inventory at late times. Additional details of the PANEL simulations and results of mobilization calculations described by Sarathi (2019d) are given in subsections below.

5.4.1 Total Mobile Concentration Limits

The PANEL code computes the total mobile concentration limit (i.e., total mobilization potential or source term) for each radionuclide of interest. The total mobile concentration limit is a constant, effective aqueous solubility limit that encompasses the dissolved (speciated and complexed with organic ligands) plus dispersed (i.e., associated with dispersed colloids) concentration limits. The total mobile concentration limits are constant throughout the course of a simulation for a given model realization, but vary among model realizations due to the solubility uncertainty factor, brine redox condition, and brine type. These total mobile concentration limit values are used by both the PANEL and NUTS codes to calculate instantaneous aqueous radionuclide concentrations as a function of time (and, for NUTS, space).

Figure 5 (Figure 14 from Sarathi 2019d²) illustrates the common logarithm (i.e., log₁₀) of the total mobilization potential (i.e., the total mobile concentration limit) for each of the five primary actinides.³ Figure 6 (Figure 15 from Sarathi 2019d) illustrates the same, but with the distribution

² This section contains boxplots to facilitate visualizing and comparing distributions of results. The convention used in this section is that the “box” bottom and top edges indicate the 25th and 75th percentiles, the box interior line indicates the 50th percentile (median), and the triangle marker indicates the mean. The “whiskers” (the extended vertical lines with horizontal bars) indicate the 2nd and 98th percentiles, and the diamond markers exterior to the bars are discrete outliers (i.e., less than the 2nd percentile or greater than the 98th percentile). Upon occasion, a particular dependent variable is constant (its independent parameters may not be sampled), and the box is collapsed to a single horizontal bar. At the other extreme, some dependent variables may have distributions where the mean is dominated by a few outliers. In those plots, only the top whisker and the outliers are visible – the box would be located below the range of the figure.

³ The common logarithm (log₁₀) values are plotted because SOLMOD3:SOLVAR and SOLMOD4:SOLVAR uncertainty distributions are defined as the logarithm of the solubility uncertainty multiplier, thus it is more appropriate to display the mean/medians of the logarithmic values rather than the logarithm of the mean/median mobilization potentials.

of results split according to the redox condition of the brine. If the brine exhibits reducing conditions, Pu(III), U(IV), and Np(IV) are assumed to exist. If the brine exhibits oxidizing conditions, Pu(IV), U(VI), and Np(V) are assumed to exist. Am(III) and Th(IV) are assumed to exist under both brine redox conditions.

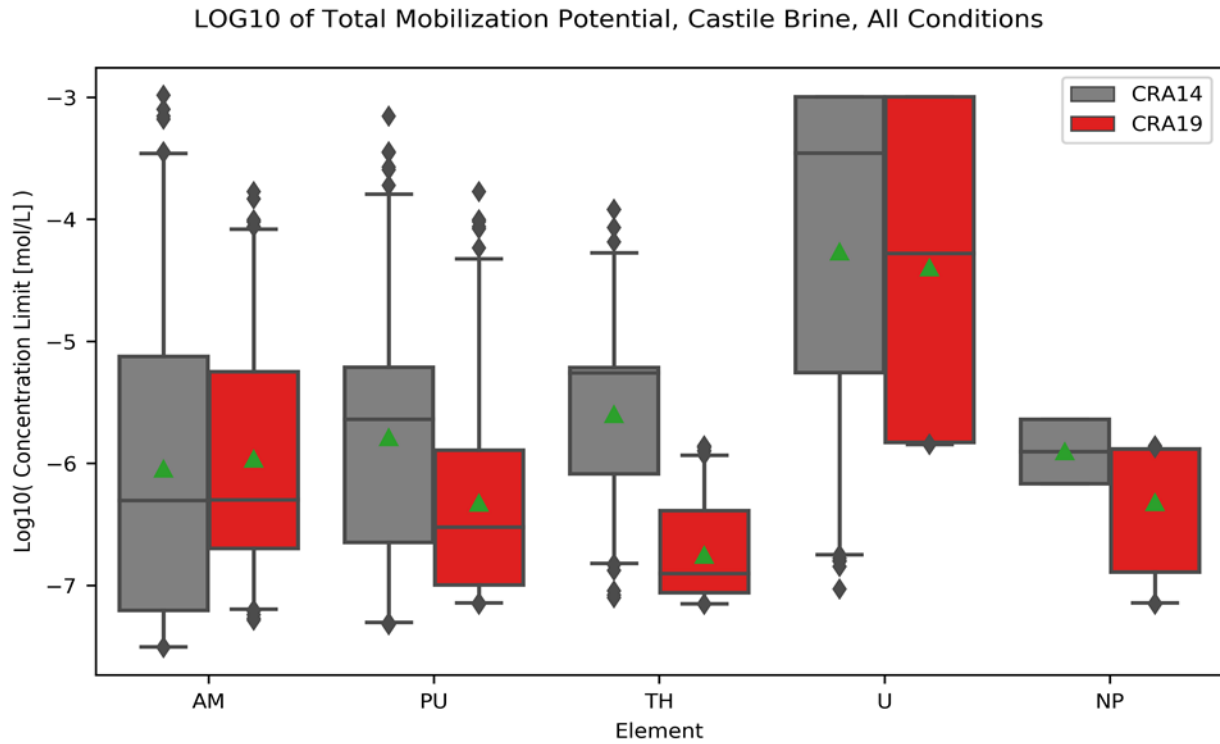


Figure 5 – Log10 of Total Mobilization Potential for Base Elements, Castile Brine, All Conditions

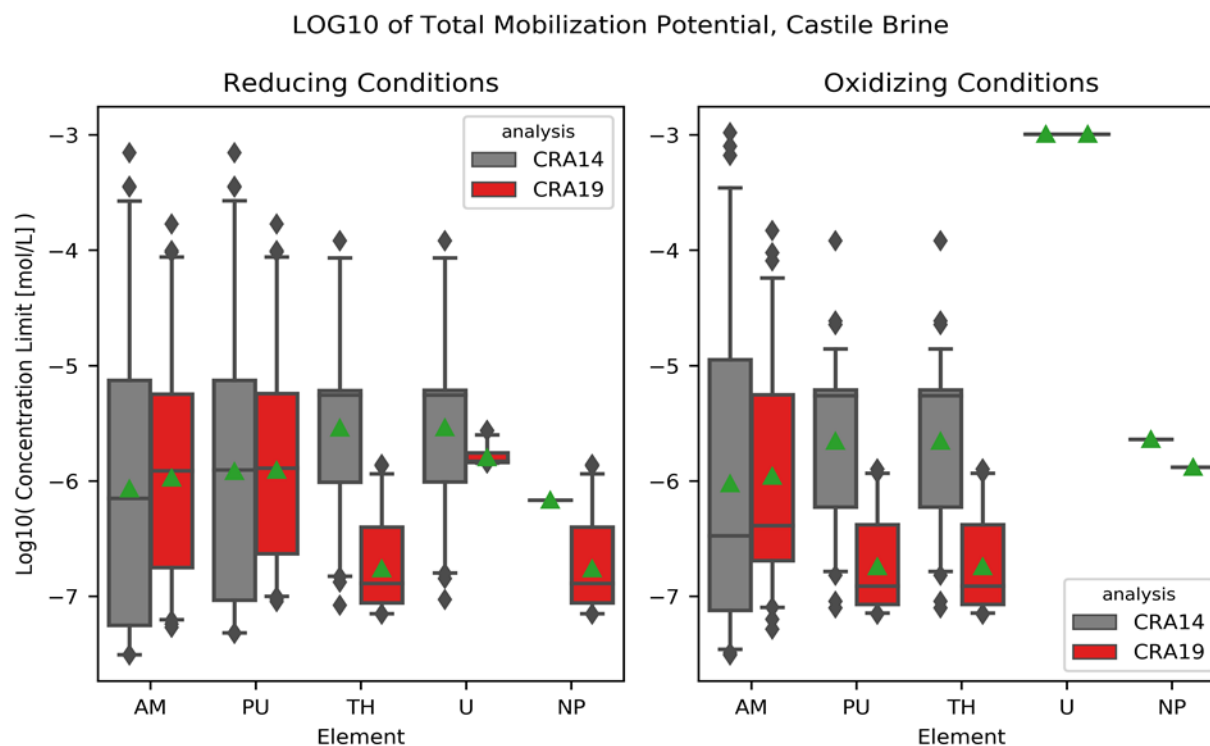


Figure 6 – Log10 of Total Mobilization Potential for Base Elements, Castile Brine, by Brine Redox Condition

For Am(III) and Pu(III), the larger percentile concentration limit values have decreased from the CRA14 analysis (evidenced by the decrease in the box-top, whiskers, and outliers), but the median values remain similar. The increase in the median of the input solubility uncertainty distribution (SOLMOD3:SOLVAR) largely offsets the decrease in the baseline solubility. For Pu(IV) and Th(IV), the decrease in the entire solubility uncertainty distribution (SOLMOD4:SOLVAR) causes the concentration limits to decrease markedly, and the median and top percentiles decrease by almost two orders of magnitude. For U(IV), the mobile concentration limit is dominated by the fixed intrinsic colloid concentration limit (U:CONCINT), which has increased for CRA19 to a value much larger than the baseline solubility (SOLMOD4:SOLCOH). The range of its distribution has shrunk because most of the dissolved concentration limit values are smaller than the intrinsic colloid concentration limit. The Np(IV) values are now sampled for CRA19 (the Np(V) values remain fixed). Np(V) values are similar, but slightly decreased due to the decrease in the CAPMIC parameter. Finally, U(VI) remains similar for CRA19, as all of the colloid terms remain small compared to its baseline solubility value.

Sarathi (2019d) also discusses the relative contributions to the total concentration limit by the dissolved and various colloid (humic, microbial, intrinsic, and mineral) components. The change in the microbial colloid implementation (Sarathi 2019a) is captured—the microbial contribution now increases linearly to the parameter CAPMIC and then plateaus (previously it ramped to a value derived from CAPMIC and then decreased to zero). For all elements, the microbial colloid term contributes little to the total concentration limit for CRA19. For Am(III), the dissolved

concentration limit comprises the majority of the total concentration limit. The same is true for Pu(III). For Pu(IV) and Th(IV), the intrinsic and mineral colloid terms contribute a large portion over the range of dissolved solubilities. The humic colloid term contributes little due to the decrease in the linear proportionality constant (PHUMOX4:PHUMSIM) for CRA19. For U(IV), the intrinsic colloid term comprises most of the total concentration limit across the entire dissolved concentration limit range because of its increase and because the An(IV) uncertainty distribution has decreased.

5.4.2 Instantaneous Mobile Concentrations

The PANEL code calculates the instantaneous aqueous radionuclide concentrations as a function of time in the waste panels. For the concentration calculations used in the calculation of DBR releases (Section 5.9.3), the PANEL code assumes that the brine volume in the waste panels is constant over time and is run for a set of brine volumes. These brine volumes, which are defined as multiples of the minimum volume of brine required for a DBR to occur (Clayton 2008), also correspond to the organic ligand concentration dilution factors (Sisk-Scott 2019) that were used in the calculation of the baseline solubility parameters.

The total mobile concentration limits presented in Section 5.4.1 are used to calculate instantaneous radionuclide concentrations in the waste panels as a function of time. These calculations consider the effects of decay/ingrowth and mass balance. The mean (across all vectors and replicates) mobile concentrations for the lumped radionuclides in 1x the minimum DBR volume is shown in Figure 7 (Figure 28 from Sarathi 2019d). The mean total radioactivity concentration at early times is dominated by AM241L and at later times by PU239L (see Sarathi 2019d for details of radionuclide lumping). The mean total radioactivity concentration has decreased for CRA19, following the trends for the overall reduction in the An(III) and An(IV) concentration limits discussed in Section 5.4.1. The increase in the late-time plateau for AM241L is due to an increase in the initial inventory of ^{245}Cm (from 1.225 to 24.47 Ci (0.00594 to 0.074 EPA Units) in CRA19), which decays with a half-life of 8,500 years to ^{241}Pu and then to ^{241}Am , and thus acts as a relatively slow source for ^{241}Am .

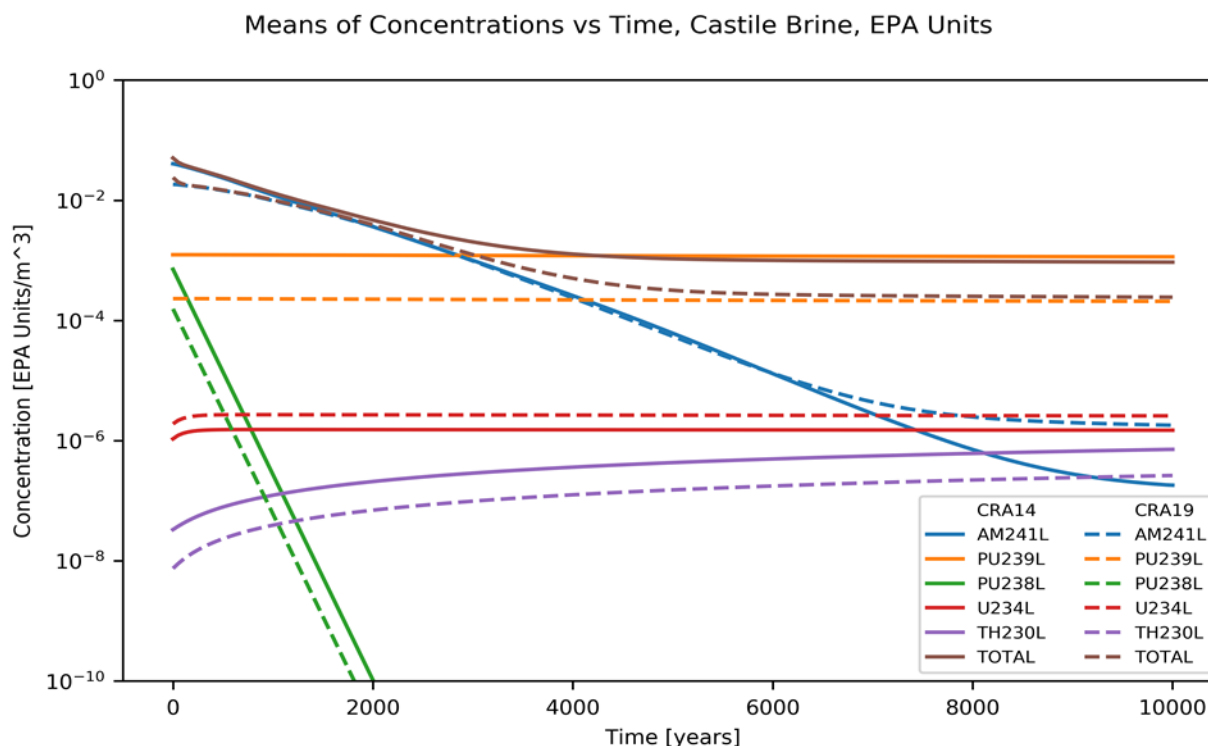


Figure 7 – Mean Mobilized Concentrations vs Time, Castile Brine

5.5 Salado Flow Results

The BRAGFLO numerical code calculates the flow of brine and gas in the vicinity of the WIPP repository over a 10,000-year regulatory compliance period. The results of these calculations are used by other codes to calculate potential radionuclide releases to the accessible environment. Changes included in the CRA-2019 PA that were observed to most substantially affect Salado flow results as compared to the CRA-2014 PA are:

- The lack of ROMPCS emplacement between Panels 3, 4, 5, 6, and 9, modeled as the southernmost panel closure area, which allows greater communication between the waste panel and the south rest-of-repository.
- Increase in the inundated steel corrosion rates and the addition of brine radiolysis which results in an increase in hydrogen gas generation.
- Addition of 5th shaft and associated access drift volume in the experimental area which increases the cross-sectional area of the shaft and increases void space in the experimental area.
- Updates to WIPP waste inventory parameters, including increased iron and cellulose mass, which contributes to increased associated corrosion and biodegradation gas generation.

Overall, the primary impacts of changes for the CRA-2019 PA in comparison to the CRA-2014 PA baseline are substantially increased waste area brine pressures and saturations for intrusion scenarios that intersect a hypothetical brine reservoir that underlies the repository. These scenarios are greatly influenced by increased total gas generation due to the availability of brine within the waste panel and south rest-of-repository that flows from the Castile brine reservoir, up the intrusion borehole, to the waste panel, and across the abandoned panel closure area to the south rest-of-repository. Undisturbed and non-Castile intruded scenarios are generally less impacted by changes, but the CRA-2019 PA results under these scenarios generally experience increased brine pressures and reduced brine saturations within the waste areas due to the increased gas generation and brine consumption induced by the associated process model and parameter modifications in comparison to the CRA-2014 PA. Additional details of the BRAGFLO simulations and results described by Day (2019b) are given in subsections below.

5.5.1 Repository Representation in BRAGFLO

The computational grid and associated material map used by BRAGFLO was altered for the CRA-2019 PA in order to implement the use of new and equivalent material names to represent the DRZ above and below emplaced panel closures and the operations and experimental area, correct for the length of the northernmost panel closure, add the additional mined volume in the repository experimental region associated with new access drifts for the 5th shaft, increase the cross-sectional area of the modeled composite shaft to accommodate the 5th shaft geometry, and accommodate modifications to the southernmost panel closure area and associated DRZ to represent the abandonment of plans to emplace ROMPCS between Panel 3, 4, 5, 6, and 9. Otherwise, the computational grid used in the CRA-2019 PA is the same as that used in the CRA-2014 PA.

The generic BRAGFLO computational grids with modeled area descriptions and cell dimensions for the CRA-2014 and CRA-2019 PA are shown in Figure 8 and Figure 9 (Figures 1 and 2 from Day 2019b), where the cell dimension changes indicated in red are associated with the northernmost panel closure extension, increased composite shaft cross-sectional area, and depth increase to accommodate the 5th shaft access drift volume in the experimental area. Also shown are the material area changes in the DRZ areas above and below and within the southernmost panel closure area which has been abandoned for the CRA-2019 PA. Detailed material maps associated with the six modeling scenarios are further defined in Section 3.2 of Day (2019b).

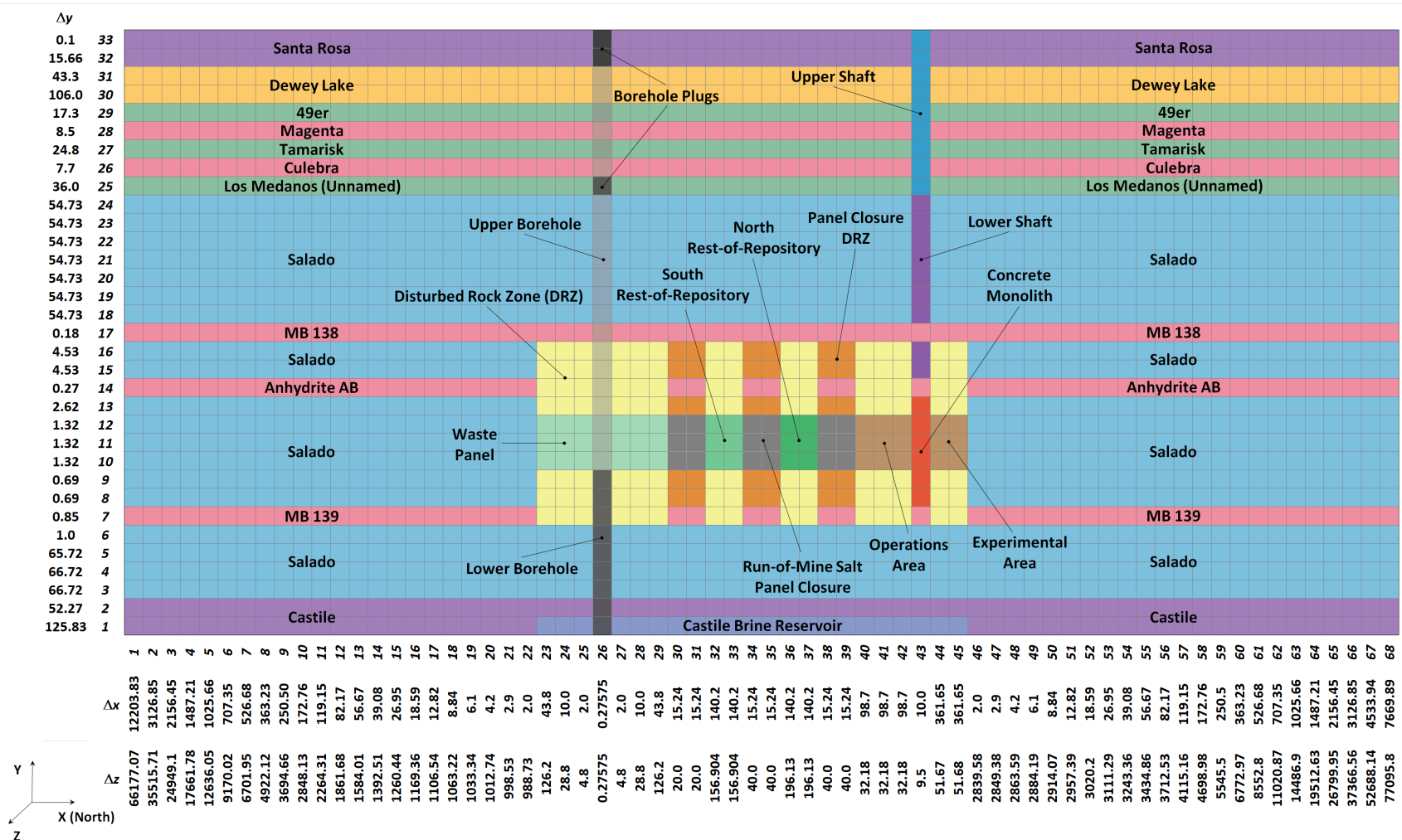


Figure 8 – Generic CRA-2014 PA BRAGFLO Grid with Modeled Area Descriptions (Δx, Δy, and Δz Dimensions in Meters)

Summary Report for the 2019 Compliance Recertification Application Performance Assessment (CRA-2019 PA)
 Rev. 0, ERMS 571376

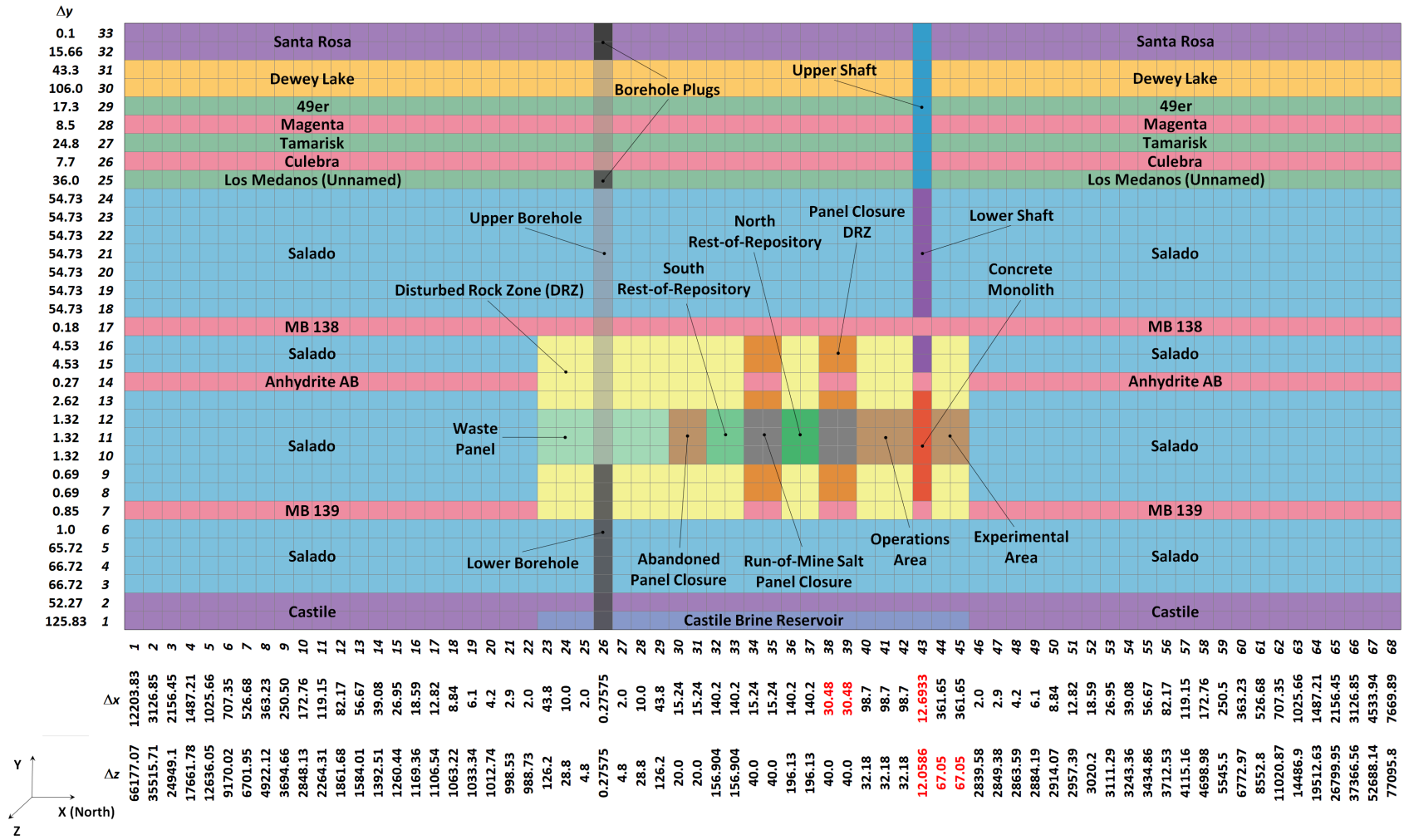


Figure 9 – Generic CRA-2019 PA BRAGFLO Grid with Modeled Area Descriptions (Δx, Δy, and Δz Dimensions in Meters)

5.5.2 Modeling Scenarios

The six BRAGFLO modeling scenarios used in the CRA-2019 PA are unchanged from those used for the CRA-2014 PA. Results obtained in the six scenarios are used to initialize flow and material properties in subsequent codes in the PA computational suite (e.g., in the calculation of direct brine release volumes). The scenarios include one undisturbed scenario (S1-BF), four scenarios that include a single inadvertent future drilling intrusion into the repository during the 10,000-year regulatory period (S2-BF to S5-BF), and one scenario investigating the effect of two intrusions into a single waste panel (S6-BF). Two types of intrusions, denoted as E1 and E2, are considered. An E1 intrusion assumes the borehole passes through a waste-filled panel and into a region of pressurized brine that may exist under the repository in the Castile formation. An E2 intrusion assumes that the borehole passes through the repository but does not encounter pressurized brine. BRAGFLO results obtained in Scenario S6-BF are used to calculate transport releases to the Culebra (Section 5.8). Table 21 summarizes the six scenarios used in WIPP PA Salado flow analyses. A total of 1,800 separate (3 replicates × 6 scenarios × 100 vectors) Salado flow simulations were run. Day (2019b) described results from scenarios S1-BF, S2-BF, S4-BF, and S6-BF only, as results from scenarios S2-BF and S3-BF are generally similar to each other, as well as results from S4-BF and S5-BF. In this summary report, results are illustrated using results plots from a subset of those described in Day (2019b).

Table 21 – BRAGFLO Modeling Scenarios

Scenario	Description
S1-BF	Undisturbed Repository
S2-BF	E1 intrusion at 350 years
S3-BF	E1 intrusion at 1,000 years
S4-BF	E2 intrusion at 350 years
S5-BF	E2 intrusion at 1,000 years
S6-BF	E2 intrusion at 1,000 years; E1 intrusion at 2,000 years

5.5.3 Gas Generation

The gas generation model was augmented for the CRA19 analysis to include the influence of brine radiolysis, a process by which brine is consumed and gas is generated. In contrast to other gas generation processes modeled in the BRAGFLO code, brine radiolysis is dependent on the radionuclide inventory, including the amount of mobilized radionuclides in brine. Mobilized radionuclide concentrations for BRAGFLO calculations are calculated identically as for PANEL calculations (Section 5.4) using solubilities based on the minimum brine volume required for a direct brine release. The initial conditions for radionuclide quantities are applied by equally distributing the sum of radiolysis-contributing contact-handled (CH) and remote-handled (RH) radionuclide inventory on a volumetric basis over all waste areas of the repository (Day 2019b).

Gas generation due to the sum of cellulose biodegradation and iron corrosion in all waste areas is marginally increased for undisturbed (S1-BF) and E2 intruded (S4-BF) scenarios and substantially increased (more than doubled on average at 10,000 years) for E1 (S2-BF) and E2E1 intruded (S6-BF) scenarios for CRA19 in comparison to CRA14 (e.g., see Figure 10 and Figure 11 (Figures 54 and 55 from Day 2019b)). Cumulative gas generation is generally higher over all scenarios for CRA19 due to the substantial increase in inundated iron corrosion rates, increased iron and cellulose mass in the waste inventory, and the addition of brine radiolysis. Cellulose biodegradation rates for CRA19 are below CRA14 for scenarios without an E1 intrusion (S1-BF, S4-BF) and higher for scenarios with an E1 intrusion (S2-BF, S6-BF) due to the respectively lower and higher overall brine saturations. Even with the variable saturation changes across scenarios, the increased inundated iron corrosion rate for CRA19 results in increased iron corrosion gas generation over all scenarios in comparison to CRA14. The total moles of gas generated from all sources under CRA19 is substantially larger than for CRA14 with iron corrosion consistently being the largest contributor and radiolytic/microbial gas generation being comparable lesser contributors under all reported scenarios (e.g., see Figure 12 and Figure 13 (Figures 58 and 59 from Day 2019b)). For scenarios involving an E1 intrusion, radiolytic gas generation exceeds (on average) gas generation from microbial degradation (Figure 13).

Cellulose biodegradation and iron corrosion gas generation statistics for CRA19 and CRA14 are summarized in Table 22 (Table 21 from Day 2019b) along with total gas generation statistics for CRA19 that includes radiolysis. Table 22 provides the 3-replicate mean (integrated over time) and 3-replicate maximum (over all time) values.

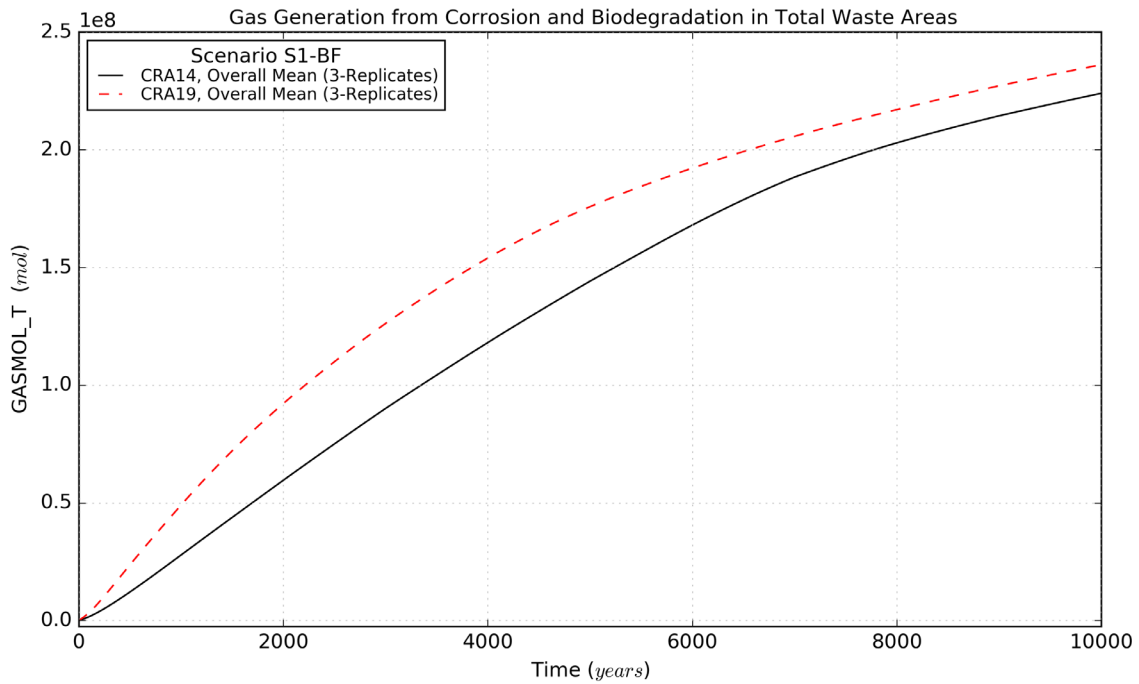


Figure 10 – Gas Generation from Corrosion and Biodegradation, Scenario S1-BF

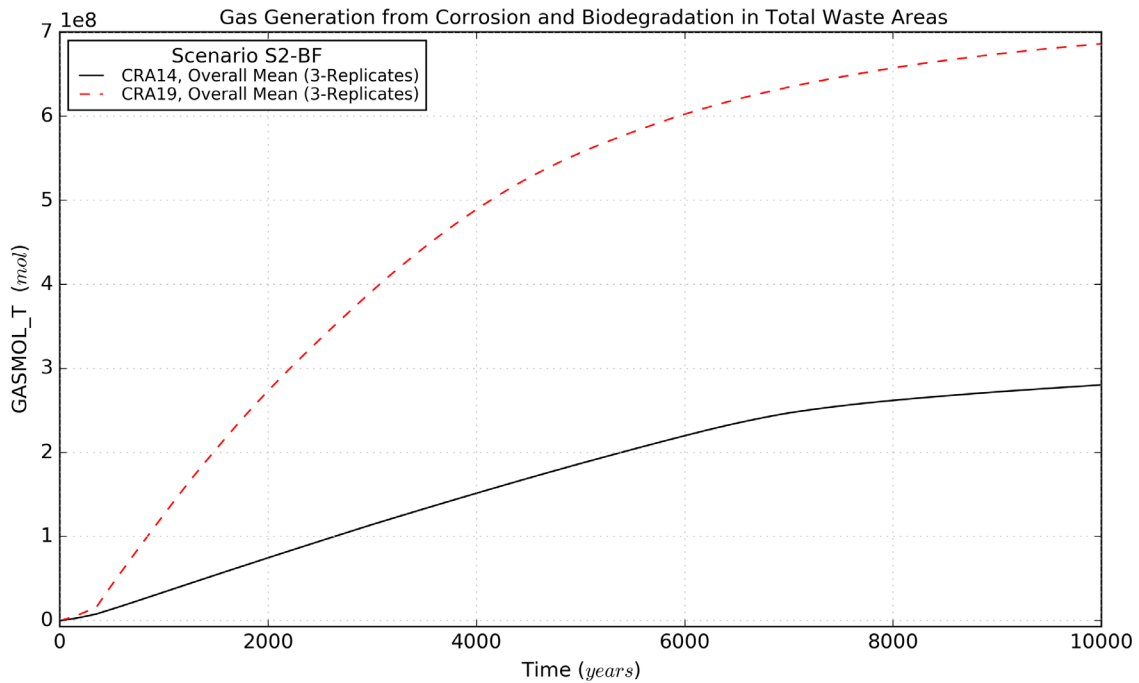


Figure 11 – Gas Generation from Corrosion and Biodegradation, Scenario S2-BF

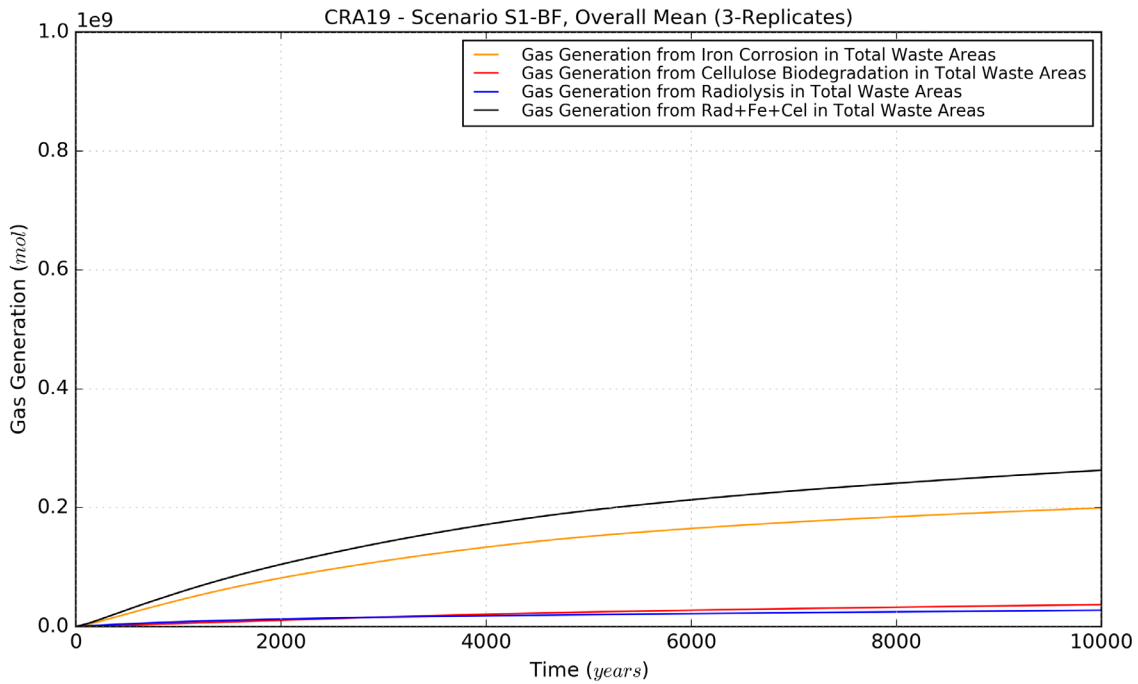


Figure 12 – CRA19 Moles of Gas Generated by All Sources, Scenario S1-BF

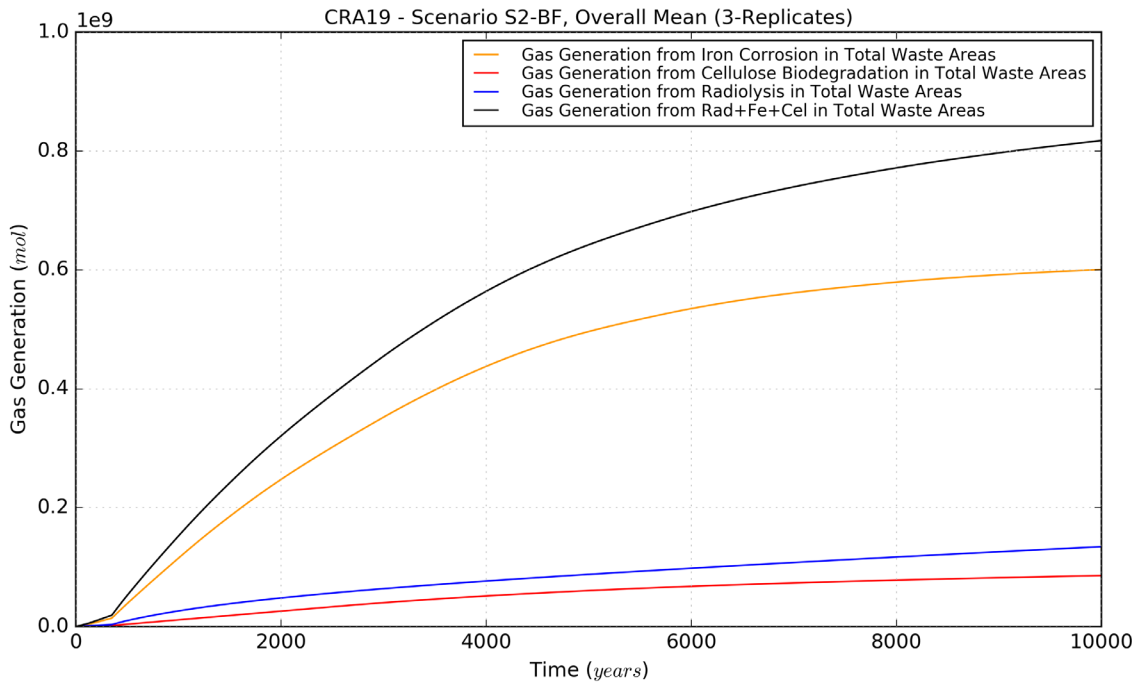


Figure 13 – CRA19 Moles of Gas Generated by All Sources, Scenario S2-BF

Table 22 – Gas Generation Statistics on Overall Means for CRA14 and CRA19

Quantity (units)	Description	Scenario	Mean Value ¹		Maximum Value ²	
			CRA14	CRA19	CRA14	CRA19
GASMOL_T (mol)	Gas Generation from Corrosion and Biodegradation in Total Waste Areas	S1-BF	1.33E+08	1.56E+08	2.24E+08	2.36E+08
		S2-BF	1.70E+08	4.75E+08	2.80E+08	6.86E+08
		S4-BF	1.43E+08	1.86E+08	2.42E+08	2.93E+08
		S6-BF	1.56E+08	3.37E+08	2.70E+08	5.58E+08
FEMOL_T (mol)	Gas Generation from Iron Corrosion in Total Waste Areas	S1-BF	1.06E+08	1.34E+08	1.78E+08	2.00E+08
		S2-BF	1.39E+08	4.22E+08	2.28E+08	6.01E+08
		S4-BF	1.15E+08	1.62E+08	1.94E+08	2.51E+08
		S6-BF	1.27E+08	2.98E+08	2.19E+08	4.88E+08
CELMOL_T (mol)	Gas Generation from Cellulose Biodegradation in Total Waste Areas	S1-BF	2.65E+07	2.20E+07	4.60E+07	3.67E+07
		S2-BF	3.12E+07	5.32E+07	5.29E+07	8.56E+07
		S4-BF	2.76E+07	2.46E+07	4.80E+07	4.19E+07
		S6-BF	2.93E+07	3.90E+07	5.13E+07	7.04E+07
ALL_HRDC (mol)	Gas Generation from Radiolysis in Total Waste Areas	S1-BF	-	1.84E+07	-	2.74E+07
		S2-BF	-	8.17E+07	-	1.34E+08
		S4-BF	-	2.48E+07	-	4.17E+07
		S6-BF	-	4.54E+07	-	8.59E+07
ALL_HHTC (mol)	Gas Generation from Rad+Fe+Cel in Total Waste Areas	S1-BF	1.33E+08	1.74E+08	2.24E+08	2.63E+08
		S2-BF	1.70E+08	5.55E+08	2.80E+08	8.18E+08
		S4-BF	1.43E+08	2.11E+08	2.42E+08	3.34E+08
		S6-BF	1.56E+08	3.82E+08	2.70E+08	6.42E+08

Notes:

- 1 Calculated as the function average (integrated) over the time interval (0-10,000 years) for the overall means (3 replicates)
- 2 Calculated as the function maximum over the time interval (0-10,000 years) for the overall means (3 replicates)

This page intentionally left blank

5.5.4 Pressure

The physical changes to the modeled repository associated with abandonment of the southernmost panel closure area, increased length of the northernmost panel closure area, increased volume of the experimental area along with gas generation and brine consumption changes resulting from an increased iron corrosion rate, addition of radiolytic gas generation, removal of iron sulfidation reactions, and increase in inventory quantities for iron and cellulose that are available for corrosion and biodegradation all impact repository pressures. Plots of mean brine pressure for the experimental area, operations area, north rest-of-repository, south rest-of-repository, and the waste panel are shown for selected scenarios in Figure 14 to Figure 26 (Figures 14, 15, 18, 19, 22, 23, 24, 26, 27, 28, 30, 31, and 32 from Day (2019b)).

For both undisturbed (S1-BF) and E2 intruded (S4-BF) scenarios, pressure within the operations and experimental areas for CRA19 are suppressed in comparison to CRA14 due to the modest change in pressures within the waste areas in concert with increased experimental area void space and enhanced isolation due to the increased length of the northernmost panel closure (e.g., see Figure 14 and Figure 16). For E1 (S2-BF) and E2E1 (S6-BF) intruded scenarios that intersect the hypothetical Castile brine reservoir, pressure within the operations and experimental areas for CRA19 are increased in comparison to CRA14 due to the increase in pressures within the waste areas that results in additional gas flow to the north from the waste areas (e.g., see Figure 15 and Figure 17).

Pressures within the north rest-of-repository are generally increased over all scenarios for CRA19 in comparison to CRA14 due to increased gas generation at early times for S1-BF and S4-BF and over all time for S2-BF and S6-BF (e.g., see Figure 18 - Figure 20). Pressures within the north rest-of-repository are increased by gas flow from the south to north and the slightly enhanced isolation from the void space within the operations and experimental areas due to the lengthened northernmost panel closure (Section 5.5.6). It is noted that gas generation rates are suppressed at later times for CRA19 in non-Castile intruded scenarios (S4-BF) due to higher early-time gas generation and brine consumption (Sections 5.5.3 and 5.5.5).

The influences on pressures discussed above are also participating in the resultant pressures within the south rest-of-repository and the waste panel. However, a primary influence on pressure is the lack of ROMPCS in the southernmost panel closure to separate these two waste areas. For undisturbed (S1-BF) and E2 intruded (S4-BF) scenarios, the lack of emplaced ROMPCS allows for pressure equilibration between the south rest-of-repository and the waste panel. With waste panel pressures historically being higher than pressures in the south rest-of-repository, the pressures in the south rest-of-repository are increased over all time for CRA19 in comparison to CRA14 for S1-BF and S4-BF while the pressures in the waste panel area are slightly higher early (due to increased early-time gas generation) and less at later times (due to equilibration) (e.g., see Figure 21, Figure 23, Figure 24, and Figure 26 (Figures 26, 28, 30, and 32 from Day 2019b)). For scenarios that intersect the hypothetical Castile brine reservoir (S2-BF and S6-BF), the lack of ROMPCS and pressure equilibration is exacerbated by flooding of both the waste panel and the south rest-of-repository with brine. This flooding substantially increases brine saturations (Section 5.5.5) within the south rest-of-repository which causes a

much higher quantity of gas generation (Section 5.5.3) and substantially increases pressures within these areas for CRA19 in comparison to CRA14 (Figure 22, and Figure 25).

Pressure statistics for CRA19 and CRA14 are summarized in Table 23 (Table 17 from Day 2019b), which provides the 3-replicate mean (integrated over time) and 3-replicate maximum (over all time) pressure values. The 3-replicate mean and maximum pressures for CRA19 as compared to CRA14 report mixed trends for pressures as both a function of scenario and location due to the interacting modifications described previously. The individual vector maximum pressure values for CRA19 are increased over CRA14 for all reported areas and scenarios with one exception – the slight reduction in maximum individual vector pressure within the waste panel for S4-BF (details shown in Day 2019b).

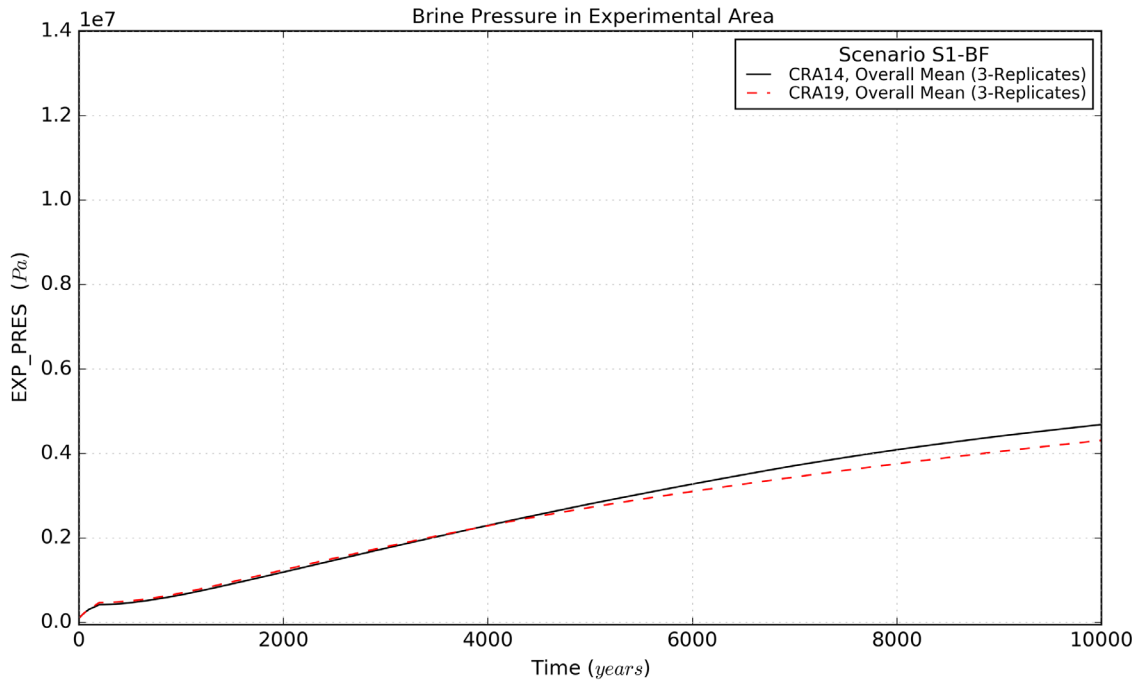


Figure 14 – Pressure Means for the Experimental Area, Scenario S1-BF

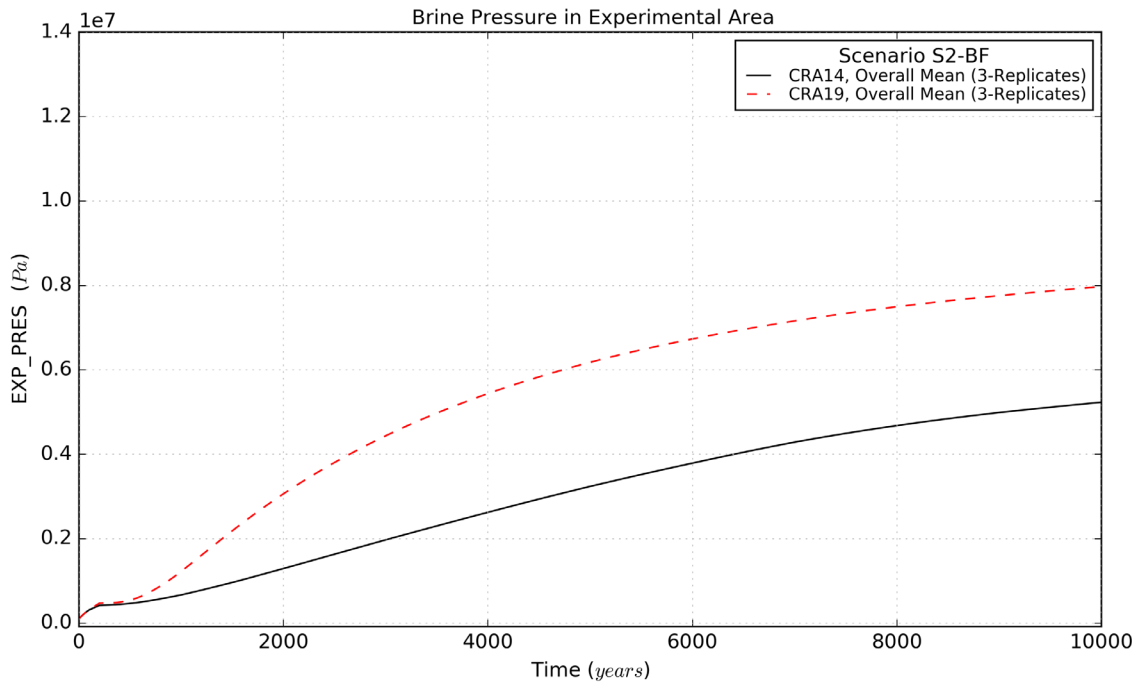


Figure 15 – Pressure Means for the Experimental Area, Scenario S2-BF

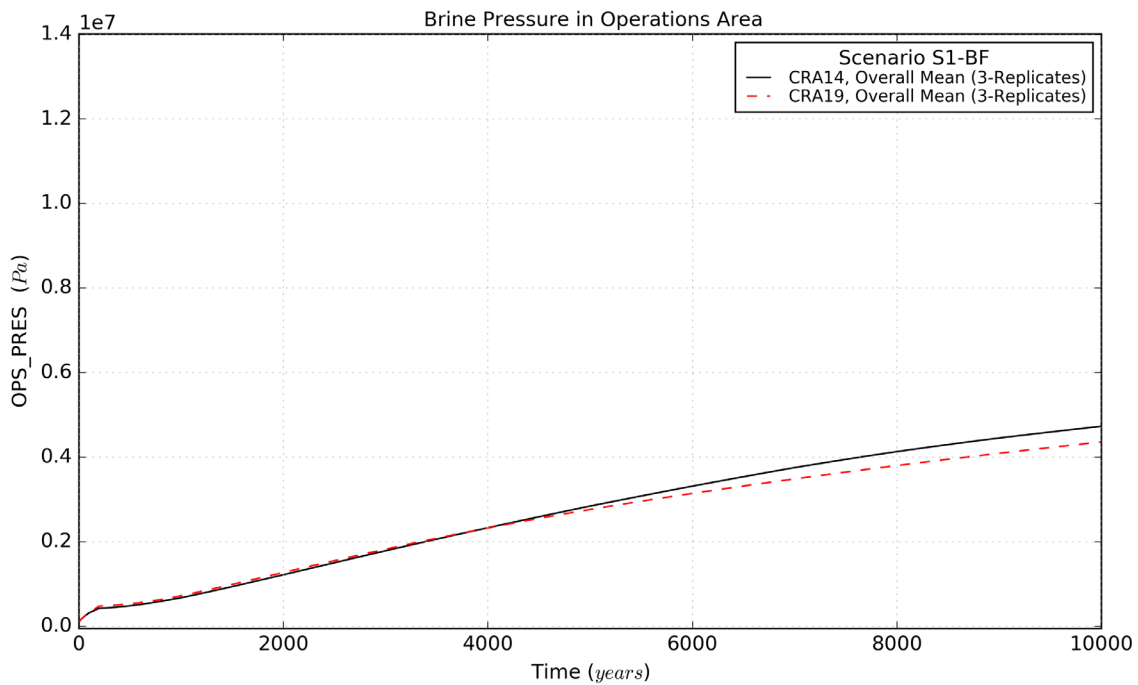


Figure 16 – Pressure Means for the Operations Area, Scenario S1-BF

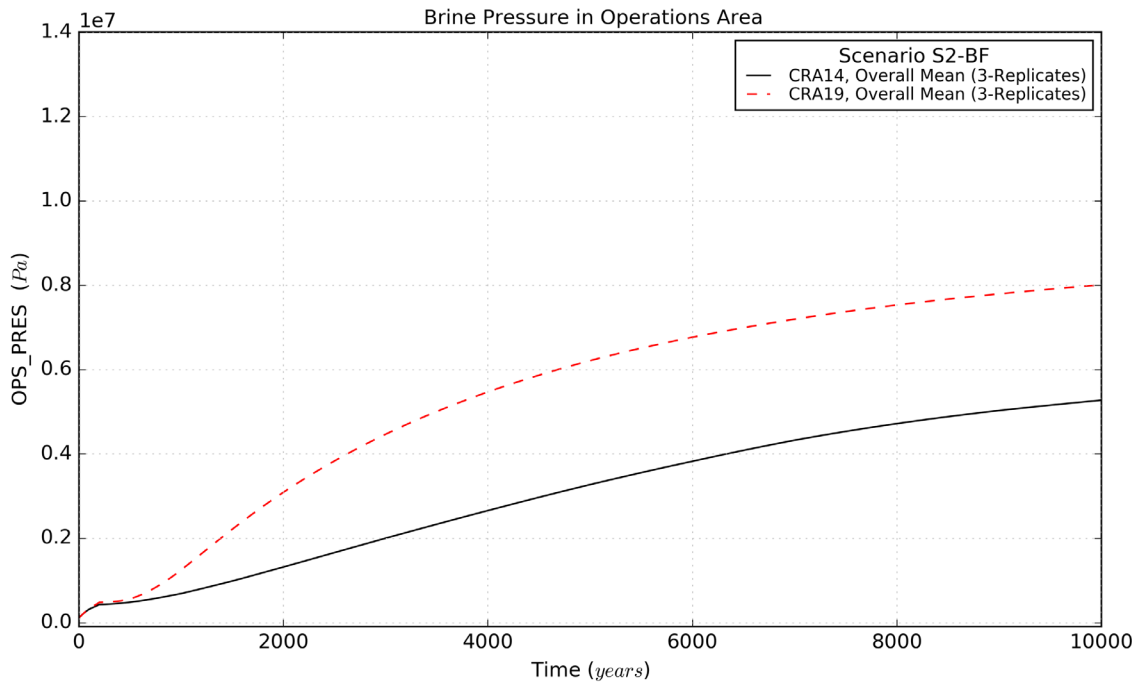


Figure 17 – Pressure Means for the Operations Area, Scenario S2-BF

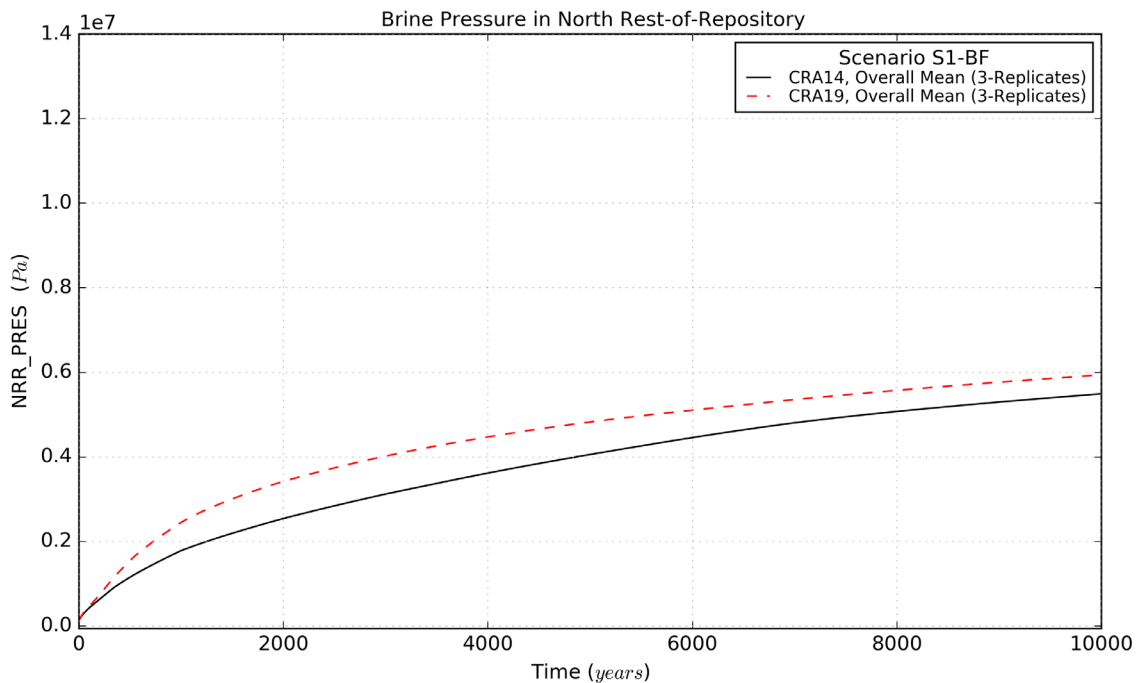


Figure 18 – Pressure Means for the North Rest-of-Repository, Scenario S1-BF

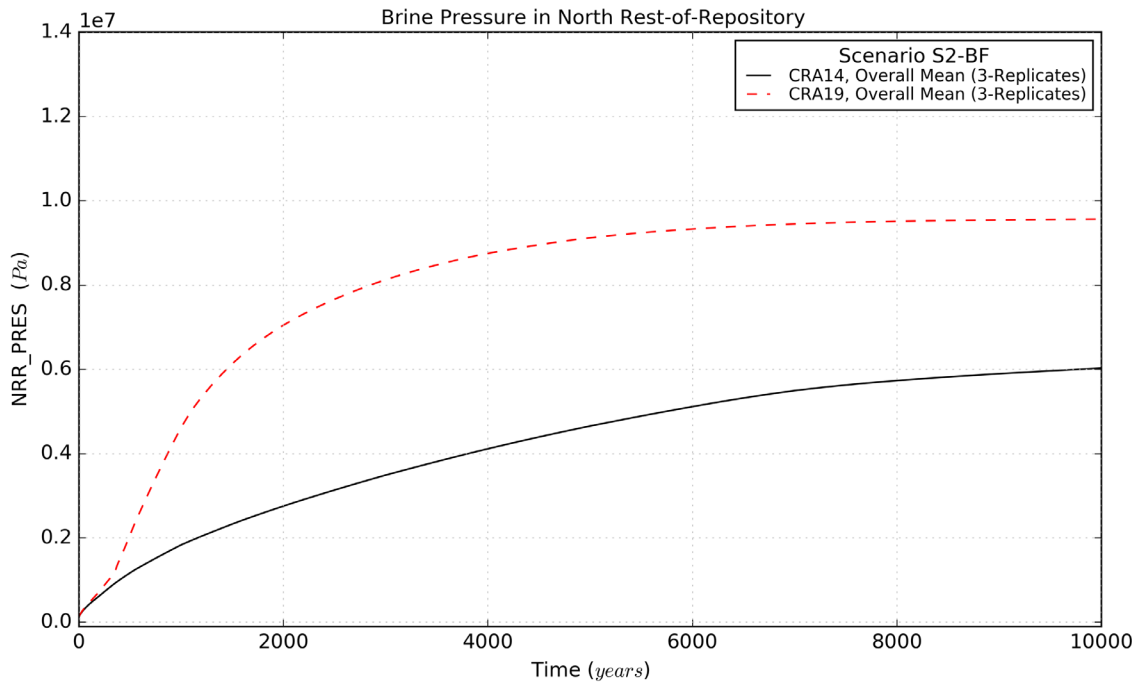


Figure 19 – Pressure Means for the North Rest-of-Repository, Scenario S2-BF

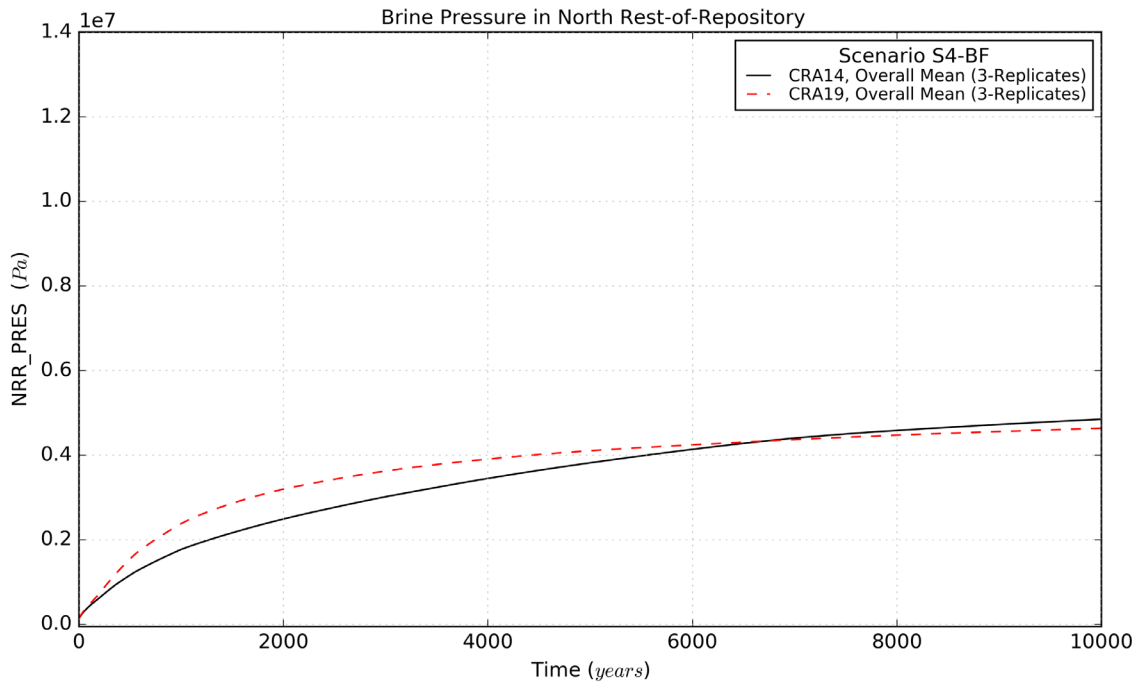


Figure 20 – Pressure Means for the North Rest-of-Repository, Scenario S4-BF

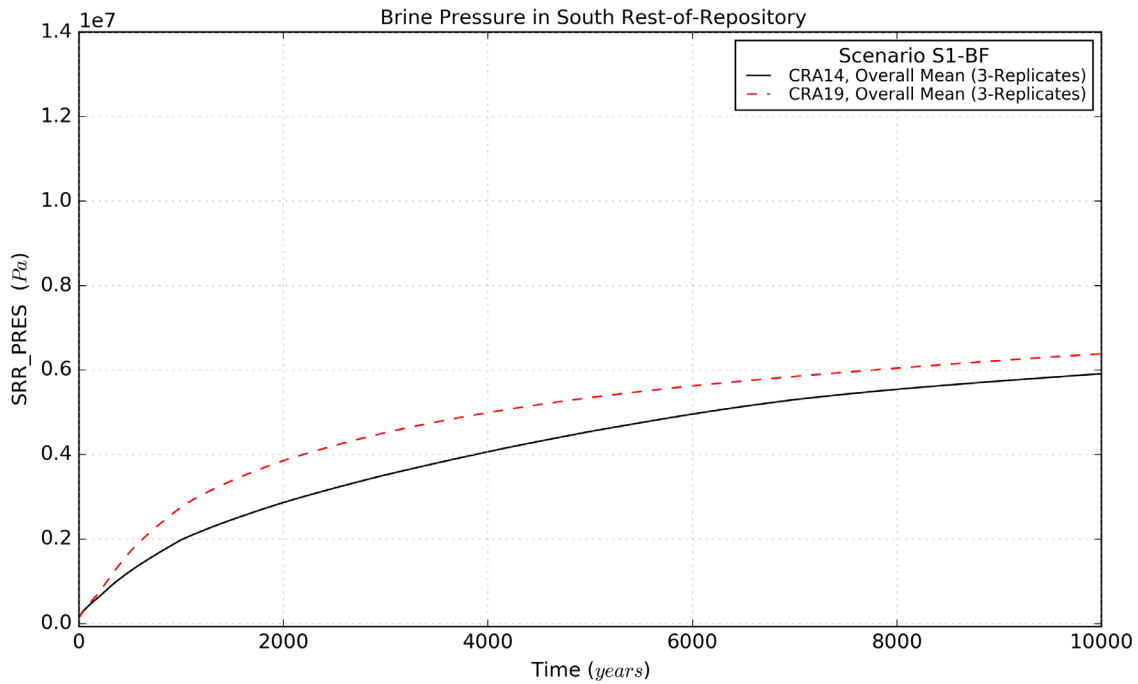


Figure 21 – Pressure Means for the South Rest-of-Repository, Scenario S1-BF

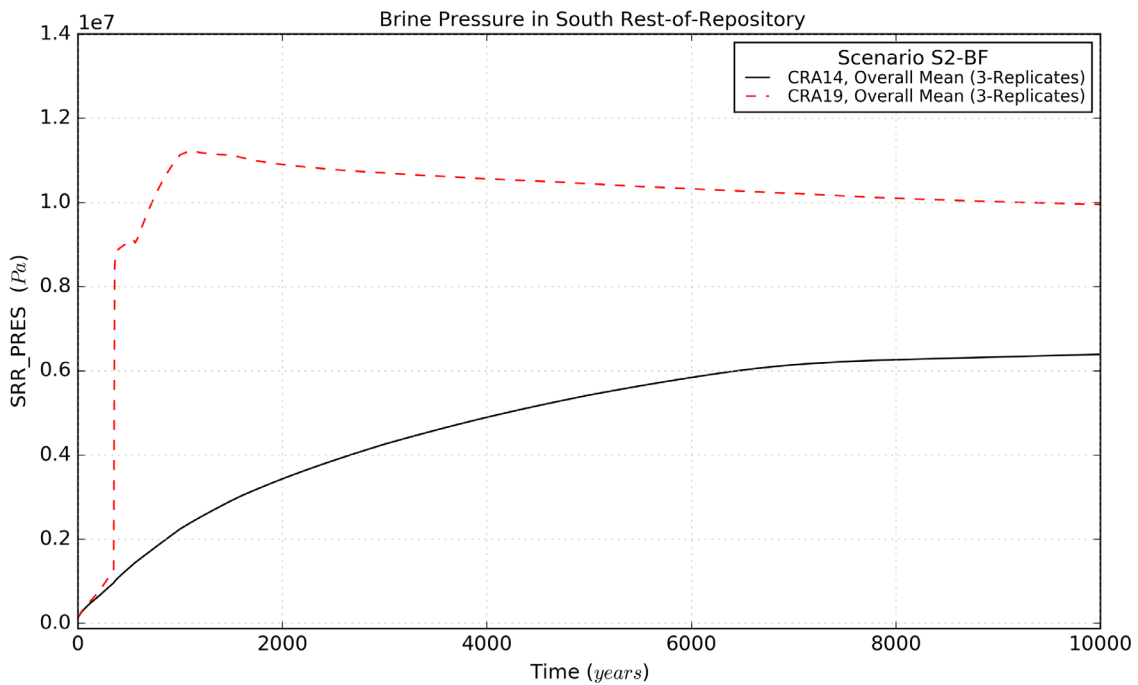


Figure 22 – Pressure Means for the South Rest-of-Repository, Scenario S2-BF

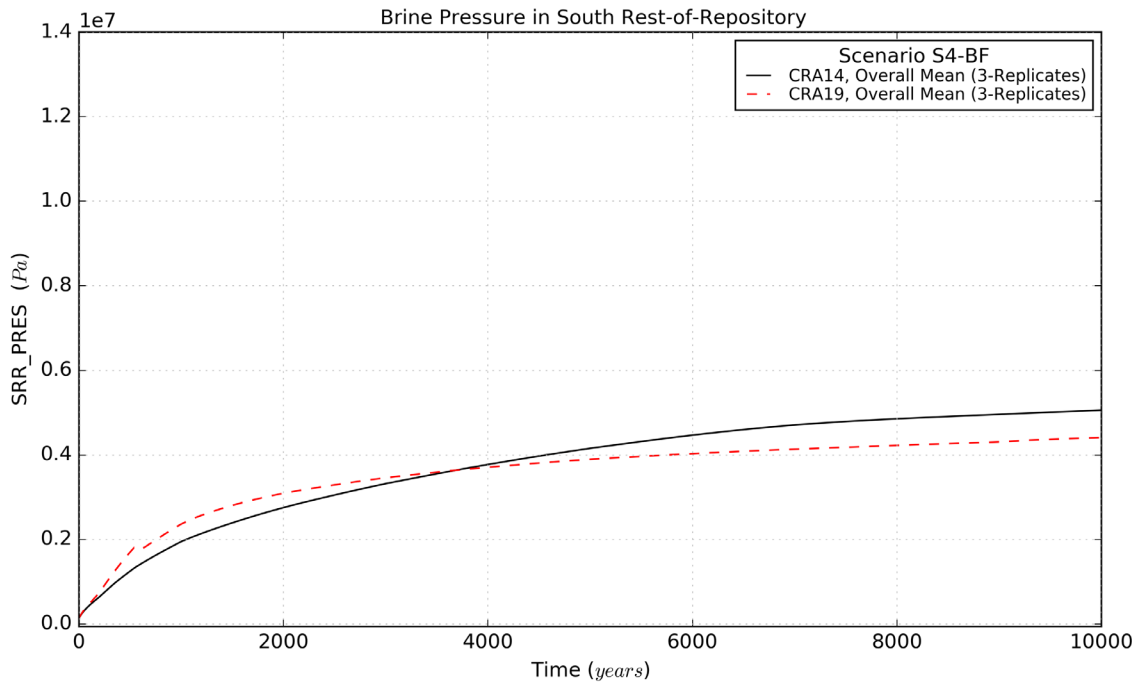


Figure 23 – Pressure Means for the South Rest-of-Repository, Scenario S4-BF

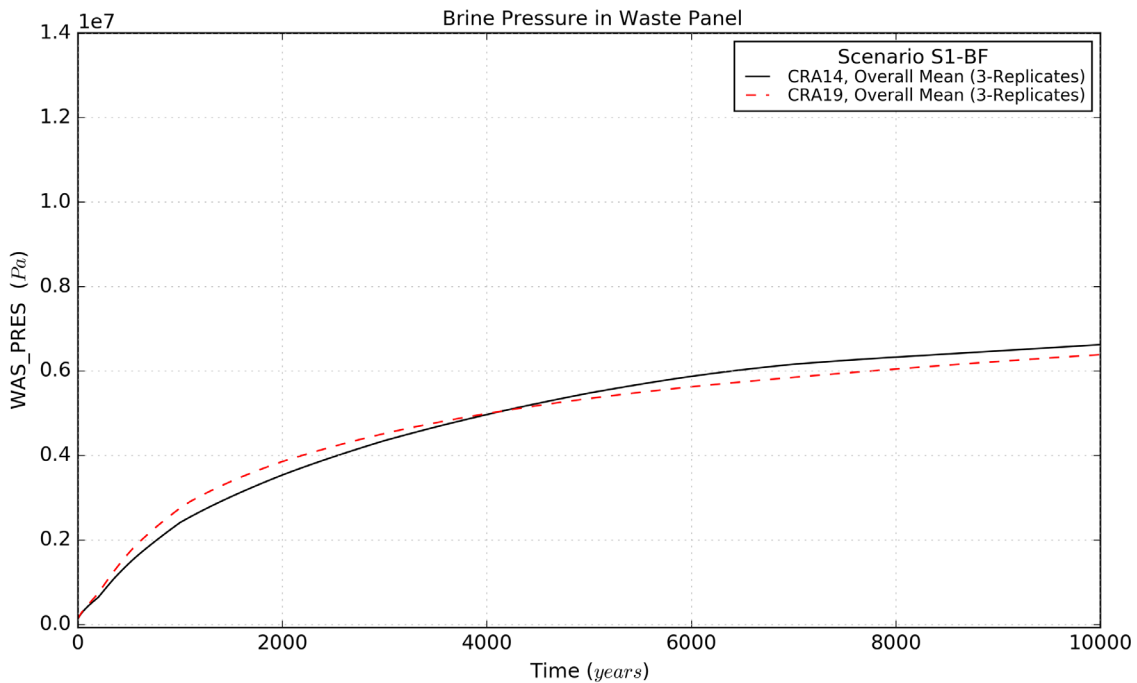


Figure 24 – Pressure Means for the Waste Panel, Scenario S1-BF

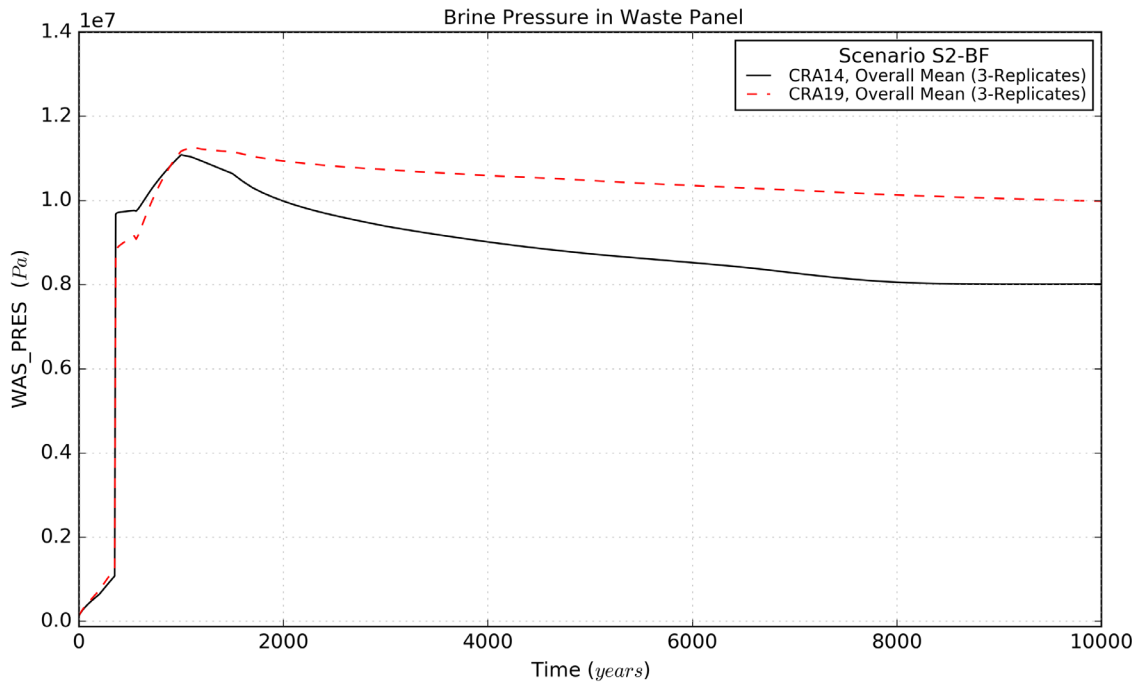


Figure 25 – Pressure Means for the Waste Panel, Scenario S2-BF

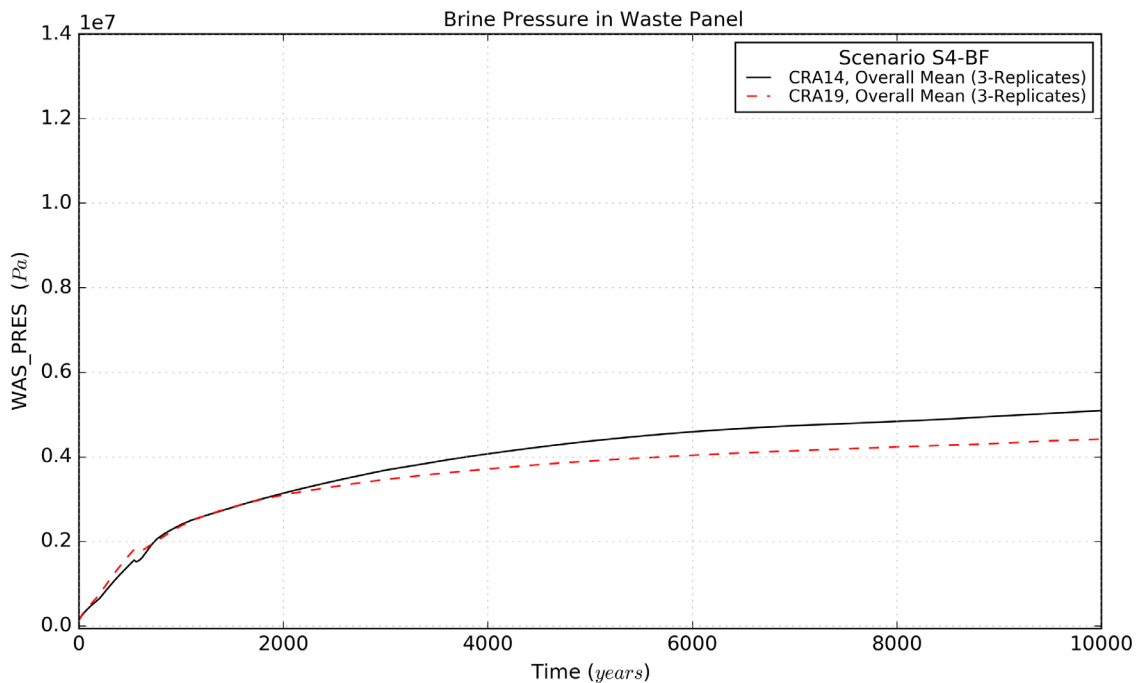


Figure 26 – Pressure Means for the Waste Panel, Scenario S4-BF

Table 23 – Pressure Statistics on Overall Means for CRA14 and CRA19

Quantity (units)	Description	Scenario	Mean Value ¹		Maximum Value ²	
			CRA14	CRA19	CRA14	CRA19
EXP_PRES (Pa)	Brine Pressure in Experimental Area	S1-BF	2.67E+06	2.54E+06	4.69E+06	4.31E+06
		S2-BF	3.03E+06	5.36E+06	5.23E+06	7.97E+06
		S4-BF	2.45E+06	2.07E+06	4.16E+06	3.37E+06
		S6-BF	2.81E+06	3.83E+06	4.99E+06	6.37E+06
OPS_PRES (Pa)	Brine Pressure in Operations Area	S1-BF	2.70E+06	2.58E+06	4.73E+06	4.36E+06
		S2-BF	3.07E+06	5.40E+06	5.28E+06	8.01E+06
		S4-BF	2.49E+06	2.11E+06	4.20E+06	3.42E+06
		S6-BF	2.84E+06	3.87E+06	5.04E+06	6.42E+06
NRR_PRES (Pa)	Brine Pressure in North Rest-of-Repository	S1-BF	3.78E+06	4.43E+06	5.49E+06	5.94E+06
		S2-BF	4.24E+06	8.05E+06	6.03E+06	9.56E+06
		S4-BF	3.51E+06	3.75E+06	4.85E+06	4.64E+06
		S6-BF	3.96E+06	6.11E+06	5.78E+06	7.96E+06
SRR_PRES (Pa)	Brine Pressure in South Rest-of-Repository	S1-BF	4.17E+06	4.87E+06	5.91E+06	6.39E+06
		S2-BF	4.83E+06	1.00E+07	6.39E+06	1.12E+07
		S4-BF	3.77E+06	3.58E+06	5.06E+06	4.41E+06
		S6-BF	4.42E+06	7.06E+06	6.15E+06	8.53E+06
WAS_PRES (Pa)	Brine Pressure in Waste Panel	S1-BF	4.92E+06	4.88E+06	6.63E+06	6.39E+06
		S2-BF	8.64E+06	1.01E+07	1.11E+07	1.13E+07
		S4-BF	3.96E+06	3.59E+06	5.10E+06	4.42E+06
		S6-BF	6.57E+06	7.08E+06	8.94E+06	8.55E+06

Notes:

- 1 Calculated as the function average (integrated) over the time interval (0-10,000 years) for the overall means (3 replicates)
- 2 Calculated as the function maximum over the time interval (0-10,000 years) for the overall means (3 replicates)

This page intentionally left blank

5.5.5 Brine Saturation

Brine pressure and saturation⁷ changes in the operations and experimental areas, north rest-of-repository, south rest-of-repository, and waste panel are typically inversely related to one another as increased repository pressures tend to reduce brine infiltration into the repository (from the DRZ/Salado) and induce flow within the repository (and possibly to the nearby strata). In addition, the iron corrosion and magnesium oxide reactions (also radiolysis in CRA19), when active, consume brine faster than the other reactions generate brine, causing waste area brine saturations to decrease over time. Brine saturations also generally increase toward the south in the repository due to the 1-degree Salado dip and the associated gravity-driven flow of brine.

This general trend of inversely related pressures and saturations is maintained for CRA19 in the experimental area, operations area, and north rest-of-repository for all scenarios (e.g., see Figure 27 - Figure 33 (Figures 34, 35, 38, 39, and 42-44 from Day 2019b)), with the saturations in the north rest-of-repository being reduced for CRA19 in comparison to CRA14 (results for scenarios involving E2 intrusions are almost identical to those from the undisturbed scenario and are not shown here). Furthermore, the trend is maintained for the south rest-of-repository in the undisturbed (S1-BF) and E2 intruded (S4-BF) scenarios (e.g., see Figure 34 and Figure 36 (Figures 46 and 48 from Day 2019b)). In contrast, the south rest-of-repository experiences substantial increases in brine saturation under scenarios that intersect the hypothetical Castile brine reservoir (S2-BF and S6-BF) due to the inflow of brine from the waste panel across the southernmost panel closure area that lacks an ROMPCS (e.g., see Figure 35 (Figure 47 from Day 2019b)). Although brine pressure in the waste panel is initially increased for CRA19 in comparison to CRA14 at early times and then decreased thereafter for the unintruded (S1-BF) and E2 intruded (S4-BF) scenarios, brine saturation within the waste panel is reduced for CRA19 over all time (e.g., see Figure 37 and Figure 39 (Figures 50 and 52 from Day 2019b)). The saturation reductions in the waste panel under S1-BF and S4-BF are attributed to the substantially increased brine consumption in the waste panel as a result of inventory increases in cellulose and iron, increased inundated iron corrosion rates, and the application of radiolytic gas generation for CRA19 in comparison to CRA14 (Section 5.5.3). For E1 (S2-BF) and E2E1 (S6-BF) intruded scenarios that intersect the hypothetical Castile brine reservoir, saturations within the waste area for CRA19 are decreased in comparison to CRA14 due to the increase in pressures within the waste areas that result in increased south to north brine flow out of the waste area into the south rest-of-repository across the “open” southernmost panel closure area (e.g., see Figure 38 (Figure 51 from Day 2019b)).

Brine saturation statistics for CRA19 and CRA14 are summarized in Table 24 (Table 19 from Day 2019b), which provides the 3-replicate mean (integrated over time) and 3-replicate maximum (over all time) brine saturation values. The 3-replicate mean and maximum brine saturations for CRA19 as compared to CRA14 report mixed trends for saturation as both a function of scenario and location due to the interacting modifications described previously. The individual vector maximum brine saturation values for CRA19 are the same or decreased under CRA14 for all reported areas and scenarios with three exceptions – the slight increase in

⁷ Gas saturation results are not explicitly provided herein, but are inferred from the brine saturation results presented in this section, with gas saturation equal to one minus the brine saturation.

maximum individual vector brine saturation within the south rest-of-repository for S2-BF, S4-BF, and S6-BF (details shown in Day 2019b).

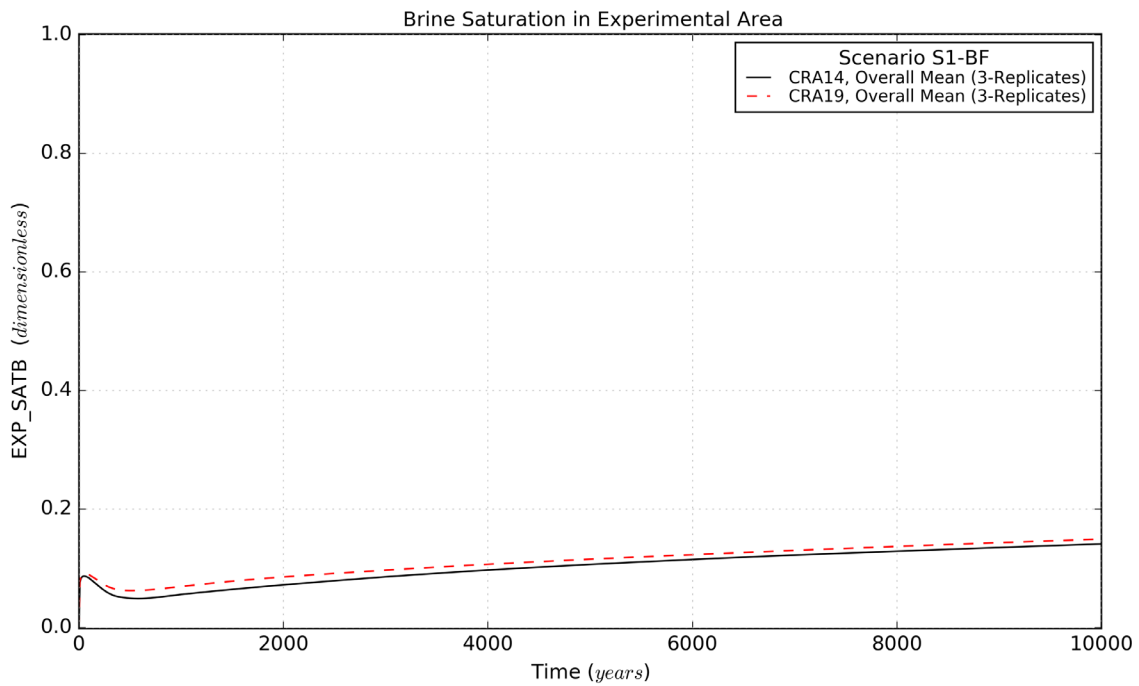


Figure 27 – Brine Saturation Means for the Experimental Area, Scenario S1-BF

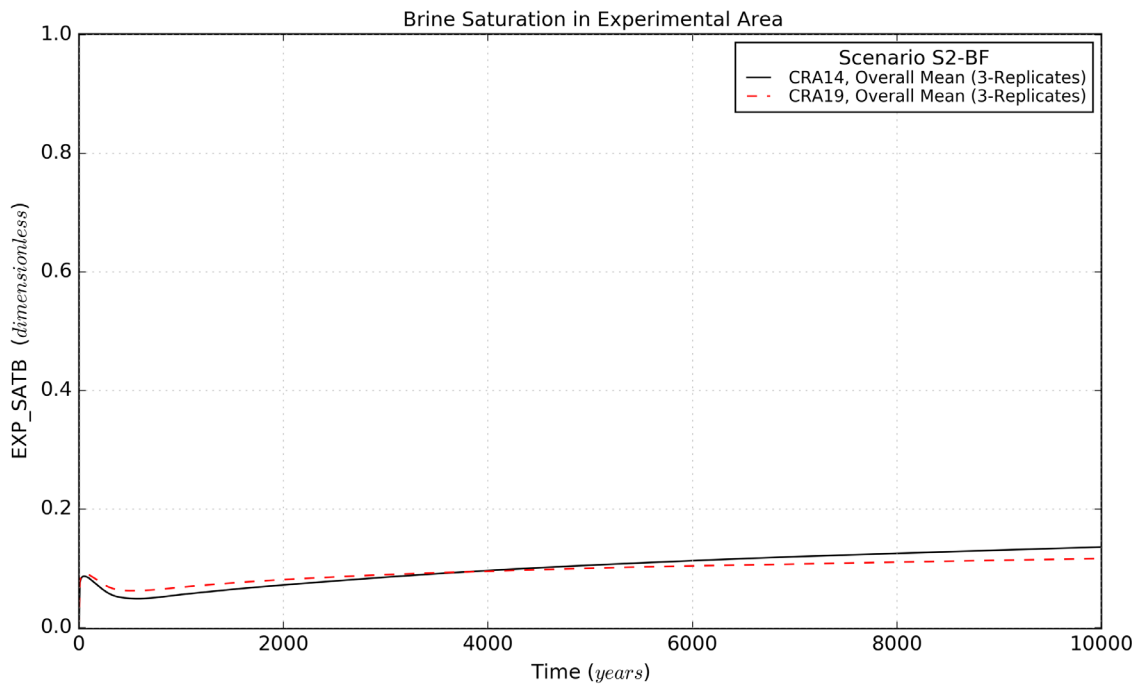


Figure 28 – Brine Saturation Means for the Experimental Area, Scenario S2-BF

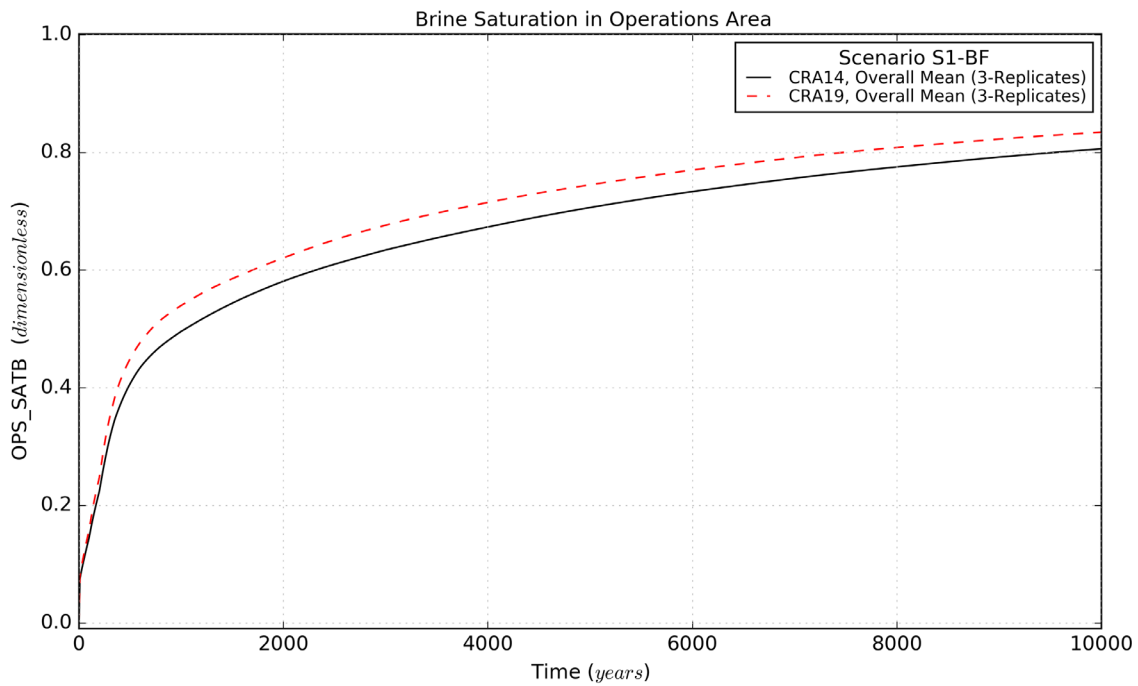


Figure 29 – Brine Saturation Means for the Operations Area, Scenario S1-BF

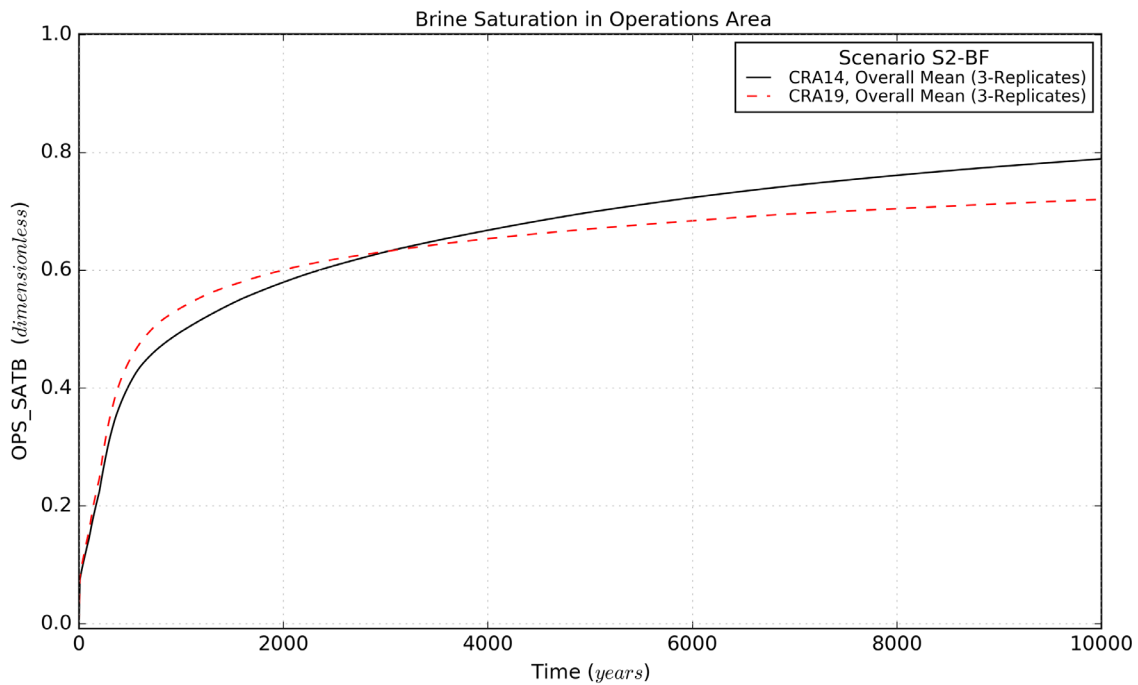


Figure 30 – Brine Saturation Means for the Operations Area, Scenario S2-BF

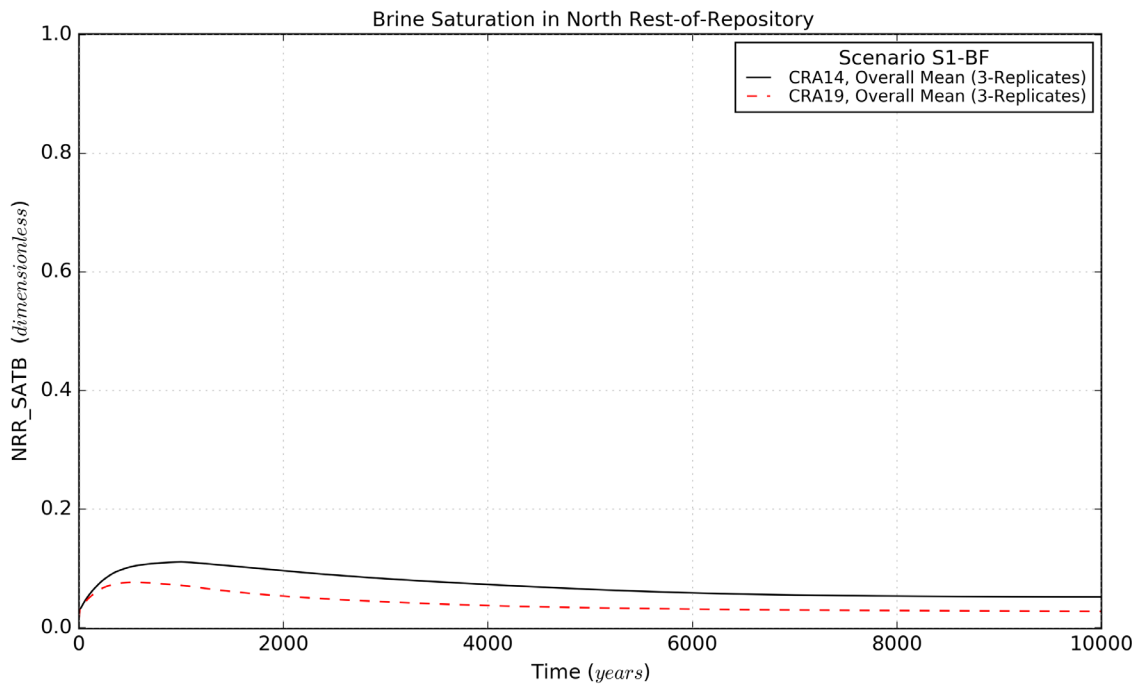


Figure 31 – Brine Saturation Means for the North Rest-of-Repository, Scenario S1-BF

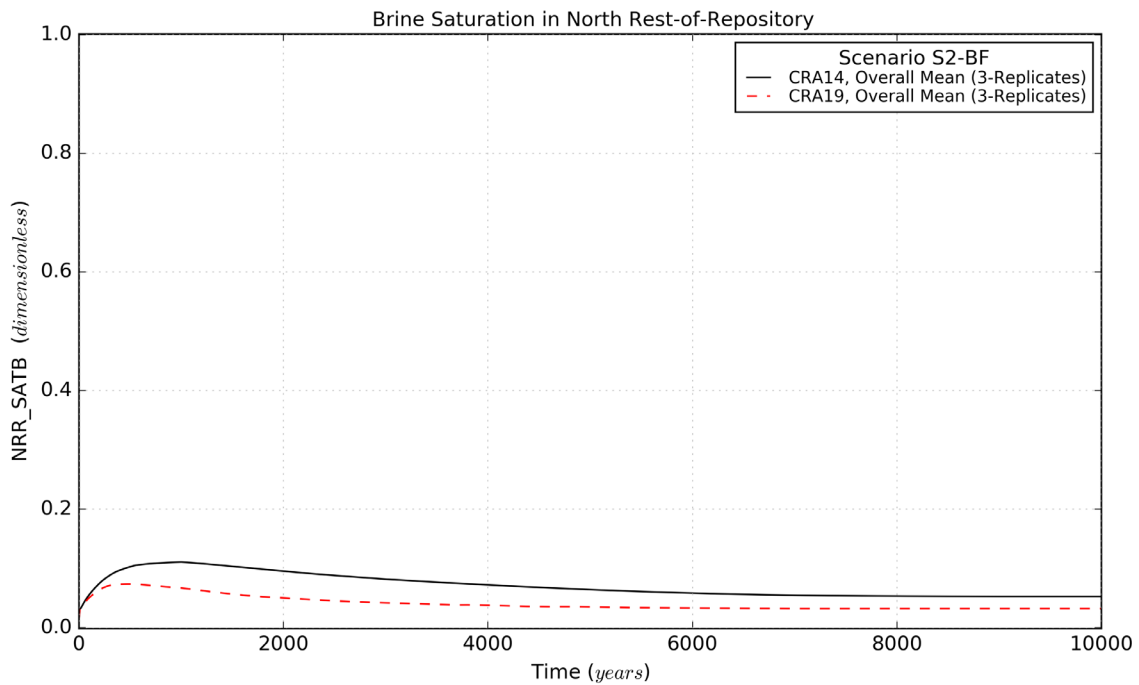


Figure 32 – Brine Saturation Means for the North Rest-of-Repository, Scenario S2-BF

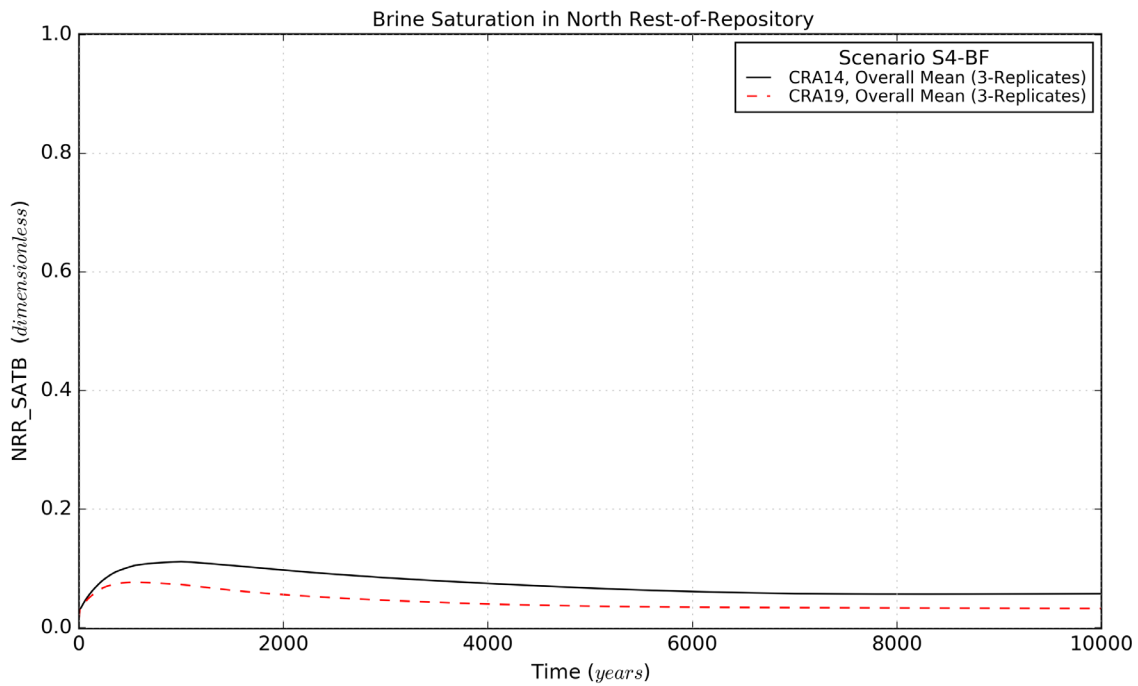


Figure 33 – Brine Saturation Means for the North Rest-of-Repository, Scenario S4-BF

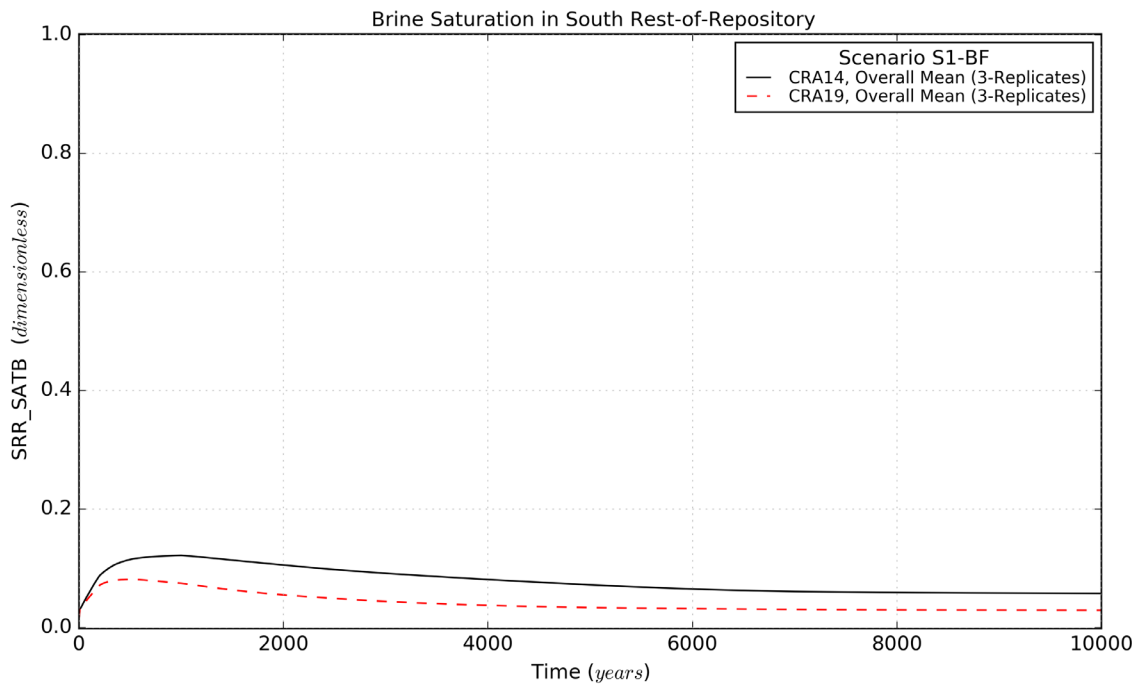


Figure 34 – Brine Saturation Means for the South Rest-of-Repository, Scenario S1-BF

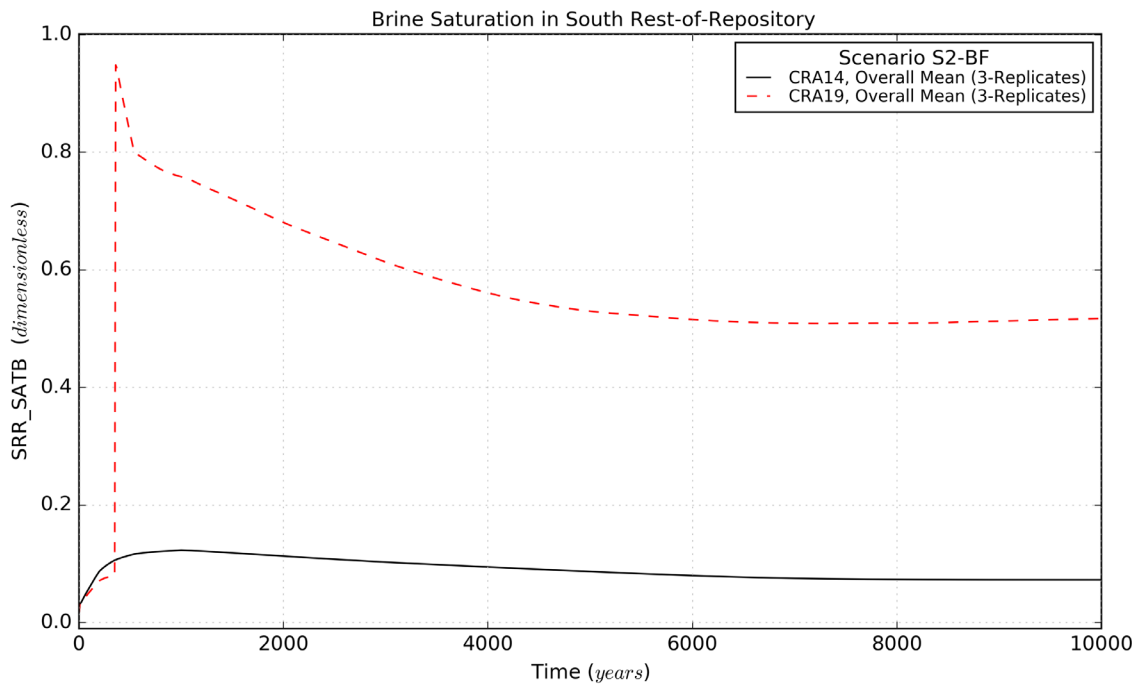


Figure 35 – Brine Saturation Means for the South Rest-of-Repository, Scenario S2-BF

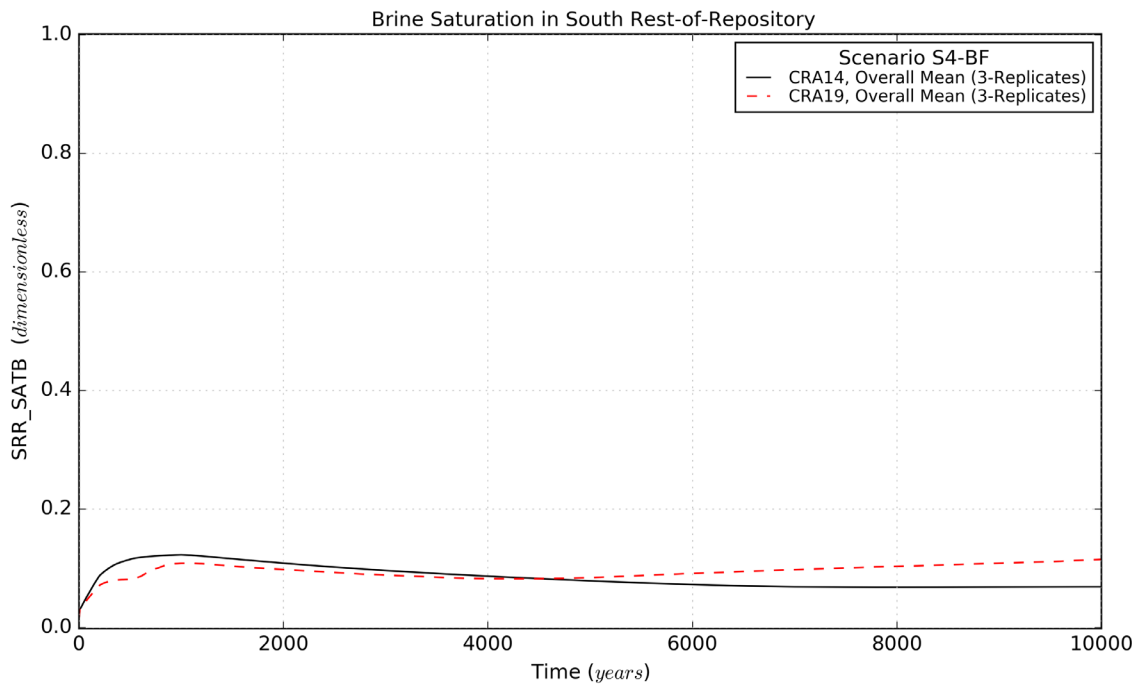


Figure 36 – Brine Saturation Means for the South Rest-of-Repository, Scenario S4-BF

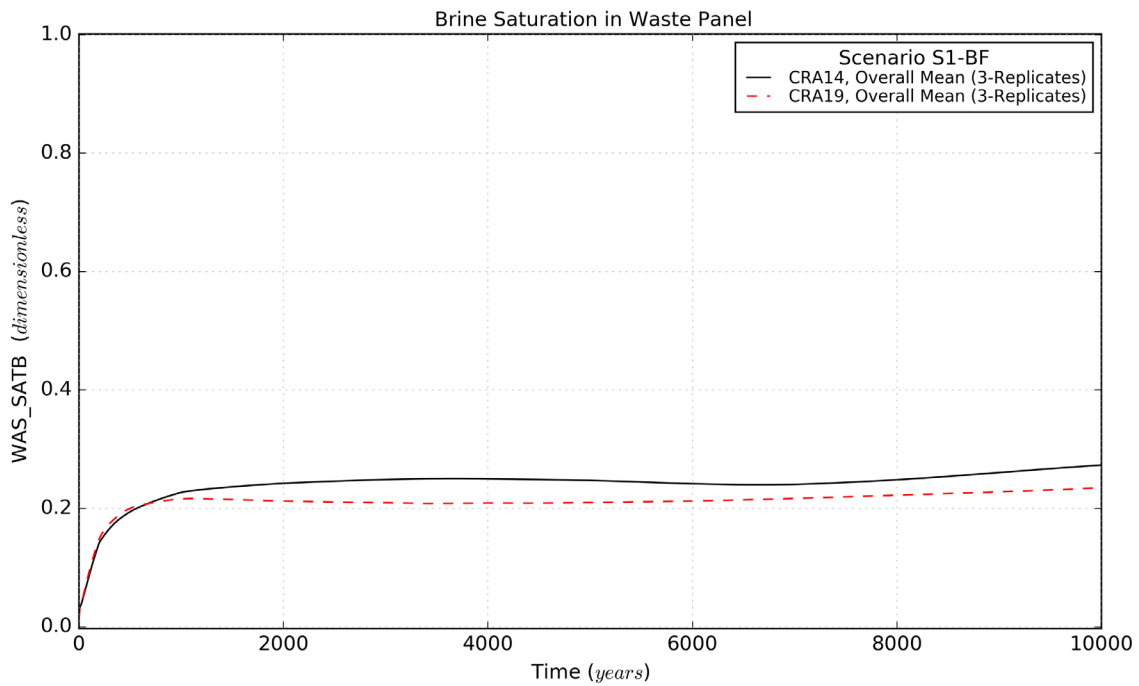


Figure 37 – Brine Saturation Means for the Waste Panel, Scenario S1-BF

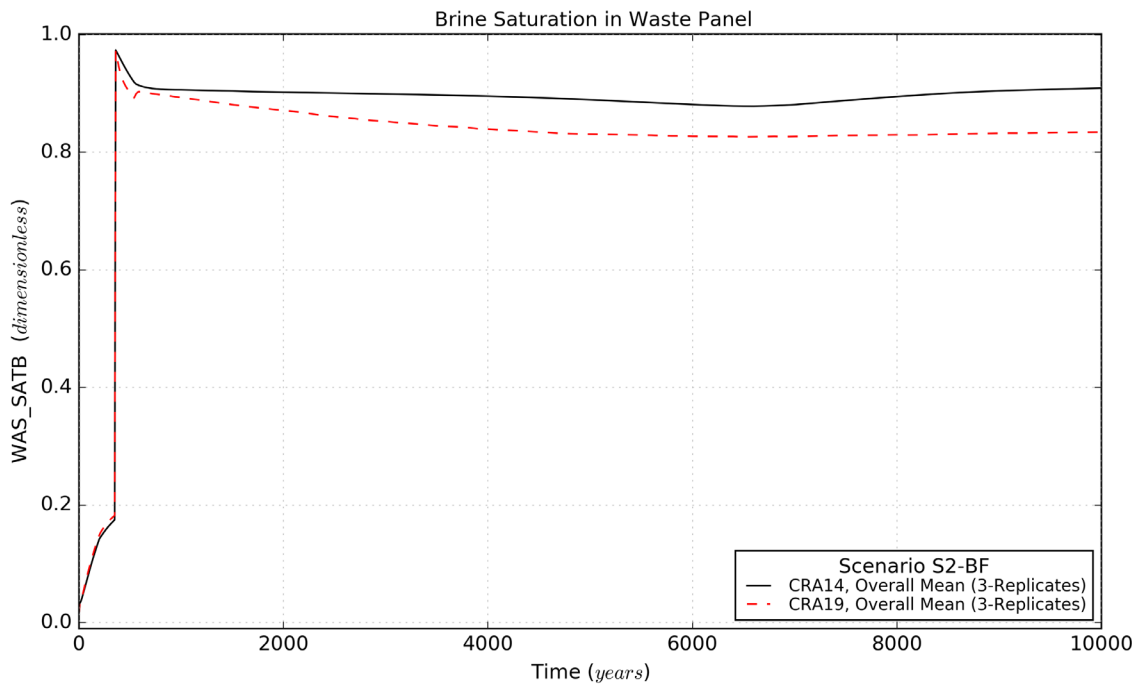


Figure 38 – Brine Saturation Means for the Waste Panel, Scenario S2-BF

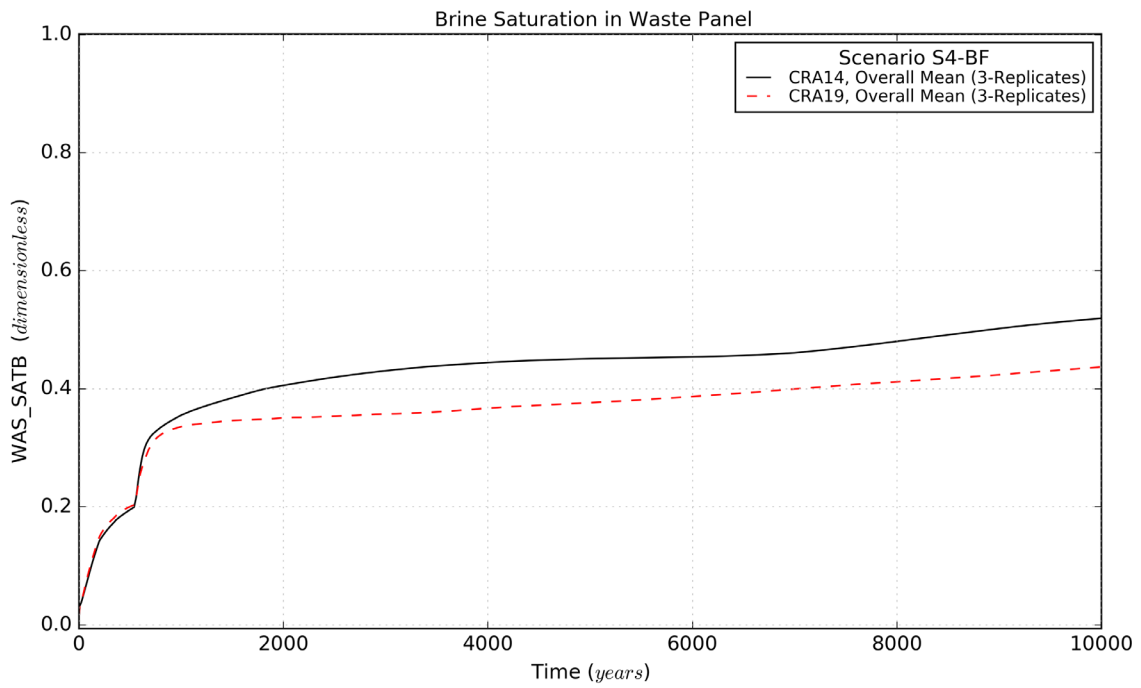


Figure 39 – Brine Saturation Means for the Waste Panel, Scenario S4-BF

This page intentionally left blank.

Table 24 – Brine Saturation Statistics on Overall Means for CRA14 and CRA19

Quantity (units)	Description	Scenario	Mean Value ¹		Maximum Value ²	
			CRA14	CRA19	CRA14	CRA19
EXP_SATB (dimensionless)	Brine Saturation in Experimental Area	S1-BF	1.02E-01	1.12E-01	1.41E-01	1.49E-01
		S2-BF	1.00E-01	9.64E-02	1.36E-01	1.17E-01
		S4-BF	1.03E-01	1.15E-01	1.44E-01	1.57E-01
		S6-BF	1.02E-01	1.05E-01	1.40E-01	1.31E-01
OPS_SATB (dimensionless)	Brine Saturation in Operations Area	S1-BF	6.67E-01	7.04E-01	8.06E-01	8.34E-01
		S2-BF	6.59E-01	6.39E-01	7.89E-01	7.21E-01
		S4-BF	6.68E-01	7.02E-01	8.08E-01	8.33E-01
		S6-BF	6.64E-01	6.78E-01	7.97E-01	7.76E-01
NRR_SATB (dimensionless)	Brine Saturation in North Rest-of-Repository	S1-BF	7.10E-02	4.04E-02	1.11E-01	7.69E-02
		S2-BF	7.07E-02	4.09E-02	1.11E-01	7.38E-02
		S4-BF	7.32E-02	4.34E-02	1.11E-01	7.69E-02
		S6-BF	7.13E-02	3.97E-02	1.11E-01	7.69E-02
SRR_SATB (dimensionless)	Brine Saturation in South Rest-of-Repository	S1-BF	7.86E-02	4.16E-02	1.22E-01	8.15E-02
		S2-BF	8.99E-02	5.61E-01	1.23E-01	9.49E-01
		S4-BF	8.48E-02	9.49E-02	1.23E-01	1.15E-01
		S6-BF	8.57E-02	3.60E-01	1.22E-01	6.28E-01
WAS_SATB (dimensionless)	Brine Saturation in Waste Panel	S1-BF	2.40E-01	2.12E-01	2.73E-01	2.35E-01
		S2-BF	8.69E-01	8.20E-01	9.74E-01	9.72E-01
		S4-BF	4.30E-01	3.68E-01	5.20E-01	4.37E-01
		S6-BF	6.93E-01	6.32E-01	8.40E-01	8.08E-01

Notes:

- 1 Calculated as the function average (integrated) over the time interval (0-10,000 years) for the overall means (3 replicates)
- 2 Calculated as the function maximum over the time interval (0-10,000 years) for the overall means (3 replicates)

This page intentionally left blank

5.5.6 Brine and Gas Flows

The larger DRZ associated with an expanded experimental area to accommodate the 5th shaft access drifts and greater communication between the waste panel and south rest-of-repository facilitated by the lack of ROMPCS emplacement in the southernmost panel closure area results in a net increase in brine inflow to the repository across all scenarios. The inflow increases associated with undisturbed (S1-BF) and non-Castile intrusions (S4-BF) are rather modest when compared to the inflow increases for intrusions that are associated with the hypothetical Castile brine reservoir (S2-BF and S6-BF). For S2-BF and S6-BF, pressure-limited flows from the Castile brine reservoir across the unemplaced southernmost panel closure flood the waste panel and south rest-of-repository, resulting in total repository brine inflows that are essentially doubled for CRA19 in comparison to CRA14. Figure 40 and Figure 41 (Figures 62 and 63 from Day 2019b) show the magnitude of brine influx to the repository for scenarios S1-BF and S2-BF (results for scenarios involving E2 intrusions are similar to those from the undisturbed scenario and are not shown here). Figure 42 (Figure 66 from Day 2019b) shows a representative case for brine influx to the experimental area under the undisturbed scenario (S1-BF).

Mean brine flows up the shaft under CRA19 remain relatively small but are increased over all scenarios in comparison to CRA14 due a combination of scenario-dependent factors such as brine pressures and saturations in the operations and experimental areas and the increased cross-sectional area of the composite shaft which includes the additional 5th shaft. The comparatively greater brine flows up the shaft observed in the S4-BF and S6-BF scenarios are associated with the higher brine pressures and saturations previously discussed (e.g., see Figure 43 to Figure 45 (Figures 67 - 69 from Day 2019b)).

Mean brine flows up the intrusion borehole under CRA19 are slightly reduced for Castile intruded scenarios (S2-BF and S6-BF) in comparison to those predicted under CRA14 (e.g., see Figure 46 (Figure 71 from Day 2019b)). The slight reduction in brine flow up the intrusion borehole for these scenarios is attributed to the reduced average brine saturations observed in the waste panel. The observed (on average) reduced brine pressures and saturations in the waste panel under S4-BF do not predict the slightly delayed and increased mean flow of brine up the intrusion borehole (e.g., see Figure 47 (Figure 72 from Day 2019b)). Further consideration of this unexpected observation is explained by the fact that the mean brine flow up the intrusion borehole under S4-BF is primarily influenced by a relatively few number of vectors (15 out of 300) that have higher than average waste panel brine pressures and saturations along with higher than average permeabilities resulting from the sampled BH_SAND borehole material (details shown in Day 2019b).

Mean gas flows out of the south rest-of-repository and north rest-of-repository (across the panel closure plane, which includes the panel closure and associated upper and lower DRZ) are increased for CRA19 in comparison to CRA14. A representative comparison of gas flows out of the south rest-of-repository (into the north rest-of-repository) and out of the north rest-of-repository (into the operations area) for S2-BF are provided in Figure 48 and Figure 49 (Figures 75 and 76 from Day 2019b) to illustrate the enhanced flow of generated gas to the north that is partially impeded by the increased length of the northernmost panel closure. The gas flow (on average) from the south rest-of-repository into the north rest-of-repository (and further north into

the operations area) is substantially increased due to the elimination of panel closures in the southern part of the repository, which drives pressure increases in the south rest-of-repository, especially for scenarios involving intrusion into Castile brine (Figure 22).

Brine flow statistics for CRA19 and CRA14 are summarized in Table 25 (Table 23 from Day 2019b), which provides the 3-replicate mean (integrated over time) and 3-replicate maximum (over all time) brine flow values. The 3-replicate mean and maximum brine flows for CRA19 as compared to CRA14 report increased brine flow into the repository and up the shaft for all scenarios along with decreased brine flow up the intrusion borehole for all applicable scenarios with the exception of S4-BF. The individual vector maximum brine flow values for CRA19 into the repository and up the shaft are increased above CRA14 for all scenarios. The individual vector maximum brine flow values for CRA19 up the intrusion borehole are decreased below CRA14 for all scenarios with one exception – the substantial increase in maximum individual vector brine flow up the intrusion borehole for S4-BF (details shown in Day 2019b).

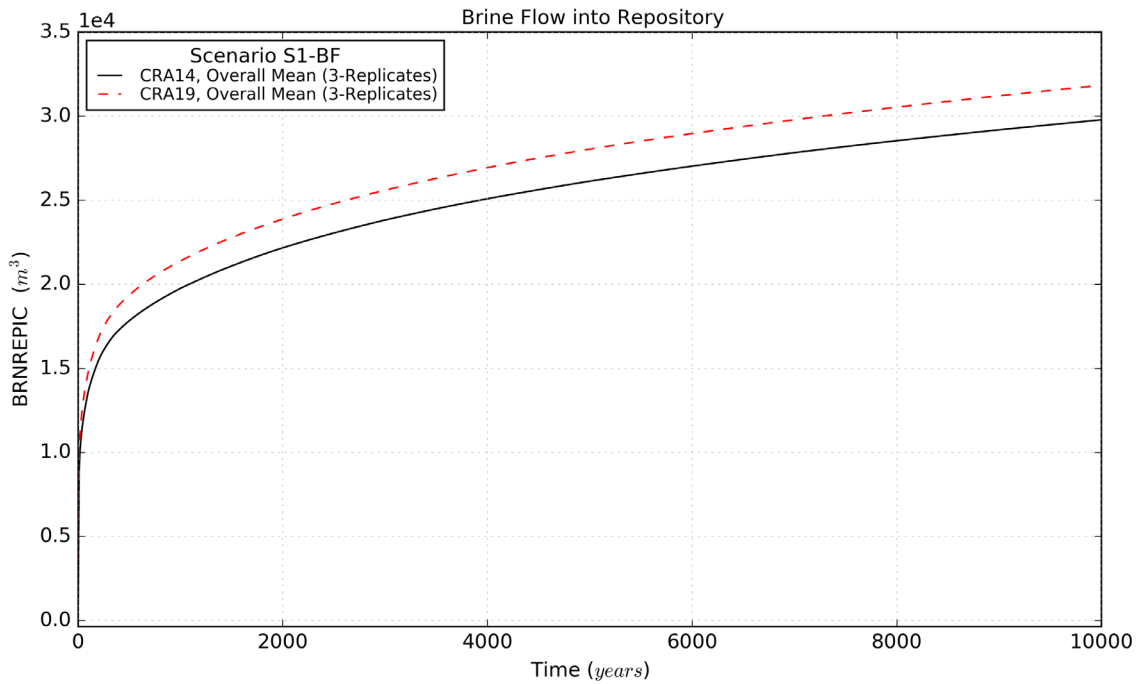


Figure 40 – Brine Flow Means into Repository, Scenario S1-BF

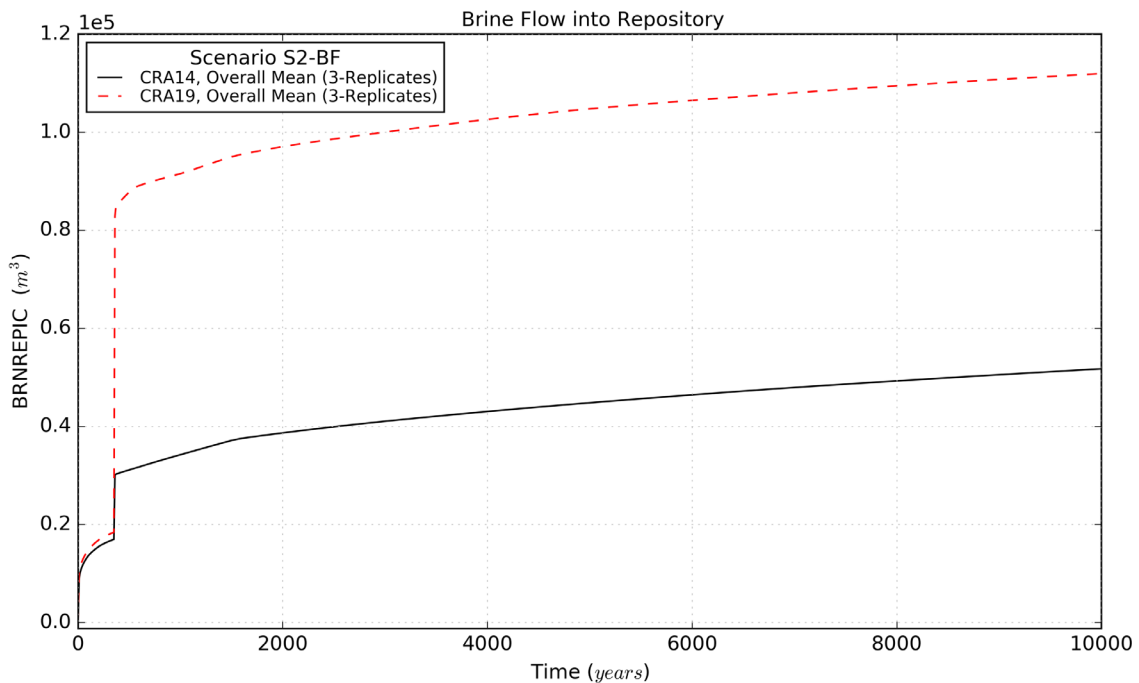


Figure 41 – Brine Flow Means into Repository, Scenario S2-BF

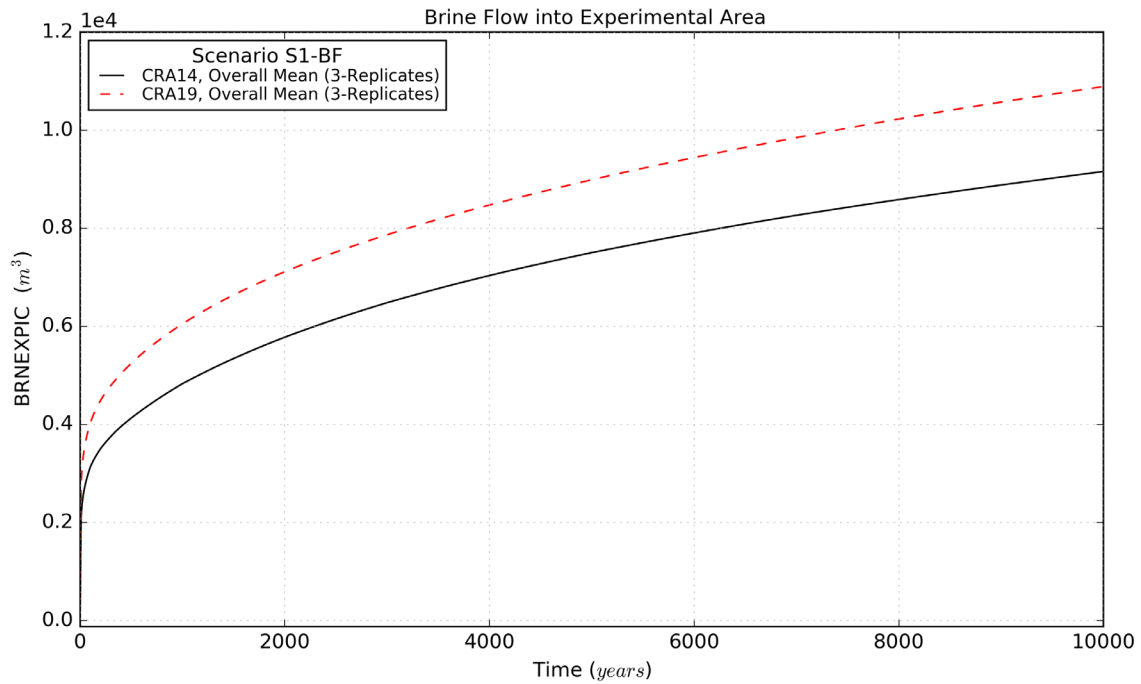


Figure 42 – Brine Flow Means into Experimental Area, Scenario S1-BF

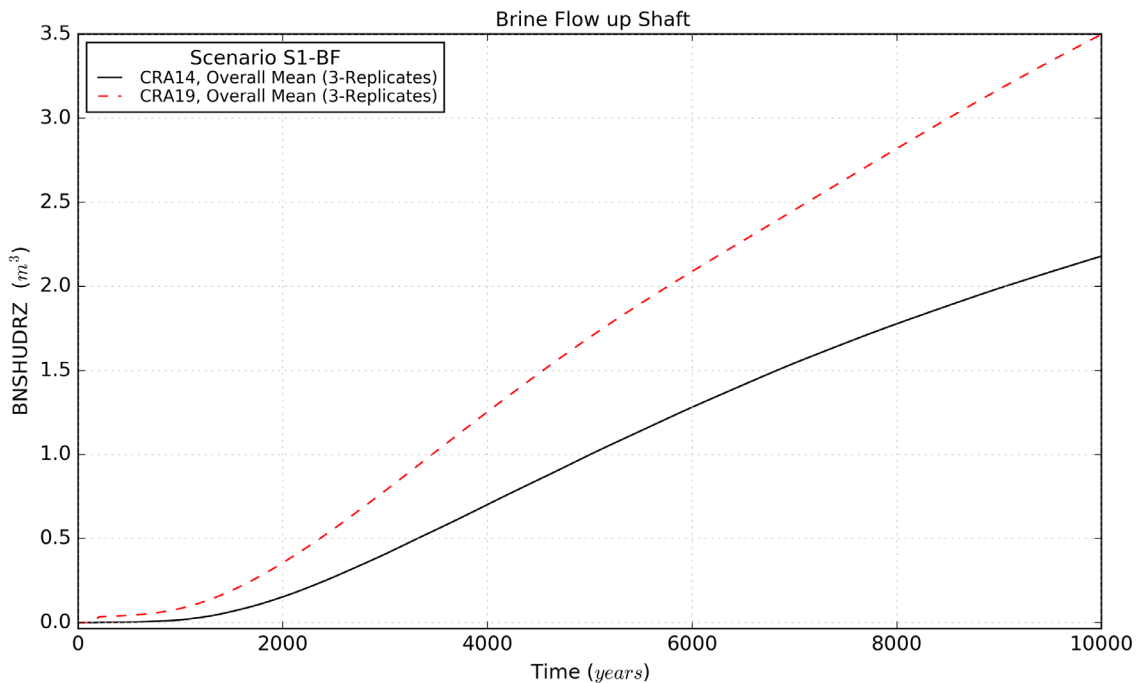


Figure 43 – Brine Flow Means up the Shaft, Scenario S1-BF

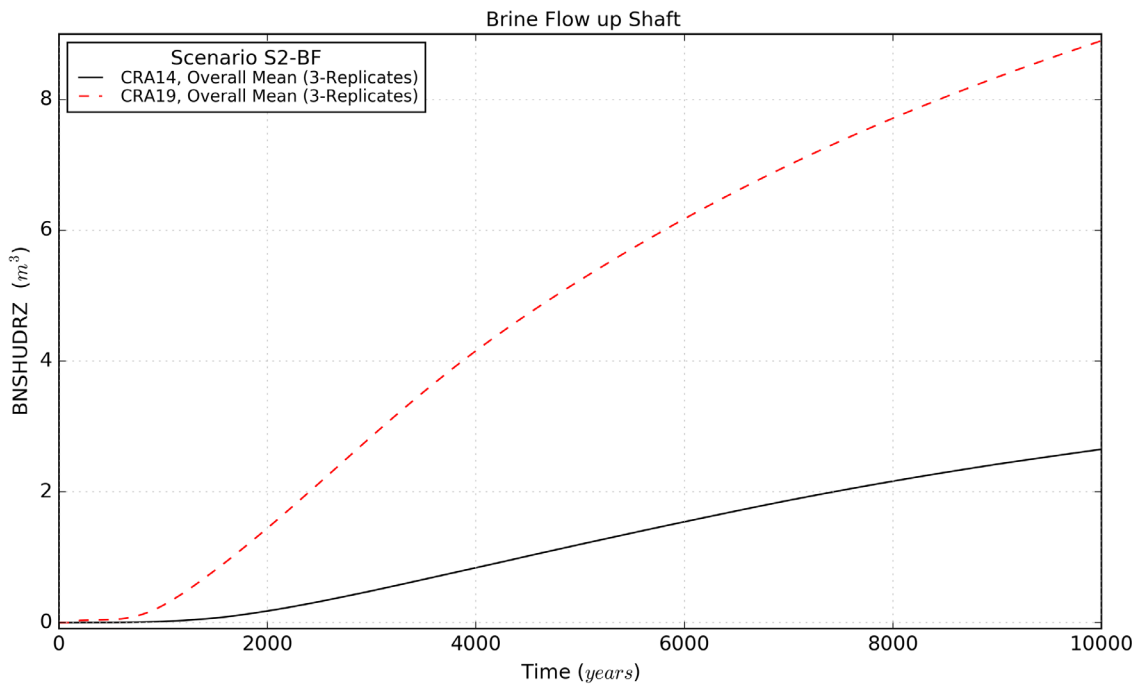


Figure 44 – Brine Flow Means up the Shaft, Scenario S2-BF

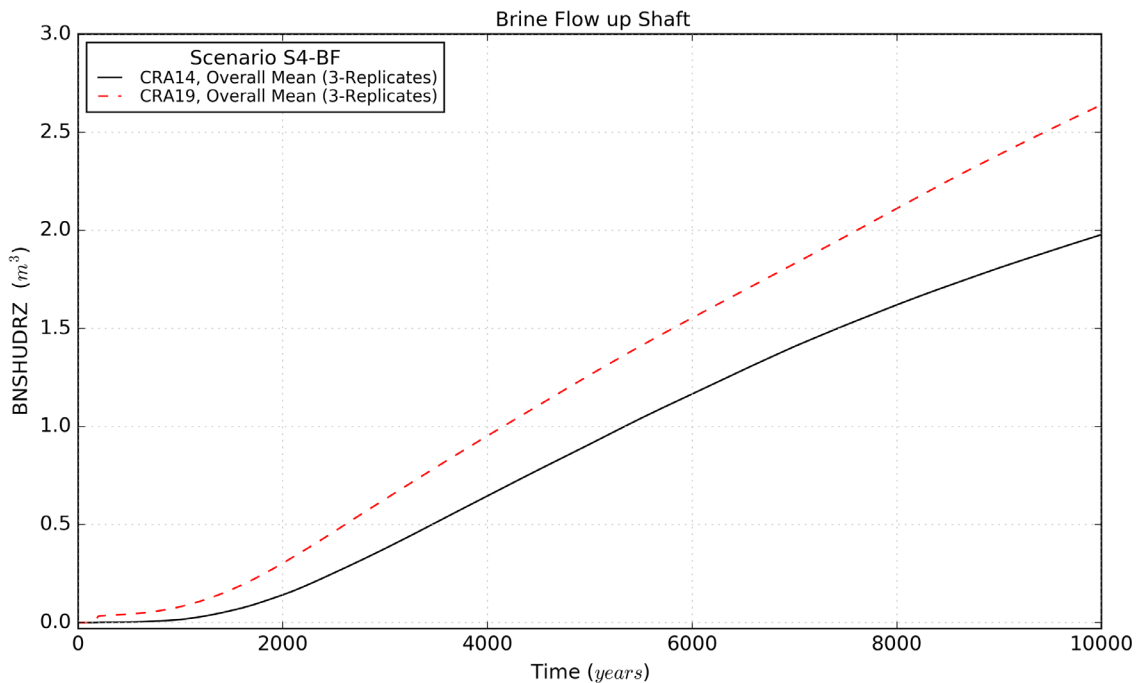


Figure 45 – Brine Flow Means up the Shaft, Scenario S4-BF

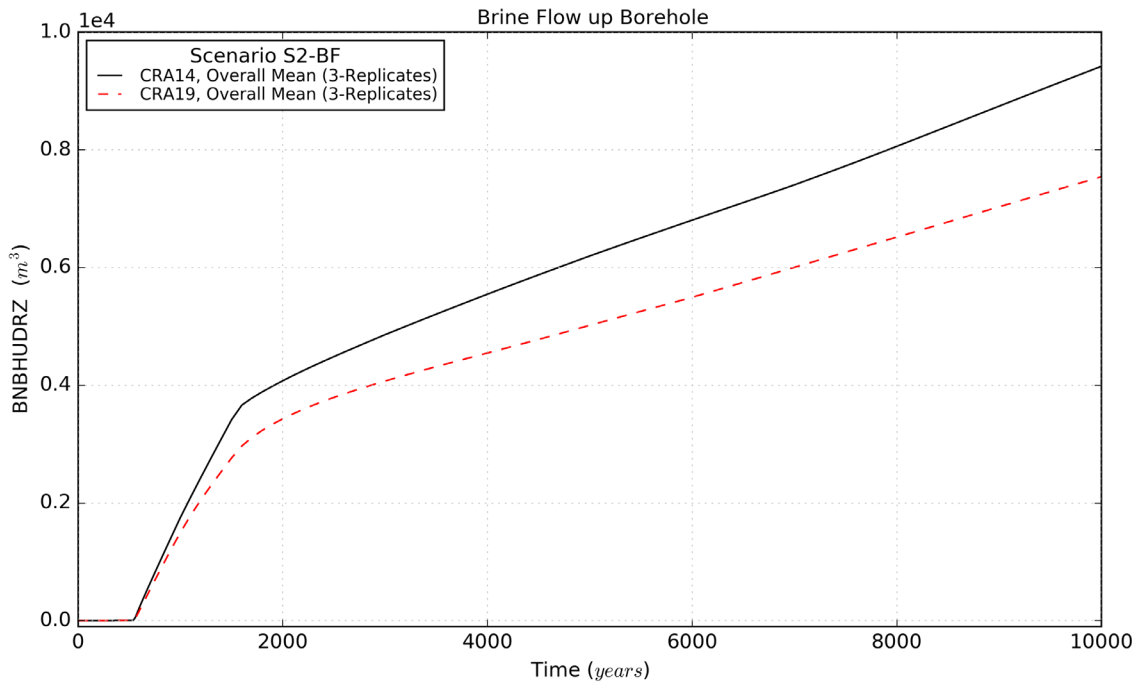


Figure 46 – Brine Flow Means up the Borehole, Scenario S2-BF

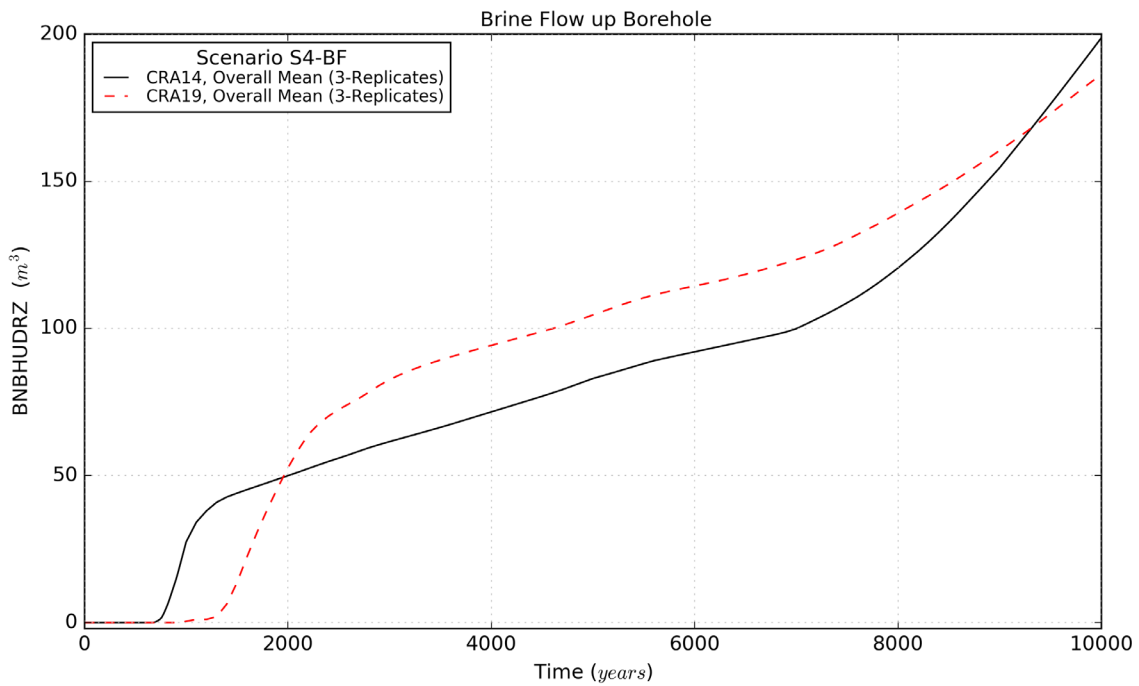


Figure 47 – Brine Flow Means up the Borehole, Scenario S4-BF

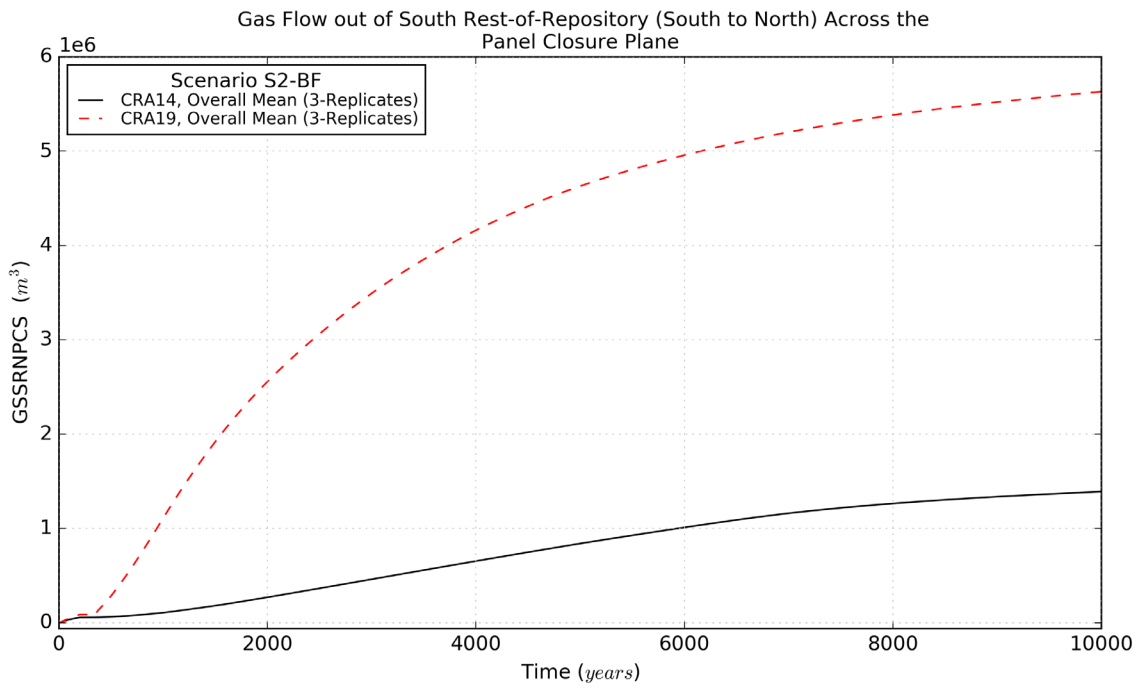


Figure 48 – Gas Flow Means out of South Rest-of-Repository (South to North) Across the Panel Closure Plane, Scenario S2-BF

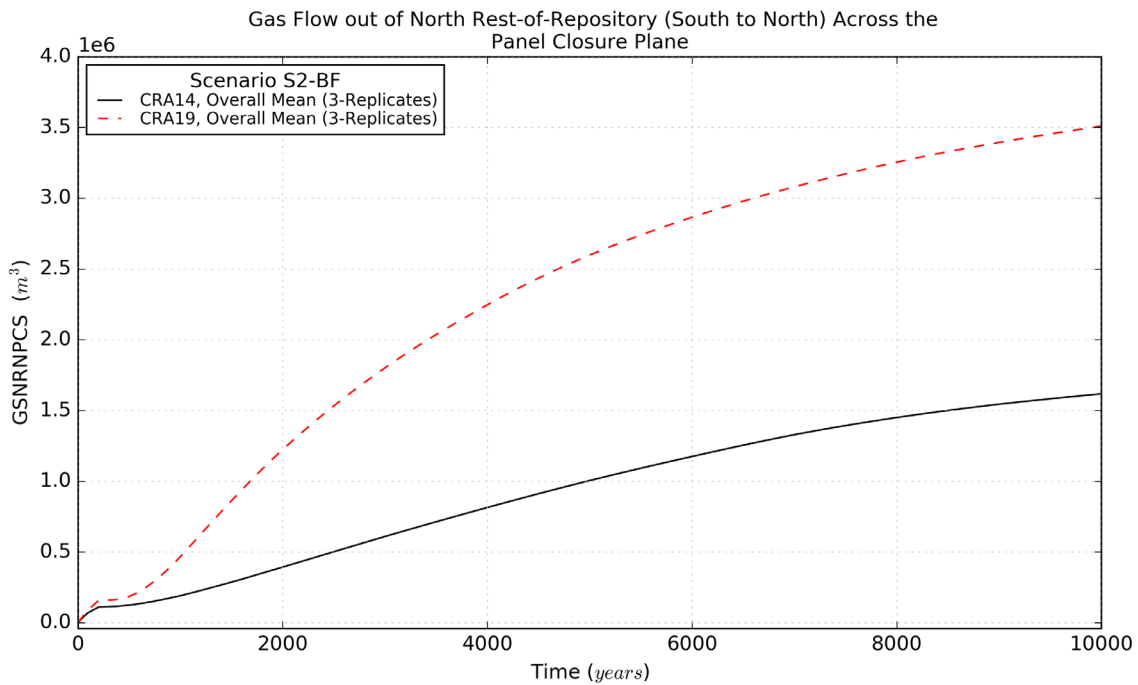


Figure 49 – Gas Flow Means out of North Rest-of-Repository (South to North) Across the Panel Closure Plane, Scenario S2-BF

This page intentionally left blank

Table 25 – Brine Flow Statistics on Overall Means for CRA14 and CRA19

Quantity (units)	Description	Scenario	Mean Value ¹		Maximum Value ²	
			CRA14	CRA19	CRA14	CRA19
BRNREPIC (m ³)	Brine Flow into Repository	S1-BF	2.52E+04	2.70E+04	2.98E+04	3.18E+04
		S2-BF	4.31E+04	1.00E+05	5.18E+04	1.12E+05
		S4-BF	2.69E+04	3.06E+04	3.24E+04	3.78E+04
		S6-BF	3.60E+04	6.00E+04	4.63E+04	7.58E+04
BNSHUDRZ (m ³)	Brine Flow up Shaft	S1-BF	9.94E-01	1.64E+00	2.18E+00	3.50E+00
		S2-BF	1.20E+00	4.76E+00	2.65E+00	8.90E+00
		S4-BF	9.07E-01	1.24E+00	1.98E+00	2.64E+00
		S6-BF	1.07E+00	3.09E+00	2.46E+00	6.81E+00
BNBHUDRZ (m ³)	Brine Flow up Borehole	S1-BF	-	-	-	-
		S2-BF	5.80E+03	4.72E+03	9.42E+03	7.54E+03
		S4-BF	8.51E+01	9.60E+01	1.99E+02	1.86E+02
		S6-BF	5.10E+03	4.17E+03	9.28E+03	7.53E+03

Notes:

- 1 Calculated as the function average (integrated) over the time interval (0-10,000 years) for the overall means (3 replicates)
- 2 Calculated as the function maximum over the time interval (0-10,000 years) for the overall means (3 replicates)

This page intentionally left blank

5.6 Cuttings, Cavings, and Spallings Results

Cuttings, cavings, and spallings are the three separate release modes used to determine the quantity of solid waste brought to the surface as the result of a drilling intrusion through a waste panel. Cuttings designates the waste contained in the cylindrical volume created by the cutting action of the drill bit passing through the waste, cavings designates the waste that erodes from the borehole in response to the upward-flowing drilling fluid within the borehole, and spallings designates the waste introduced into the borehole by the release of waste-generated gas escaping to the lower-pressure borehole. The releases associated with these processes are computed within the CUTTINGS_S code. There were no observed changes to cuttings results. The change included in the CRA-2019 PA that was observed to most substantially affect cavings results as compared to the CRA-2014 PA was:

- Refinement to the effective shear strength of WIPP waste.

Changes included in the CRA-2019 PA that were observed to most substantially affect spallings results as compared to the CRA-2014 PA are (Note: each change is related to the impact on waste area pressures as described in Section 5.5.4):

- The lack of ROMPCS emplacement between Panels 3, 4, 5, 6, and 9, modeled as the southernmost panel closure area, which allows greater communication between the waste panel and the south rest-of-repository and results in increased waste area pressures.
- Addition of 5th shaft and associated access drift volume in the experimental area which increases the cross-sectional area of the shaft and increases void space in the experimental area.
- Increase in the inundated steel corrosion rates and the addition of brine radiolysis which results in an increase in hydrogen gas generation.
- Updates to WIPP waste inventory parameters, including increased iron and cellulose mass, which contributes to increased associated corrosion and biodegradation gas generation.

Overall, the primary impacts of changes for the CRA-2019 PA in comparison to the CRA-2014 PA baseline are identical cuttings areas, similar cavings areas, and increased spallings release volumes. Additional details of the cuttings, cavings, and spallings results from deterministic calculations using the CUTTINGS_S code described by Kicker (2019c) are presented in subsections below. Normalized cuttings, cavings, and spallings releases for stochastically-derived intrusion events calculated by the CCDFGF code are described in Sections 5.9.1 and 5.9.2.

5.6.1 Modeling Scenarios

The CUTTINGS_S code calculates an area for cuttings and cavings and a spillings volume for each combination of replicate, vector, scenario, drilling location¹, and intrusion time (the CCDFGF code calculates releases based on these areas and volumes along with the radionuclide concentrations calculated by the EPAUNI code). PA calculations for direct solids releases (i.e., cuttings, cavings, spillings, and DBRs) are run for the scenarios summarized in Table 26. A total of 23,400 areas (3 replicates × 100 vectors × 3 drilling locations × 26 intrusion times) and 23,400 volumes were determined.

Table 26 – PA intrusion Scenarios Used in Calculating Direct Solids Releases

Scenario	First Intrusion Time and Type	Subsequent Intrusion Times
	Year	Year
S1-DBR	None	100, 350, 1000, 3000, 5000, 10000
S2-DBR	350, E1	550, 750, 2000, 4000, 10000
S3-DBR	1000, E1	1200, 1400, 3000, 5000, 10000
S4-DBR	350, E2	550, 750, 2000, 4000, 10000
S5-DBR	1000, E2	1200, 1400, 3000, 5000, 10000

Notes: For the first intrusions in each scenario, the repository conditions are obtained from BRAGFLO intrusion scenarios. An E1 intrusion scenario is defined as an intrusion into the repository that creates a pathway to a pressurized brine pocket below the repository. An E2 intrusion scenario is defined as an intrusion into the repository that does not create a pathway to a pressurized brine pocket below the repository.

5.6.2 Cuttings Area Results

The solid material removed from the repository and carried to the surface by the drilling fluid during the process of drilling a borehole is comprised of cuttings and cavings components. The volume of cuttings removed and transported to the surface in the drilling mud corresponds to the drill bit area and height of waste, each of which are constant in PA calculations. Therefore, cuttings results for the CRA19 analysis are identical to those from the CRA14 analysis (Kicker 2019b).

5.6.3 Cavings Area Results

WIPP PA estimates cavings removal with a model based on the effect of shear stress on the material located adjacent to the edge of the borehole. The uncertain parameter BOREHOLE:TAUFAIL is used to represent the effective shear strength for erosion of WIPP waste. Subsequent to the submittal of the CRA-2014, the EPA requested that the DOE reconsider the subset of the Herrick data to be included in the TAUFAIL distribution, including

¹ Drilling location refers to the waste panel, south rest-of-repository, and north rest-of-repository and is further discussed in Section 5.7.

lowering the lower bound of the distribution and therefore a relatively small change to the parameter distribution (the mean decreased from 39.61 to 39.30 Pa) was implemented for use in the CRA-2019 PA (Section 1.1.6).

The analysis performed by Kicker (2019b) showed that cavings area results for the CRA19 analysis are overall similar to those from the CRA14 analysis, with differences attributed to decreasing the lower bound of the TAUFAIL distribution (Figure 50 (Figure 2 from Kicker 2019b)). The change in the parameter distribution did not change the mean cavings areas much, but did serve to increase maximum cavings areas.

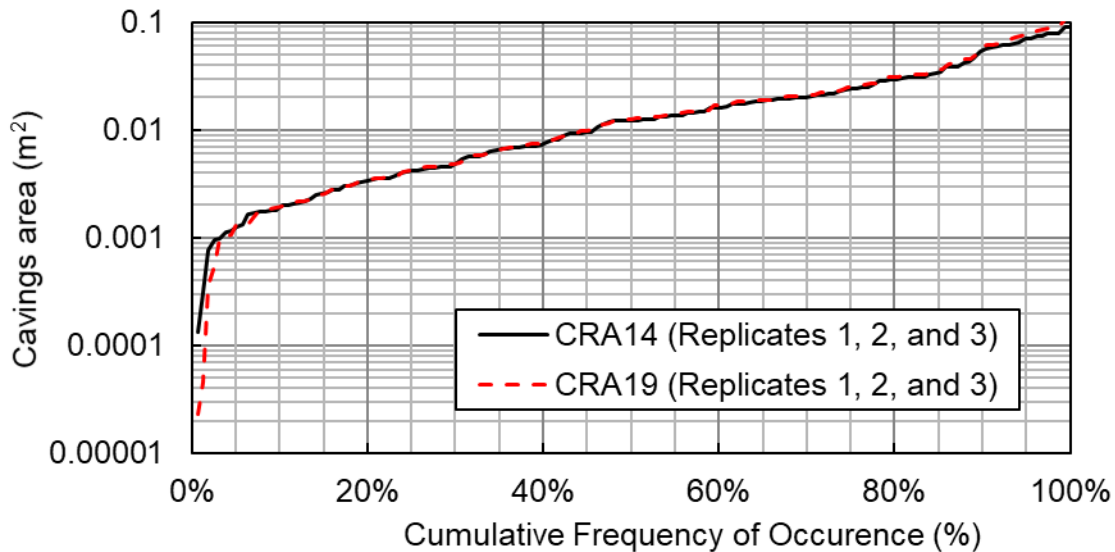


Figure 50 – Cumulative Frequency of Cavings Areas

5.6.4 Spallings Volume Results

The change in spallings volumes between the CRA19 and CRA14 is the result of changing repository pressures observed in BRAGFLO calculations for the CRA-2019 PA (Section 5.5).² Waste area pressures are generally increased for the CRA19 analysis, as discussed in Section 5.5. Because spallings volumes directly depend on waste area pressures, an increase in waste area pressures translates into larger spallings volumes. Since there is a minimum threshold pressure of 10 MPa required to create spallings (Kicker 2019b), an increase in repository pressure also increases the percentage of vectors with nonzero spallings volumes.

² The CRA14 analysis results used for comparison in this section and throughout this report are the CRA14 (Rev. 2) analysis results from Kirchner et al. (2015), which included the correction of an error in the DRSPALL code. The correction of that error resulted in increased spallings releases upon rerunning the CRA-2014 PA calculations for the CRA14 (Rev. 2) analysis. The increased spallings releases observed for the CRA19 analysis are therefore not due in any part to the correction of the DRSPALL code.

5.6.4.1 Overall Spallings Volumes

The cumulative frequency of spallings volumes for CRA19 and CRA14 (replicates 1, 2, and 3) is shown in Figure 51 (Figure 7 from Kicker 2019b). This figure provides a summary of spallings results from all scenarios, repository regions, and times. Figure 51a considers only those simulations in which nonzero spallings occur, showing that the cumulative distributions of nonzero spallings volumes for the CRA19 and CRA14 analyses are similar, with larger CRA19 spallings volumes compared to CRA14 at corresponding cumulative frequency levels. Figure 51b considers all simulations, including those that result in zero spallings volumes and shows that the CRA19 cumulative distribution of spallings volumes is quite different from the CRA14 results. The shift in the cumulative frequency of occurrence curve for the CRA19 spallings volumes (Figure 51b) is the result of more simulations with nonzero spallings, which is due to increased waste area pressures.

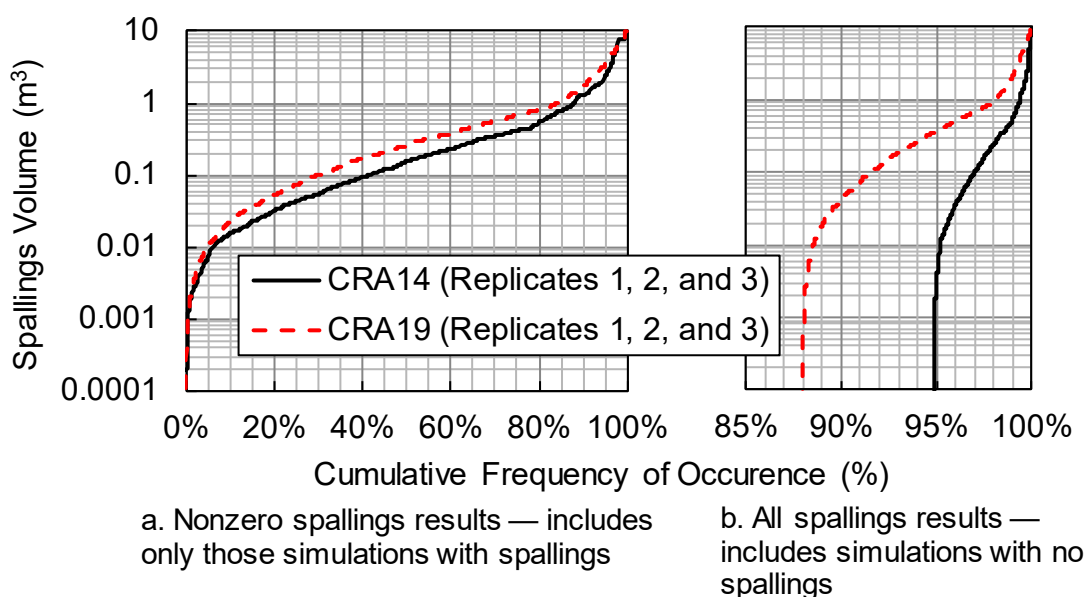


Figure 51 – Cumulative Frequency of Spallings Volumes

5.6.4.2 Spallings Volumes by Scenario

Summary statistics of spallings volumes for the solids release intrusion scenarios (Table 26) are shown in Table 27 (Table 6 from Kicker 2019b) for the CRA19 and CRA14 analyses. Results presented in that table are combined for all replicates, times, vectors, and drilling locations. The maximum spallings results for the CRA19 and CRA14 analyses are similar for all five scenarios. The average spallings release volume for the CRA19 analysis has increased by 15% for the previously undisturbed scenario (S1-DBR). For scenarios with E1 intrusions (S2-DBR and S3-DBR), the average spallings release volumes for the CRA19 analysis have increased by 27% to 54%. For the scenarios with E2 intrusions (S4-DBR and S5-DBR), the average spallings release volumes for the CRA19 analysis have decreased by 5% to 8%. However, there is an increase in the number of nonzero spallings in the CRA19 analysis compared to the CRA14 analysis across all scenarios.

Table 27 – Summary of Spallings Volumes by Scenario

Scenario	Maximum Volume (m ³)		Average Nonzero Volume (m ³)		Number of Nonzero Volumes (Percentage of Realizations that Result in a Nonzero Spallings Volume)	
	CRA14	CRA19	CRA14	CRA19	CRA14	CRA19
S1-DBR	7.47	7.47	0.63	0.72	200 (3.7%)	258 (4.8%)
S2-DBR	9.84	10.23	0.54	0.83	473 (10.5%)	1254 (27.9%)
S3-DBR	9.80	10.23	0.54	0.68	329 (7.3%)	1063 (23.6%)
S4-DBR	7.47	7.47	0.62	0.59	86 (1.9%)	105 (2.3%)
S5-DBR	7.47	7.47	0.61	0.56	109 (2.4%)	135 (3.0%)

5.6.4.3 Spallings Volumes by Drilling Intrusion Location

Summary statistics of spallings volumes for the three drilling intrusion locations are shown in Table 28 (Table 7 from Kicker 2019b) for the CRA19 and CRA14 analyses. Results presented in that table are combined for all replicates, times, vectors, and scenarios. For the CRA19 analysis, maximum and average nonzero releases have increased for all locations (except average nonzero volumes in the NROR) and are largest (and nearly identical) for intrusions into the WP (Lower Region) and SROR (Middle Region). Nonzero volumes from intrusions into the NROR (Upper Region) are only slightly smaller in magnitude compared to the other locations, but only occur at about half the frequency of the other locations. The average nonzero volumes in the Lower and Middle regions have increased 10% to 54% compared to CRA14, while the average volume in the Upper Region has slightly decreased by 4%. Spallings volumes for the Lower and Middle Regions are similar for the CRA19 analysis due to the removal of the southernmost panel closure, which has allowed for equilibration of pressures between the WP and SROR (Section 5.5.4). The percentages of realizations with nonzero volumes has increased for all locations. Further details regarding the locations of repository sub-regions and repository pressures are discussed in Section 5.5.

Table 28 – Summary of Spallings Volumes by Intrusion Location

Intrusion Location	Maximum Volume (m ³)		Average Nonzero Volume (m ³)		Number of Nonzero Volumes (Percentage of Realizations that Result in a Nonzero Spallings Volume)	
	CRA14	CRA19	CRA14	CRA19	CRA14	CRA19
Lower Region (Waste Panel)	9.84	10.23	0.49	0.76	770 (9.9%)	1135 (14.6%)
Middle Region (South Rest-of-Repository)	7.47	10.23	0.68	0.75	240 (3.1%)	1128 (14.5%)
Upper Region (North Rest-of-Repository)	7.47	9.85	0.73	0.71	187 (2.4%)	552 (7.1%)

5.7 Direct Brine Release Volume Results

If the WIPP repository were to be penetrated by a borehole while under conditions of sufficient repository brine pressure and saturation, brine could migrate up through the intruding borehole to reach the land surface. Such an event is defined as a direct brine release (DBR). The BRAGFLO DBR analysis uses the BRAGFLO code to numerically evaluate the volumetric flux of brine that enters the borehole over the duration of the release.

As defined for WIPP PA, minimum pressure and saturation conditions must exist within the waste panel for brine to flow to the surface during an intrusion and produce a DBR. Pressure in the intruded waste panel must be great enough to overcome the static pressure exerted by a column of drilling fluid at the repository depth, assumed to be equal to 8 megapascals (MPa). Brine saturation in the intruded waste panel must be above the residual brine saturation of the waste (a sampled parameter), i.e., the brine must be mobile.

The change included in the CRA-2019 PA that was observed to most substantially affect direct brine release volume results as compared to the CRA-2014 PA was:

- The lack of ROMPCS emplacement between Panels 3, 4, 5, 6, and 9, modeled as the southernmost panel closure area, which allows greater communication between the waste panel and the south rest-of-repository.

(Note: the many changes observed to impact brine pressure (Section 5.5.4) and saturation (Section 5.5.5) also impacted DBR volume results.) Overall, the primary impacts of changes for the CRA-2019 PA in comparison to the CRA-2014 PA baseline are substantially higher average DBR event magnitudes and nonzero frequencies, and higher maximum DBR volumes. These changes are driven by higher pressures throughout the BRAGFLO DBR modeling domain, and substantially higher saturations in the middle intrusion locations. The increases are accounted for primarily in the scenarios that simulate the effects of a hydraulic connection between a

hypothetical brine reservoir underlying the repository and the lower intrusion region. Average DBR volumes from both the lower and middle intrusion locations increased by a similar magnitude, but because middle intrusion events had previously produced much smaller DBR volumes than lower intrusion events, the increase in the middle intrusion DBR volumes represents a much more substantial relative change. Additional details of the BRAGFLO DBR simulations and results described by Bethune (2019a) are given in subsections below.

5.7.1 Repository Representation in BRAGFLO

The BRAGFLO_DBR model explicitly represents the vicinity of the waste panels, including specific repository features such as individual panels and panel closures, in a 2-dimensional rectilinear grid. Like the BRAGFLO Salado Model, the grid dips 1° to the south. The DBR numerical grid and material map used in the CRA-2019 PA calculations are shown in Figure 52 (Figure 1 from Bethune 2019a). Relative to the CRA-2014 DBR grid, the CRA-2019 grid has replaced eight of the panel closures in the south end of the mine with the material PCS_NO, a material intended to capture the absence of panel closures (Zeitler et al. 2017). The same three drilling locations considered in the CRA-2014 PA are considered in the CRA-2019 PA, namely: upper (up-dip), middle, and lower (down-dip) locations. They are also shown in Figure 52.

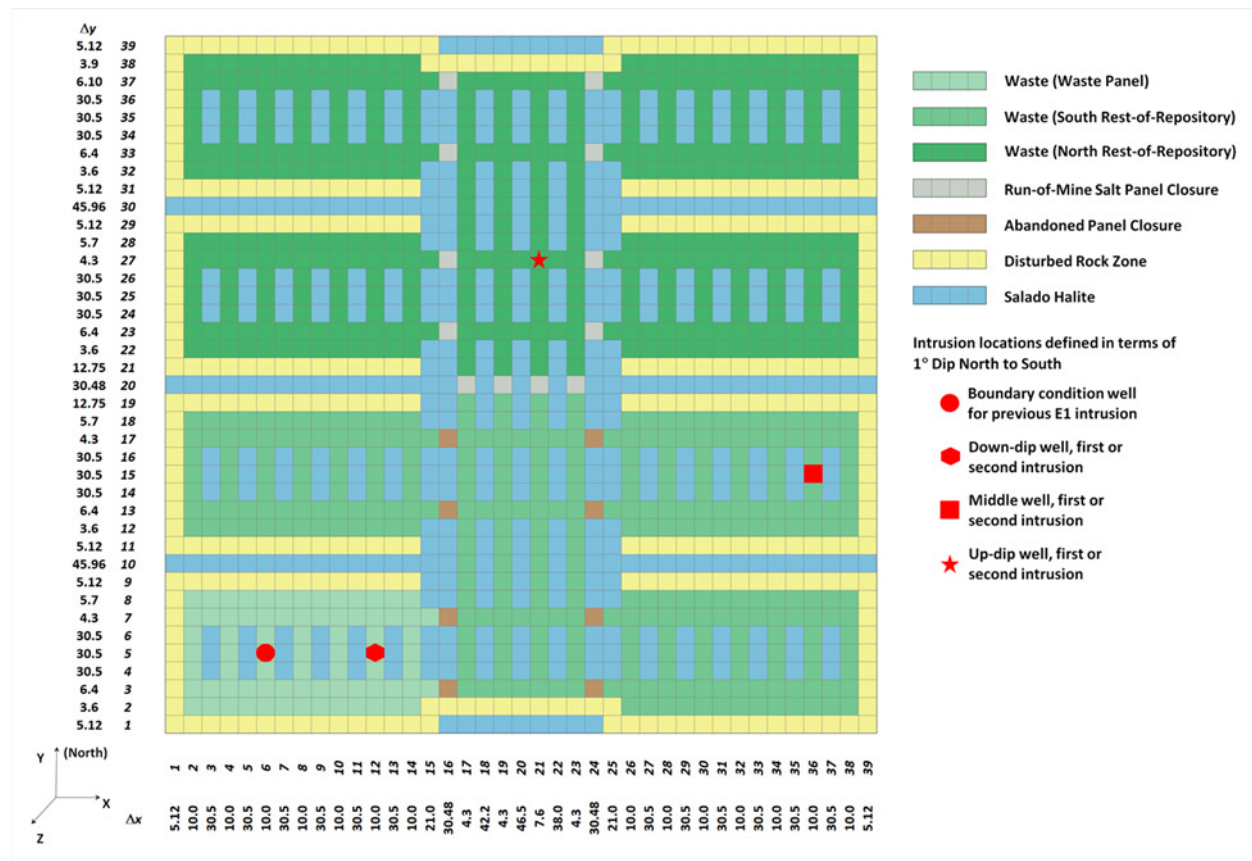


Figure 52 – CRA-2019 PA DBR Grid with Simulated Intrusion Locations

5.7.2 Modeling Scenarios

Volume averaged brine pressures and brine saturations are calculated during the BRAGFLO Salado simulations (Day 2019), interpolated to the DBR intrusion times in the CUTTINGS_S code (Kicker 2019), and then used as initial conditions in the DBR simulations. PA calculations for direct releases (i.e., cuttings, cavings, spillings, and DBRs) are run for the scenarios summarized in Table 26. A total of 23,400 DBR volumes (3 replicates \times 100 vectors \times 3 drilling locations \times 26 intrusion times) were determined.

5.7.3 Initial Conditions for DBRs

CRA19 DBR mean initial conditions are presented in Table 29 (Table 9 from Bethune 2019a) with CRA14 values for comparison. Boxplots of initial pressure (Figure 53 (Figure 9 from Bethune 2019a)³) and saturation (Figure 54 (Figure 10 from Bethune 2019a)) are also shown below with all intrusion values included in the distributions.

Average CRA19 initial brine pressures for DBR events have risen relative to CRA14 in scenario S2-DBR in both the lower and middle intrusion locations.⁴ In both analyses, most lower intrusions encounter pressure conditions above the 8 MPa⁵ threshold for a DBR. Average initial pressure in the middle intrusion is substantially higher in CRA-2019 relative to CRA-2014. The distribution of pressure in the middle location has shifted up, such that the median values are above all but the outliers of the CRA-2014 values. This shift has resulted in more CRA-2019 initial pressure values above the 8 MPa threshold for a DBR event than there were in CRA-2014.

Brine saturations show two distinct trends in the lower and middle locations. In the lower location, brine saturation is decreased slightly relative to CRA-2014, with a slightly decreased median value and lower outlier values (Figure 54 (Figure 10 from Bethune 2019a)). Brine saturation in the lower location in both analyses is high though, and the difference between them is on average relatively small. Average saturation in the middle location is much higher in CRA-2019 than CRA-2014, and the entire distribution of values has shifted up and shows greater spread about the median. The average saturation values are decreased at later intrusion times, but remain much higher than the CRA-2014 values, and the distribution becomes wide enough to span nearly the entire range of possible values.

In general, the initial conditions of the middle location are more similar to the lower location in CRA-2019 than they had been in CRA-2014. In CRA-2014 the pressures of the middle location are on average more than 8 MPa below those of the lower location in the 550-year intrusions,

³ Results are presented in boxplots which graphically depict the distribution of the data by drawing boxes around the 25th and 75th percentiles of the distribution with a bisecting line at the median. The box whiskers extend out from the box an additional $1.5 \times (Q_{75} - Q_{25})$ or to the full range of the data, whichever is closer to the median. All datapoints used to derive the boxplot are also plotted on top of the boxplot for visualization of any outliers. Note that intrusion time is treated categorically when used as an axis on the boxplots in this section.

⁴ For the CRA-2014 PA, DBR initial conditions (i.e., brine pressures and saturations) were derived independently of radionuclide inventory and mobilized concentration. Due to the introduction of brine radiolysis to the gas generation model implemented in the Salado flow calculations from which DBR initial conditions are derived for the CRA-2019 PA, there is now some influence of radionuclide inventory and mobilized concentrations on DBRs.

⁵ Bethune (2019) incorrectly states the threshold as 6 MPa.

and are still on average more than 1.5 MPa below those of the lower location in the 10,000-year intrusions. In CRA-2019, on the other hand, pressures in the middle location remain within 0.5 MPa of the lower location at all simulated intrusion times (this can be attributed to the increased communication between the waste panel and south rest-of-repository as a result of the abandoned plan to emplace panel closures in the south end of the repository (Section 5.5)). Saturation values are similarly closer in the lower and middle locations in CRA-2019 than they are in CRA-2014. In CRA-2014, the saturations of the middle location are on average 0.80 below those of the lower location in the 550-year intrusions, and become even further apart at late-time intrusions. In CRA-2019, saturations in the middle location remain within 0.10 to 0.31 of the lower location at all simulated intrusion times.

Table 29 – S2-DBR Mean Initial Conditions, Lower and Middle Locations

Location Time	Brine Pressure (MPa)			Brine Saturation (-)		
	CRA14	CRA19	Change	CRA14	CRA19	Change
L	9.44	10.17	0.74	0.91	0.87	-0.04
550	9.76	9.17	-0.59	0.92	0.89	-0.03
750	10.40	10.18	-0.22	0.91	0.90	-0.01
2000	9.99	10.94	0.95	0.90	0.87	-0.03
4000	9.02	10.59	1.58	0.90	0.84	-0.06
10000	8.02	9.99	1.97	0.91	0.83	-0.07
M	3.59	10.14	6.55	0.10	0.67	0.56
550	1.43	9.14	7.72	0.12	0.79	0.68
750	1.80	10.14	8.34	0.12	0.78	0.66
2000	3.44	10.90	7.47	0.11	0.68	0.57
4000	4.90	10.56	5.67	0.09	0.56	0.47
10000	6.39	9.95	3.56	0.07	0.52	0.44
Average	5.39	8.85	3.46	0.37	0.53	0.16

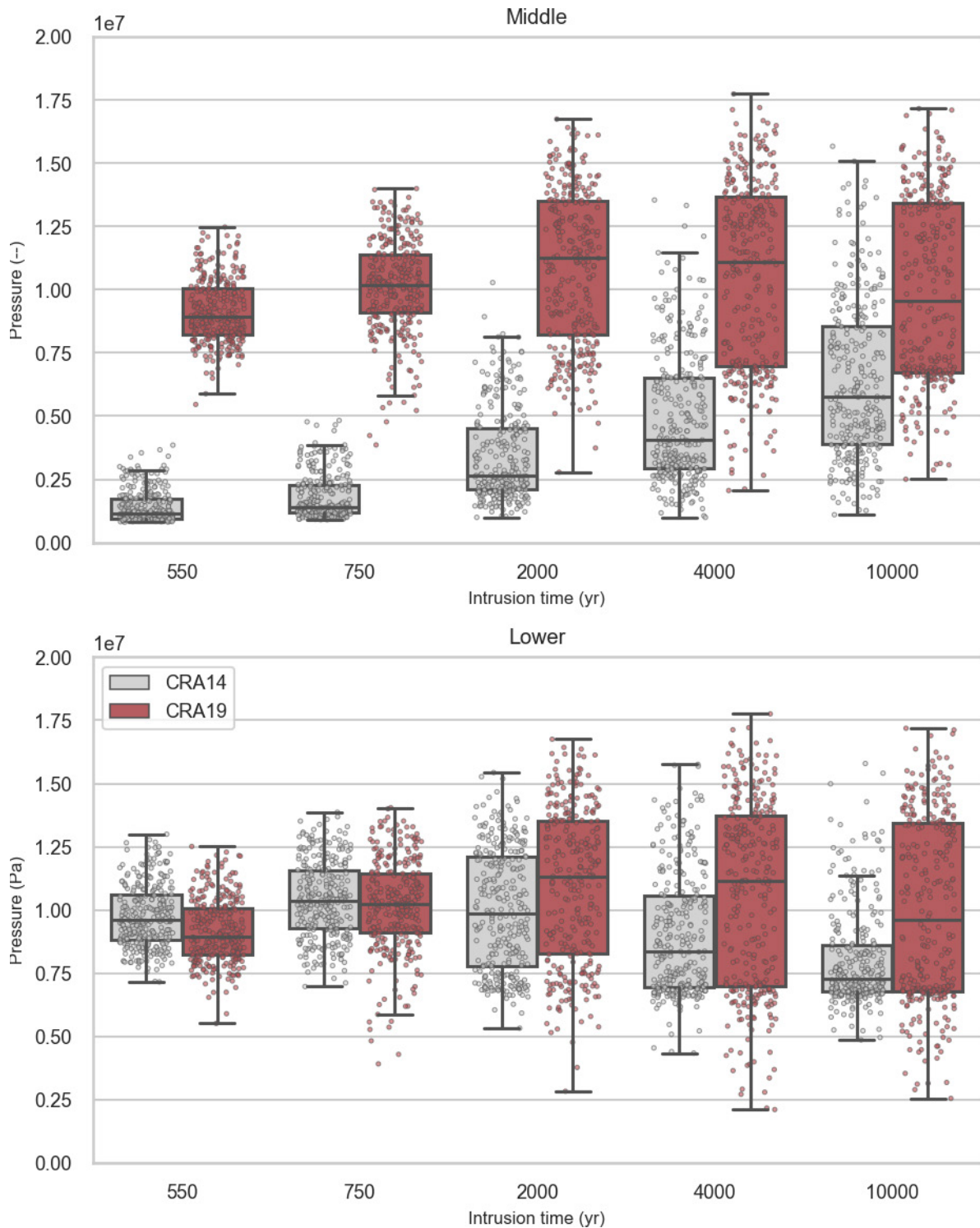


Figure 53 – S2-DBR Brine Pressure, All Lower and Middle Intrusions

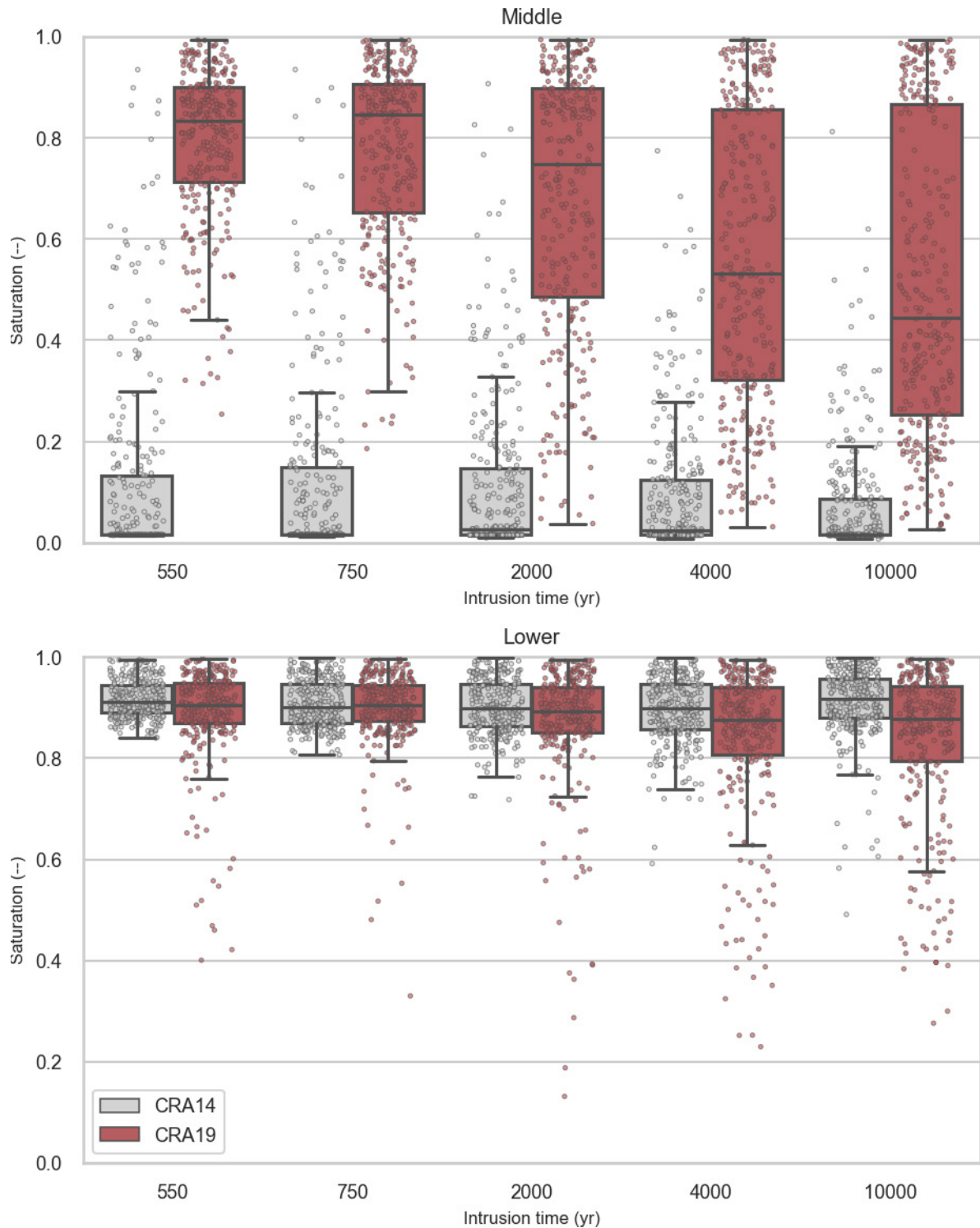


Figure 54 – S2-DBR Brine Saturation, All Lower and Middle Intrusions

5.7.4 DBR Volumes

As a result of the changes to initial conditions relative to CRA-2014, nonzero DBR volumes increased in both mean magnitude and frequency, resulting in increases to the overall mean DBR volume (Table 30 (Table 4 from Bethune 2019a)). Releases of all magnitude increased in frequency (Figure 55 (Figure 4 from Bethune 2019a)), and maximum DBR volumes have also increased (seen in the outliers of Figure 56 (Figure 5 from Bethune 2019a)). Despite the increases, only 18% of modeled intrusions produce nonzero⁶ DBRs, and less than 15% of modeled intrusions produce DBR events greater than 1.00 m³.

While mean DBR volumes increased in all scenarios, the increases were most substantial in S2-DBR and S3-DBR (Figure 57, Figure 7 from Bethune 2019a, shows results for S2-DBR; results for S3-DBR are similar). Releases from scenarios S2-DBR and S3-DBR had already represented the majority of total release volume (together 93.4% in CRA-2014), and with the increases noted above, now represent an even greater proportion (96.4% in CRA-2019). These results show that the majority of the non-zero DBR volumes occur when there is a previous E1 intrusion, as has been observed previously (Clayton et al. (2010); Pasch and Camphouse (2011), and Malama (2013)).

Lower intrusions continue to produce the largest average release volumes, but relatively larger increases to the average Middle release volumes result in Middle intrusions representing a greater proportion of the total release volumes (from 3.0% in CRA-2014, 33.6% in CRA-2019). Releases from the upper location have decreased slightly, both in frequency and magnitude.

The DBR volume analysis also revealed that at low saturations, DBR intrusions are more sensitive to panel saturation than they are to pressure, but once saturation increases enough to produce a brine dominated flow regime, panel saturation becomes much less important than panel pressure. Fully saturated panels are sensitive to both panel saturation and panel pressure.

⁶ For consistency with previous analyses, in calculating average non-zero DBR volumes and rates, non-zero volumes are defined as volumes that are greater than 10⁻⁷ m³. Tabulated results are rounded to two decimal places.

Table 30 – DBR Volume Summary

Intrusion	Mean Brine Released (m ³)			Nonzero Release Rate			Mean Non-Zero (m ³)		
	CRA14	CRA19	Diff.	CRA14	CRA19	Diff.	CRA14	CRA19	Diff.
S1-DBR	0.15	0.26	0.10	4%	3%	-2%	3.80	10.11	6.31
Lower	0.37	0.70	0.33	7%	5%	-1%	5.56	12.87	7.31
Middle	0.08	0.07	-0.02	3%	1%	-2%	2.54	5.62	3.08
Upper	0.01	0.00	-0.01	2%	1%	-1%	0.49	0.30	-0.19
S2-DBR	3.31	8.29	4.97	25%	47%	22%	13.12	17.55	4.43
Lower	9.84	15.64	5.80	70%	74%	4%	14.10	21.27	7.18
Middle	0.09	9.21	9.12	4%	66%	62%	2.63	13.94	11.31
Upper	0.01	0.00	-0.01	2%	2%	0%	0.43	0.15	-0.28
S3-DBR	2.14	5.23	3.09	22%	40%	19%	9.79	12.94	3.15
Lower	6.32	10.83	4.52	59%	67%	8%	10.75	16.27	5.52
Middle	0.10	4.86	4.76	4%	53%	49%	2.47	9.19	6.72
Upper	0.01	0.00	-0.01	3%	2%	-1%	0.44	0.22	-0.22
S4-DBR	0.09	0.07	-0.02	2%	1%	-1%	3.82	7.14	3.31
Lower	0.19	0.22	0.04	3%	2%	0%	6.85	9.83	2.98
Middle	0.07	0.00	-0.07	2%	0%	-2%	3.15	0.18	-2.97
Upper	0.01	0.00	-0.01	2%	0%	-2%	0.48	0.01	-0.47
S5-DBR	0.11	0.12	0.02	3%	2%	-1%	3.73	7.70	3.97
Lower	0.22	0.36	0.14	4%	2%	-2%	5.87	10.10	4.23
Middle	0.09	0.01	-0.08	3%	0%	-2%	3.43	1.38	-2.05
Upper	0.01	0.00	-0.01	2%	0%	-2%	0.49	0.01	-0.48
Lower	3.27	5.37	2.09	28%	29%	2%	11.89	18.29	6.41
Middle	0.09	2.72	2.63	3%	23%	20%	2.77	11.65	8.88
Upper	0.01	0.00	-0.01	2%	1%	-1%	0.47	0.18	-0.29
ALL	1.12	2.70	1.57	11%	18%	7%	10.19	15.02	4.83

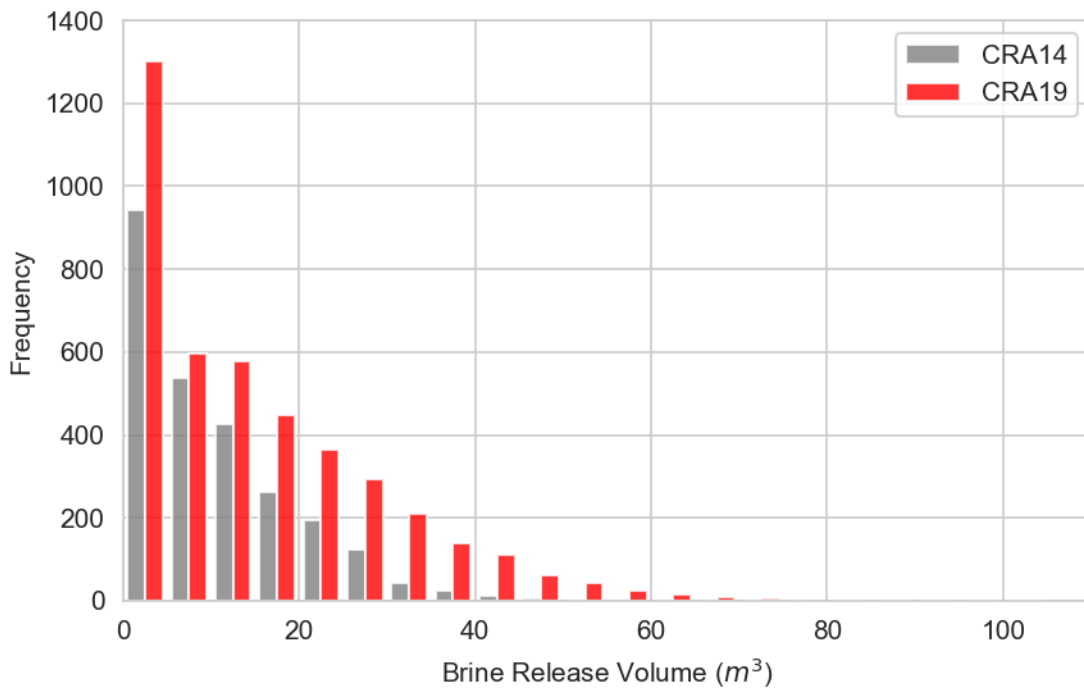


Figure 55 – Release Volume Frequency, All Intrusions

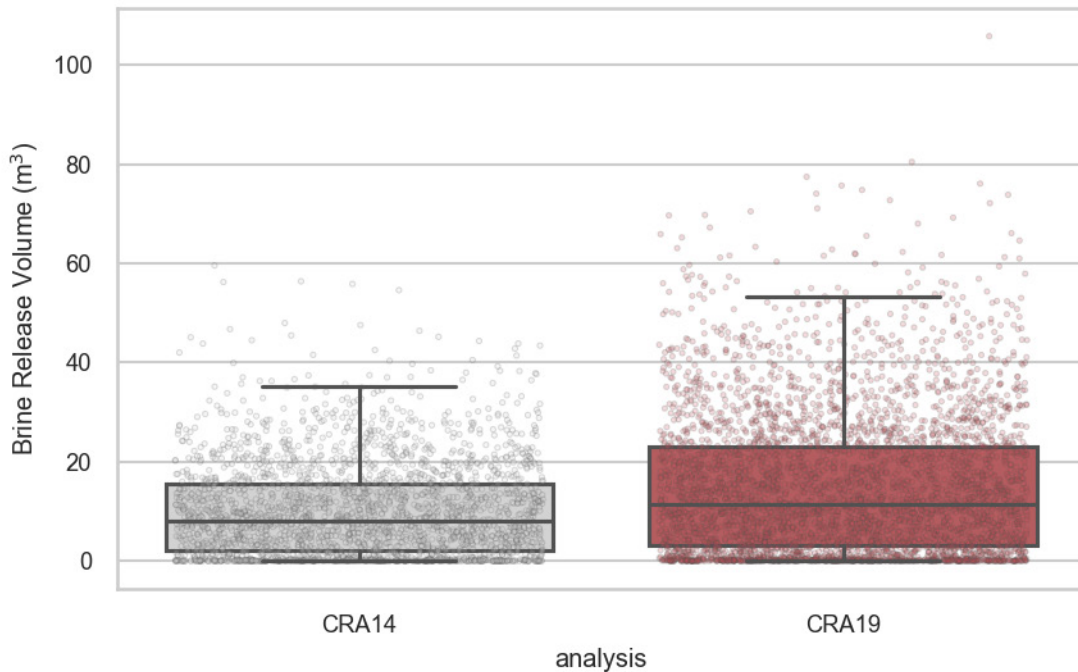


Figure 56 – Release Volume Boxplots, All Nonzero Events

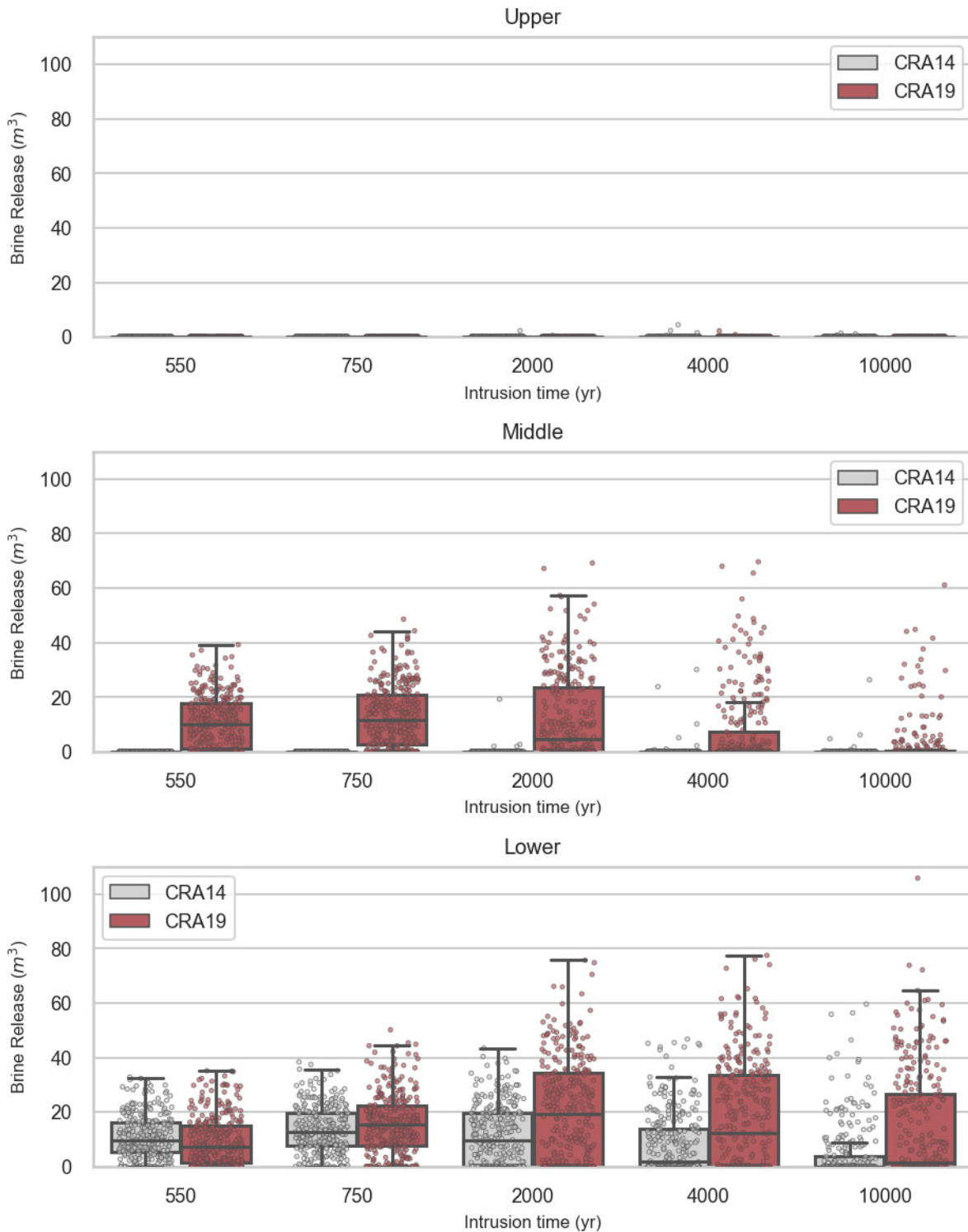


Figure 57 – S2-DBR Release Volumes, All Intrusions

5.8 Salado Transport Results

The NUTS and PANEL codes simulate radionuclide transport in the Salado formation in order to track radionuclides exiting the repository as a function of time over the 10,000 year regulatory compliance period. The cumulative radionuclide discharges through the shaft and borehole are assumed to flow into the overlying Culebra member of the Rustler formation and are used by the CCDFGF code to calculate releases from the Culebra (Section 5.9.4). The Salado transport model is also used to estimate releases through the anhydrite marker beds across the land withdrawal boundary (LWB). The NUTS code performs decay and mass balance calculations using only the five initially lumped radionuclides (see Kicker 2019a for information on radionuclide lumping). This is in contrast to PANEL, which performs decay and mass balance calculations on the full set of 30 individual radionuclides, lumps radionuclides, and then reports the lumped values at each timestep. The total mobile concentration limits presented in Section 5.4.1 are also used in the radionuclide transport simulations.

Changes included in the CRA-2019 PA that were observed to most substantially affect Salado transport results as compared to the CRA-2014 PA are:

- Those changes impacting the Salado flow results, which show decreased brine flow up the intrusion borehole due to reduced average waste panel brine saturations (Section 5.5.6, Figure 46 and Section 5.5.5, Figure 38).
- Decreased total mobile concentration limits for most lumped radionuclides due to updates to colloid enhancement and radionuclide solubility (and solubility uncertainty) parameters.

Overall, the result of changes for the CRA-2019 PA in comparison to the CRA-2014 PA baseline is similar or decreased mean radionuclide discharges across the various disturbed repository scenarios. The undisturbed repository scenario continues to show negligible releases for the CRA-2019 PA. Additional details of the PANEL and NUTS simulations and results of Salado transport calculations described by Sarathi (2019d) are given in subsections below.

5.8.1 Repository Representation and Modeling Scenarios

The NUTS code is used to model radionuclide transport in the Salado for scenarios S1-BF through S5-BF (the BRAGFLO scenarios with zero or one borehole intrusion), and the PANEL code is used for scenario S6-BF (the scenario with a sequence of two borehole intrusions). Both codes rely on BRAGFLO simulation results for brine flux and brine volume data. NUTS uses the same two-dimensional grid as BRAGFLO (Section 5.5.1). PANEL neglects spatial information and simply performs a mass balance calculation over a fixed number of waste panels (one for CRA-2014, five for CRA-2019). The cumulative discharges up the borehole are tabulated and comprise the *to Culebra* discharges. For scenarios 1-5, the radionuclide discharge through the shaft and the radionuclide discharge through the anhydrite marker beds (all three combined) to the LWB are also tabulated.

5.8.2 Transport Results for an Undisturbed Repository

For the undisturbed repository scenario (scenario S1-BF), one vector (replicate 2, vector 1) produced a nonzero discharge up the shaft of $1e-133$ EPA units, which is a small enough number to be within the numerical noise of the calculation methods and thus to be of little or no concern. The maximum (across vectors) discharge through all anhydrite marker beds combined was $3e-10$ EPA units, which is insignificant compared to other release pathways. Thus, calculated long term releases up the shaft and through anhydrite marker beds for an undisturbed repository continue to be negligible for the CRA-2019 PA.

5.8.3 Transport Results for a Disturbed Repository

Figure 58 (Figure 39 from Sarathi 2019d⁷) illustrates the cumulative radionuclide discharge through the intrusion borehole for the disturbed repository scenarios S2-BF through S5-BF (there is no borehole for scenario S1-BF). Figure 59 (Figure 40 from Sarathi 2019d) illustrates the cumulative brine discharge through the borehole (see Section 5.5.6) for these scenarios. Because high consequence radionuclide solubilities are not correlated with high consequence brine discharges, the results are mixed (i.e., small radionuclide releases may result for cases with high solubilities or high brine discharges). Overall, the mean radionuclide discharges are similar for the Castile brine pocket intrusion scenarios (scenarios S2-BF, S3-BF, and S6-BF), but the median has decreased while the high-consequence outliers have increased. A somewhat similar trend is apparent in the brine discharges (though the outliers have slightly decreased). The means and outlier radionuclide discharges for scenarios S4-BF and S5-BF have slightly decreased. However, because there are few simulations in scenarios S4-BF and S5-BF with meaningful brine discharges, the change in radionuclide discharges is likely impacted by this small population size more than other phenomena.

⁷ This section contains boxplots to facilitate visualizing and comparing distributions of results. The convention used in this section is that the “box” bottom and top edges indicate the 25th and 75th percentiles, the box interior line indicates the 50th percentile (median), and the triangle marker indicates the mean. The “whiskers” (the extended vertical lines with horizontal bars) indicate the 2nd and 98th percentiles, and the diamond markers exterior to the bars are discrete outliers (i.e., less than the 2nd percentile or greater than the 98th percentile). Upon occasion, a particular dependent variable is constant (its independent parameters may not be sampled), and the box is collapsed to a single horizontal bar. At the other extreme, some dependent variables may have distributions where the mean is dominated by a few outliers. In those plots, only the top whisker and the outliers are visible – the box would be located below the range of the figure.

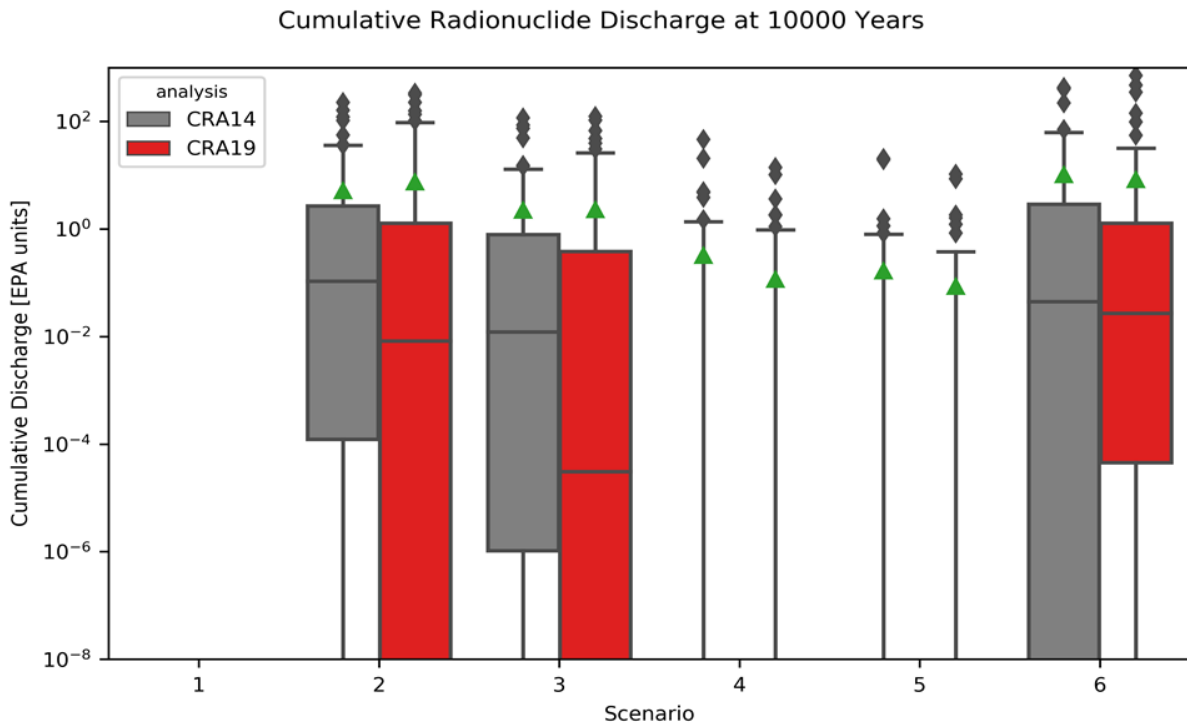


Figure 58 – Cumulative Radionuclide Discharge Up Borehole at 10000 Years

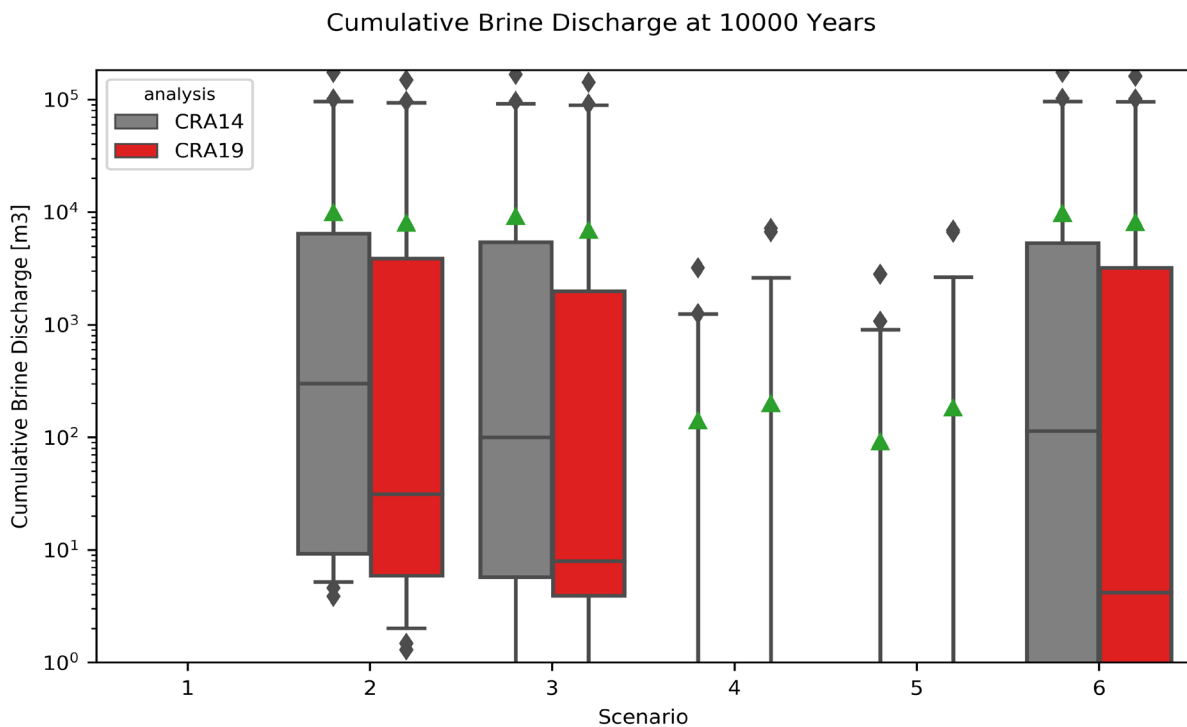


Figure 59– Cumulative Brine Discharge Up Borehole at 10000 Years

Sarathi (2019d) also describes the cumulative radionuclide discharges for each lumped radionuclide across scenarios S2-BF through S6-BF, including horsetail plots of the full time-history of the *to Culebra* cumulative radionuclide discharges to the Culebra that are later used by the CCDFGF code to calculate releases to and from the Culebra (Section 5.9.4). For most simulations, especially in scenarios S2-BF and S3-BF, the majority of the discharge occurs in the first few hundred years after the borehole plug degrades (which occurs 200 years after the intrusion). Notably, the U234L cumulative discharges have increased due to the increase in its isotope-to-element mole fraction. This is important because U(VI) is assumed to have low adsorption (i.e., low linear matrix partition coefficient, K_D) in the Culebra, and thus is more likely to reach the LWB in the Culebra.

5.9 Normalized Releases

This section presents a discussion of normalized releases for each of the four release mechanisms (cuttings and cavings, spallings, DBRs, and releases from the Culebra) that contribute to total normalized releases, followed by a discussion of total normalized releases obtained in the CRA-2019 PA. Normalized releases are calculated with the CCDFGF code, which uses stochastic processes to simulate intrusion events by drilling and the occurrence of mining for natural resources. The CCDFGF code assembles the results from the deterministic models (described above in Sections 5.1 through 5.8) and selects the most appropriate scenario data provided by these models to use as the simulation of a 10,000 year future progresses.

The futures constructed by the CCDFGF code are generated by the random and repeated sampling of: (1) the time between drilling events (derived from the drilling rate, Section 1.1.11); (2) the location of drilling events (among the 10 panels); (3) the activity level of the solid waste penetrated by each drilling intrusion (Section 5.3); (4) the plug configuration of the borehole (Section 1.1.11); (5) the penetration of a Castile brine reservoir (Section 1.1.4); and (6) the occurrence of mining in the disposal system. For the CRA-2019 PA, the drilling rate has increased, increasing the number of borehole intrusions modeled. The mean probability of intersecting pressurized Castile brine has increased, increasing the probability of E1 intrusions; however, the plugging pattern changes have led to a decreased probability of E1 and E2 intrusions (Brunell 2019).⁸

In the results that follow, the overall mean CCDF is computed as the arithmetic mean of the mean CCDFs from each replicate. Normalized releases calculated in the CRA-2019 PA are fully discussed in Brunell (2019). Sensitivities of normalized releases to uncertain parameters used in WIPP PA are documented in a separate report (Zeitler 2019e) and summarized in Section 5.10.

5.9.1 Cuttings and Cavings Normalized Releases

Cuttings and cavings releases are calculated from cuttings areas, cavings volumes, and radionuclide concentrations derived from sampled waste streams. Compared to the CRA14 analysis, the CRA19 analysis cuttings areas are identical (Section 5.6.2) and cavings areas are

⁸ Selection by the CCDFGF code of plug pattern one leads to an E0 scenario, while selection of plug pattern three leads to an E2 scenario. Selection of plug pattern leads to either an E1 or E2 scenario depending on the sampled value of the PBRINE parameter.

overall very similar (Section 5.6.3). Cuttings and cavings concentrations are also similar between the analyses on average (Section 5.3.2), but because of the stochastic nature of waste stream selection in WIPP PA, there are expected differences in radionuclide concentrations among the intrusions for the two analyses. The substantial increase in drilling rate (Section 1.1.11) leads to increases in cuttings and cavings releases due to the increased number of borehole intrusions modeled. Overall, mean cuttings and cavings releases have increased for the CRA19 analysis for all probabilities (Figure 60 (Figure 4 from Brunell 2019)).

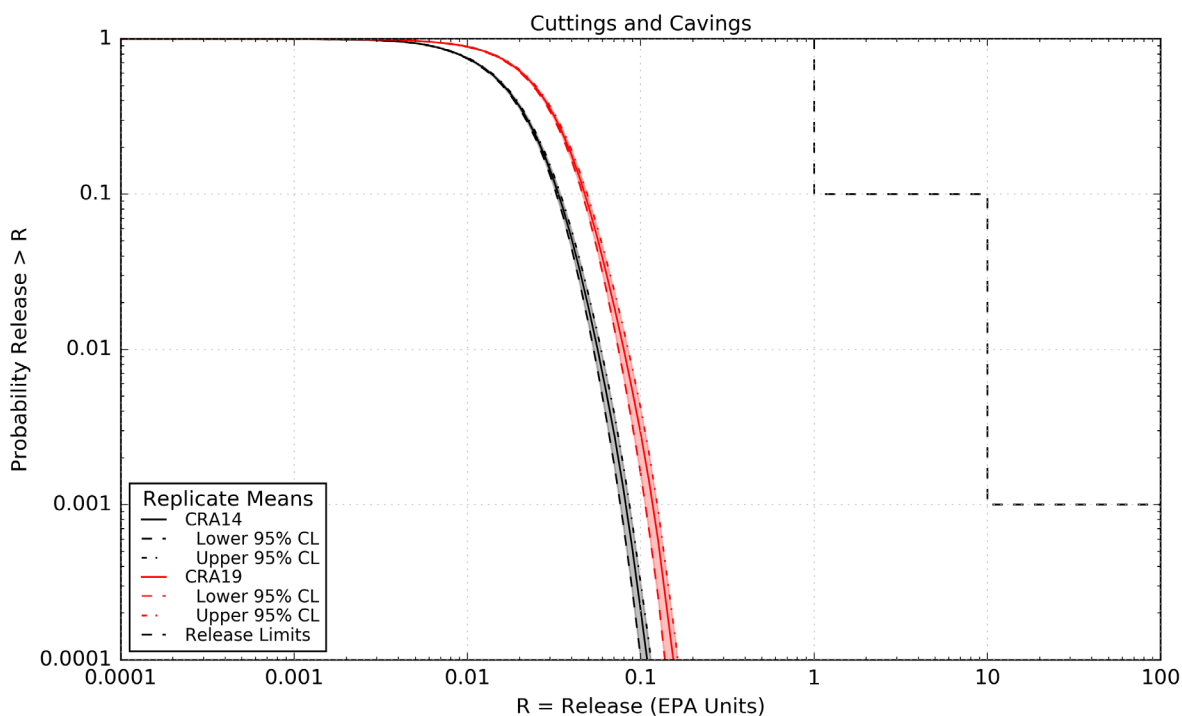


Figure 60 –Overall Mean for Cuttings and Cavings Normalized Releases with Confidence Limits

5.9.2 Spallings Normalized Releases

Spallings releases are calculated from spallings volumes and spallings concentrations. Compared to the CRA14 analysis, the CRA19 spallings volumes have increased (Section 5.6.4) and spallings concentrations are overall very similar (Section 5.3.3). Spallings volumes have increased due to increased waste area pressures (Section 5.5.4). The substantial increase in drilling rate (Section 1.1.11) also leads to increases in spallings releases due to the increased number of borehole intrusions modeled. The increased mean value of PBRINE leads to increased spallings releases due to an increased probability of relatively high-pressure E1 intrusions. However the plugging pattern changes resulted in a decrease in spallings releases due to a decreased probability of E1 and E2 intrusions (Section 1.1.11) (Brunell 2019). Overall, mean spallings releases have increased for the CRA19 analysis for all probabilities (Figure 61 (Figure 9 from Brunell 2019)).

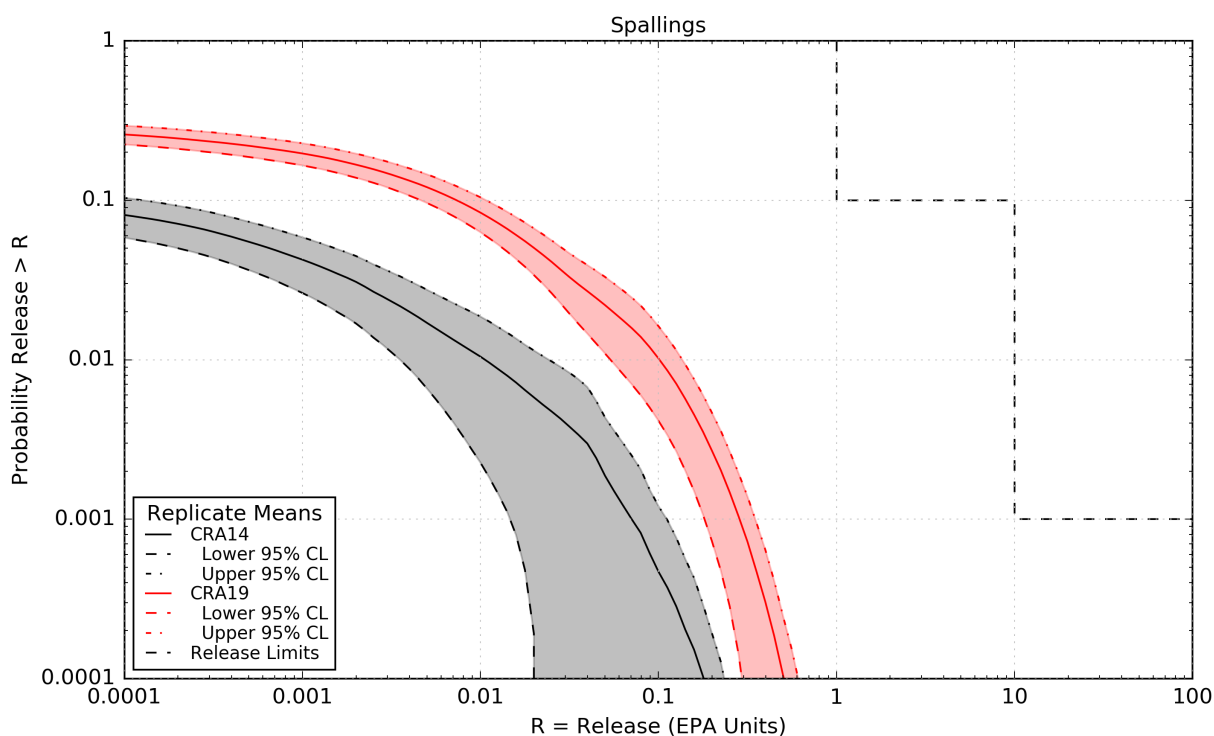


Figure 61 –Overall Mean for Normalized Spallings Releases with Confidence Limits

5.9.3 Normalized Direct Brine Releases

Direct brine releases are calculated from DBR volumes and mobilized actinide concentrations in brine. Compared to the CRA14 analysis, the CRA19 analysis DBR volumes have increased (Section 5.7.4) and radionuclide concentrations in brine are overall similar despite many changes to radionuclide solubility parameterization (Section 5.4.2). DBR volumes have increased as a result of increased waste area brine saturations (Section 5.5.5) and pressures (Section 5.5.4). The substantial increase in drilling rate (Section 1.1.11) leads to increased DBRs due to the increased number of borehole intrusions modeled. The increased mean value of PBRINE leads to increased spallings releases due to an increased probability of relatively high-pressure E1 intrusions. However the plugging pattern changes lead to a decrease in spallings releases due to a decreased probability of E1 and E2 intrusions (Section 1.1.11) (Brunell 2019). Overall, mean direct brine releases have increased for the CRA19 analysis for all probabilities (Figure 62 (Figure 14 from Brunell 2019)).

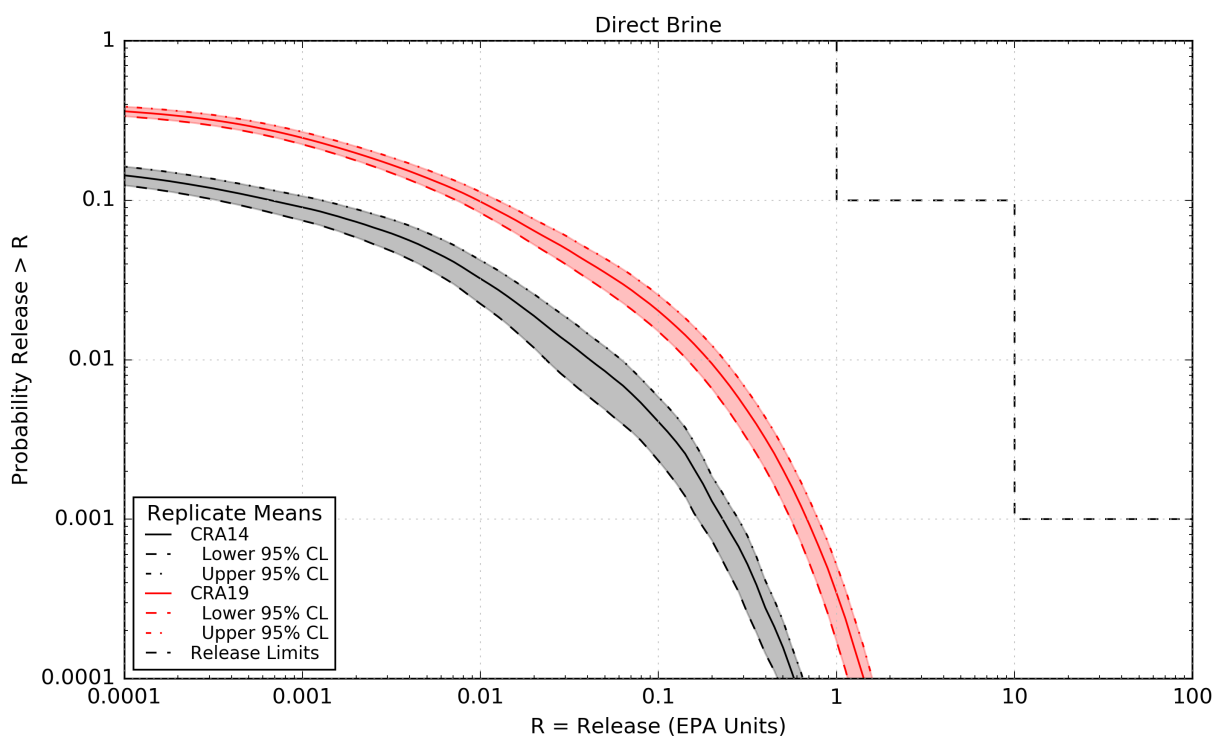


Figure 62 – Overall Mean for Normalized Direct Brine Releases with Confidence Limits

5.9.4 Normalized Culebra Transport Releases

Releases from the Culebra at the LWB releases are calculated from cumulative radionuclide-loaded brine discharges to the Culebra and the results of Culebra transport calculations. Compared to the CRA14 analysis, the CRA19 transport of radionuclides to the Culebra (Section 5.8) is overall similar or decreased across the disturbed repository scenarios. The SECOTP2D Culebra transport calculations are identical between the two analyses⁹; however, these calculations are based on a unit source, such that differing radionuclide concentrations reaching the Culebra will result in different Culebra releases. There is some impact of the drilling rate, plugging pattern probabilities, and probability of intersecting brine, as described above. However, releases from the Culebra are relatively low and rare compared to releases from those mechanisms discussed above. Overall, mean releases from the Culebra have increased for the CRA19 analysis for all probabilities (Figure 63 (Figure 20 from Brunell 2019)).

⁹ The cumulative mass flux results to the LWB from the SECOTP2D calculations show several instances with unphysical negative cumulative releases, ranging from $-1.08e-4$ kg to less than $-1e-100$ kg. An analysis was performed by Bethune (2019b) to bound the unaccounted for potential releases, and determined it to have no impact at the compliance level.

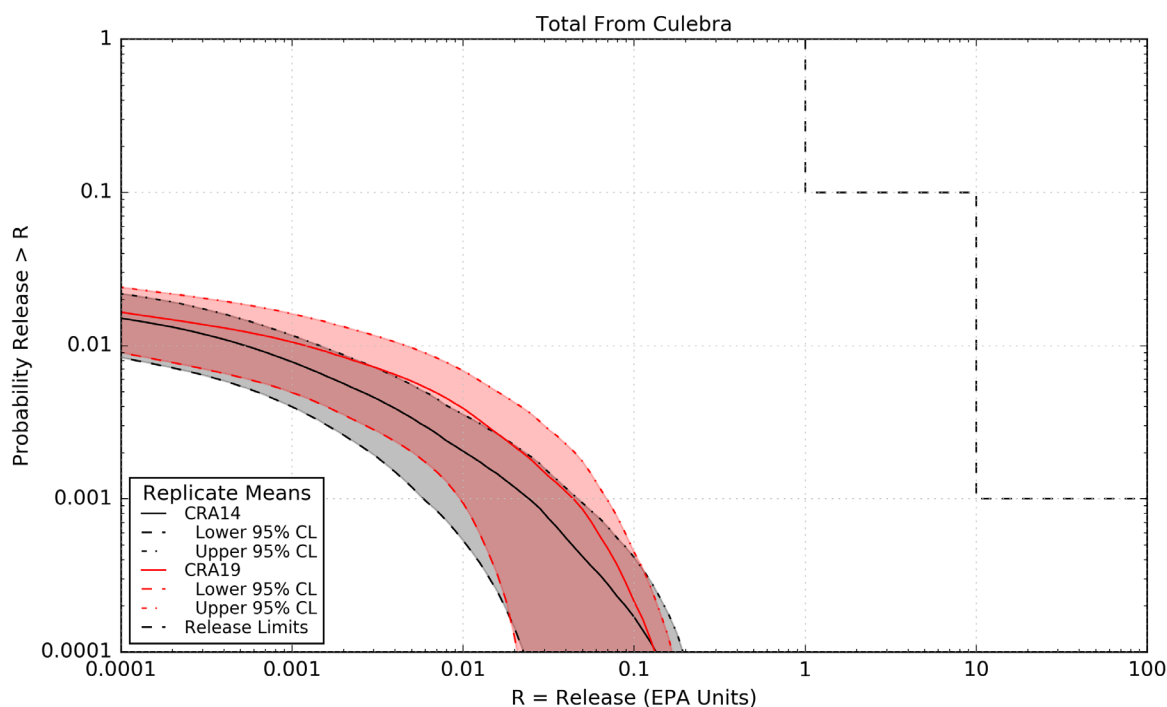


Figure 63 –Overall Means for Transport Releases from the Culebra with Confidence Limits

5.9.5 Total Normalized Releases

Individual “horsetail” plots of total releases for the CRA19 analysis are shown for Replicates 1-3 in Figure 64-Figure 66 (Figures 22-24 from Brunell 2019). Compared to the CRA14 analysis, the CRA19 releases for each individual release mechanism have increased. Total releases for the CRA19 analysis are dominated by cuttings and cavings releases at high probabilities and DBRs at low probabilities (Figure 67 (Figure 25 from Brunell 2019)); total releases for the CRA14 analysis were similarly dominated by these two release mechanisms despite the many differences between the two analyses. Overall, total normalized releases have increased for the CRA19 analysis for all probabilities. As seen in Figure 68 (Figure 26 from Brunell 2019) and Table 31, the overall mean for normalized total releases and its lower/upper 95% confidence limits are well below acceptable release limits. Accordingly, the WIPP remains in compliance with the containment requirements of 40 CFR Part 191.

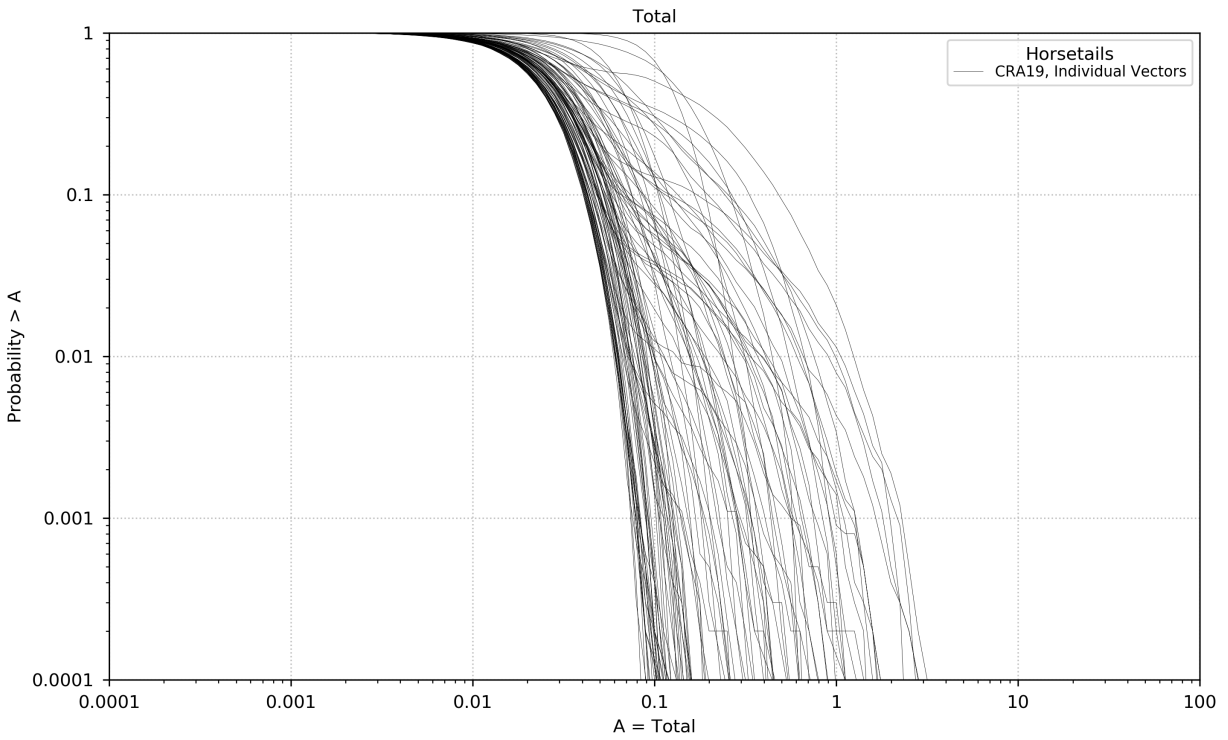


Figure 64 – Replicate 1 Total Normalized Releases

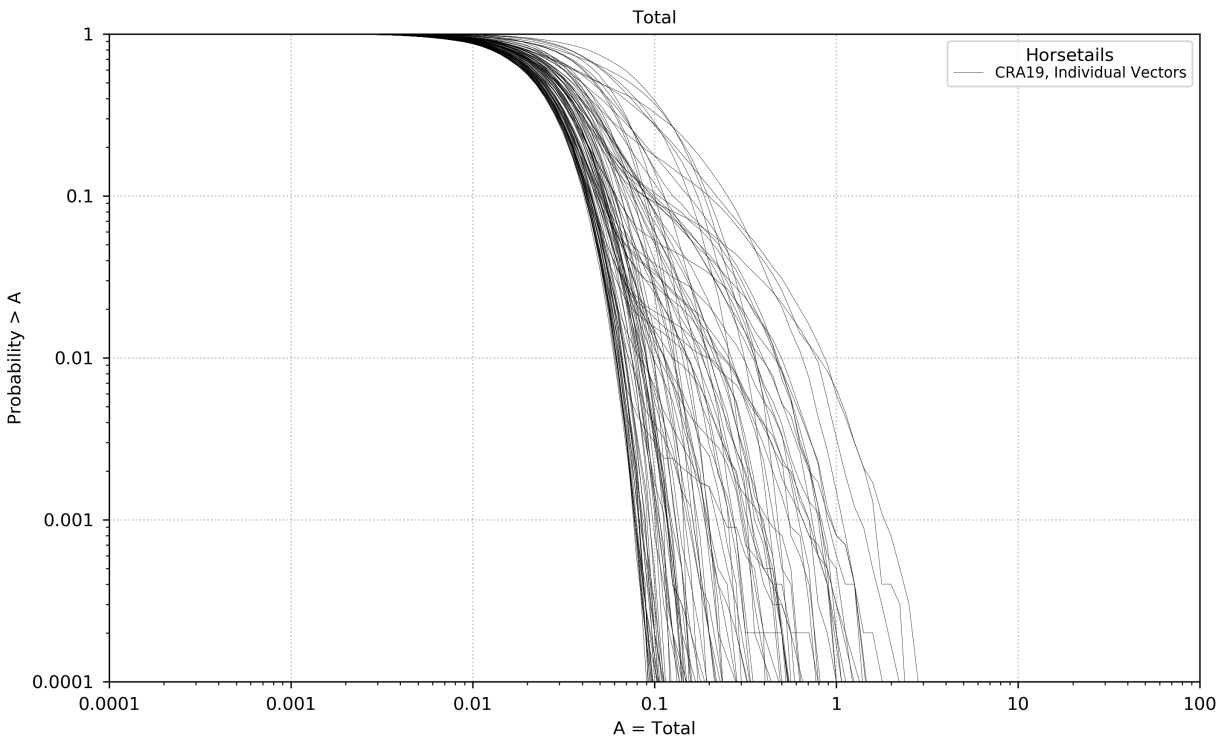


Figure 65 – Replicate 2 Total Normalized Releases

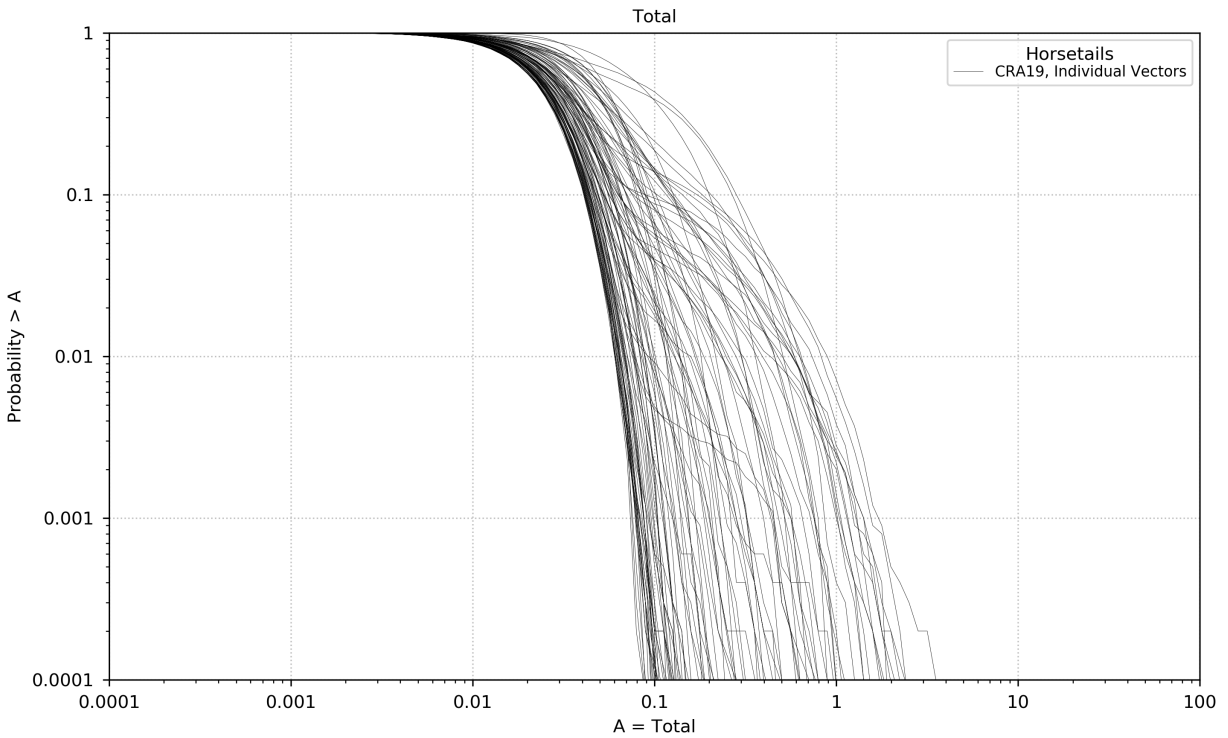


Figure 66 – Replicate 3 Total Normalized Releases

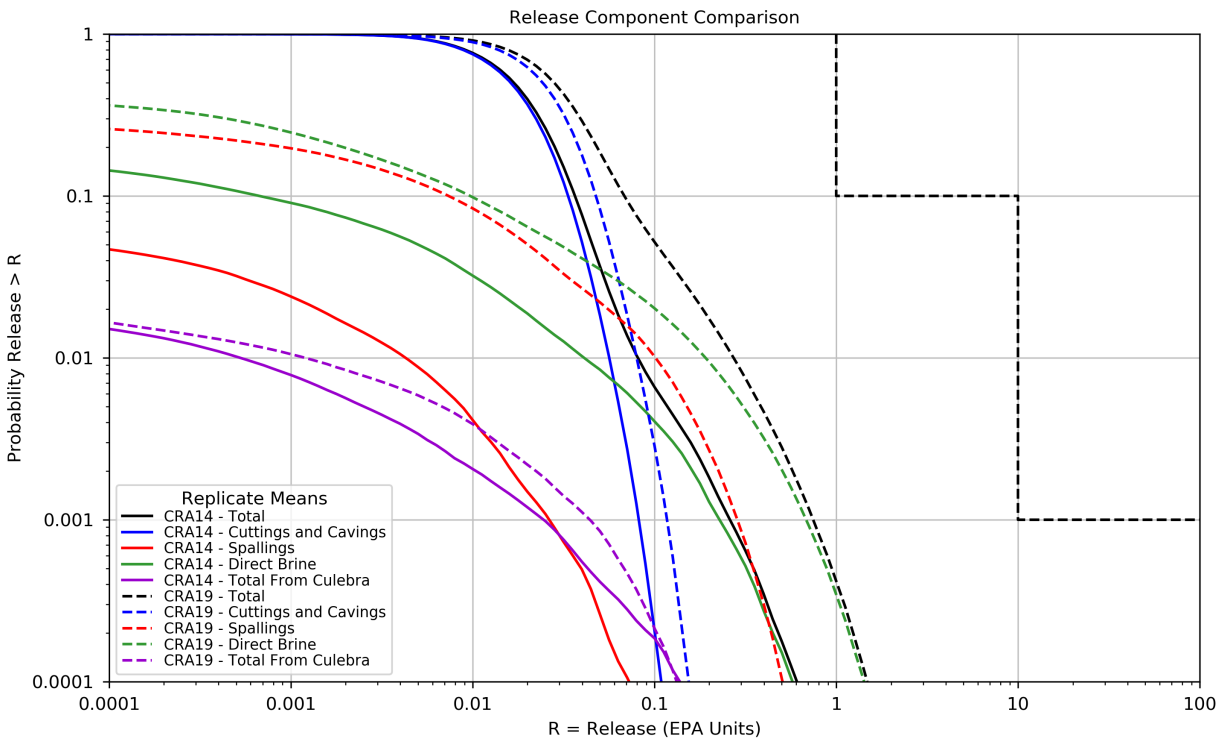


Figure 67 – Comparison of Overall Means for Release Components

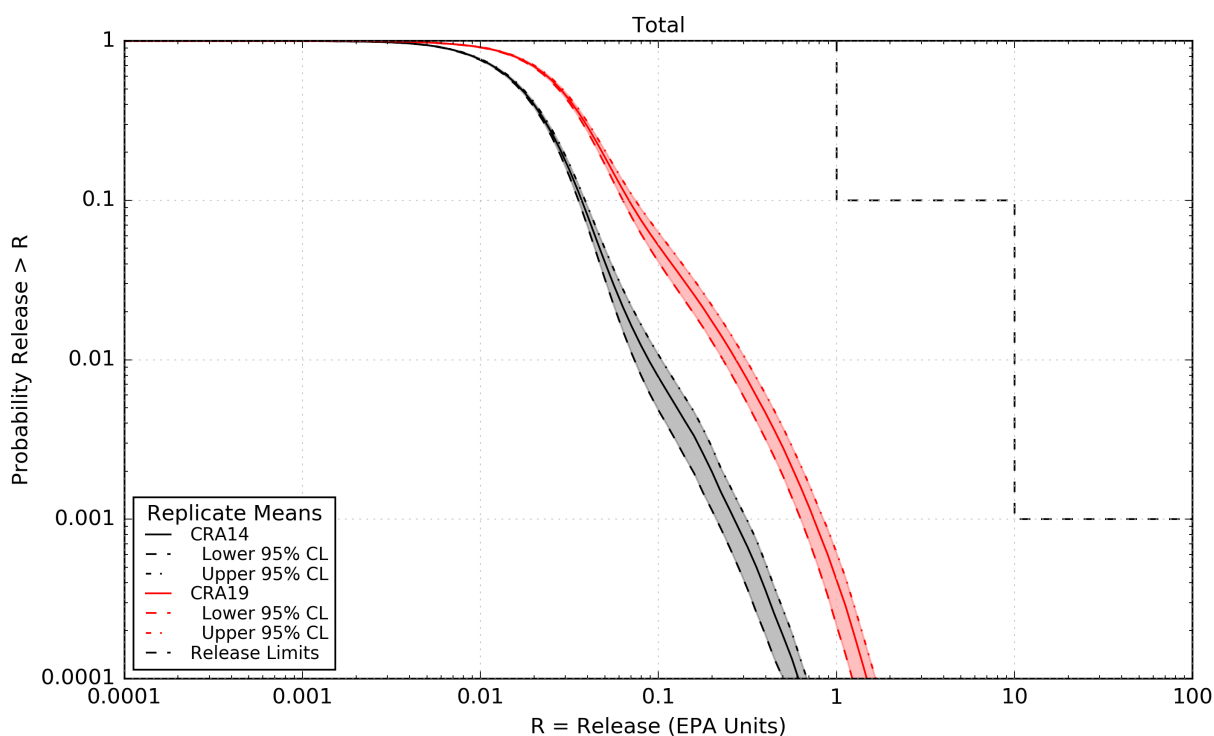


Figure 68 – Overall Mean for Total Normalized Releases with Confidence Limits

Table 31 – Statistics on the Overall Mean for Total Normalized Releases

Probability	Analysis	Mean Total Release	Lower 95% CL	Upper 95% CL	Release Limit
0.1	CRA14	0.0373	0.0355	0.0388	1
	CRA19	0.0685	0.0631	0.0745	
0.001	CRA14	0.2677	0.2124	0.3132	10
	CRA19	0.7505	0.6301	0.8501	

5.10 Sensitivity of Releases to Uncertain Parameters

A stepwise linear multiple regression (“sensitivity”) analysis was performed to determine the relative importance of the sampled parameters on the calculated releases (Zeitler 2019e). The sensitivity analysis was used to resolve the question of which sampled parameters contribute most to the variability (uncertainty) observed in the mean releases by vector. The sensitivity of mean releases of each individual release mechanism, as well as total releases, to sampled parameters was analyzed.

Parameter and model changes between the CRA14 and CRA19 analyses have contributed to changes in calculated releases as described above. Two new sampled parameters have been added and one subtracted, for a total of 64 sampled parameters that could potentially contribute to the variability in releases across the 100 vectors in each of three replicates. The sensitivity of each individual release mechanism, as well as total releases, to sampled parameters was analyzed using a stepwise linear multiple regression analysis.

Whereas for the CRA14 analysis the BOREHOLE:TAUFAIL parameter (waste shear strength) was the most dominant parameter with regard to controlling total releases in all three replicates, the SOLMOD3:SOLVAR parameter (solubility multiplier for III oxidation states) is now the most dominant parameter contributing to variability in total releases in all three replicates (tied with parameter BH_SAND:PRMX_LOG in replicate 3). The increased importance is due in part to the shifting of the distribution mean to a higher value (thus making it more impactful on DBRs), as well as in part to the increased contribution of DBRs to total releases. Nonzero DBR volumes have also increased, such that some intrusions that previously had zero DBRs (and thus zero contribution of the SOLMOD3:SOLVAR parameter to DBRs) now have nonzero DBRs.

The BOREHOLE:TAUFAIL parameter is now the second-most dominant parameter for total releases. It has decreased in importance, not due to the minor change in assigned distribution, but to the increased impact of the variability in waste stream concentrations.

The BH_SAND:PRMX_LOG parameter (the (logarithm of the) permeability of the silty-sand-filled borehole) has increased in importance in the CRA19 analysis due to the impact on DBRs. The CASTILER:PRESSURE parameter continues to be one of the more important parameters in terms of variability in total releases, due to its impact on DBRs.

The updated distribution for the STEEL:CORRMCO2 parameter (inundated iron corrosion rate) has led to increased importance in the variability of DBRs, but the correlation with DBRs is negative—increased gas generation rates associated with this parameter lead to decreased DBRs due to the impact of repository pressure to reduce waste area saturations.

The influence of the GLOBAL:PBRINE (probability that a drilling intrusion penetrates the pressurized brine in the Castile) parameter on DBRs was somewhat increased in comparison to the CRA14 due to the change in assigned distribution and increased impact of DBRs on total releases.

Of the other sampled parameters that were changed or were new since the CRA14, none had any substantial impact on releases. The change in the distribution of SOLMOD4:SOLVAR (solubility multiplier for IV oxidation states) had little impact on DBR or releases from the Culebra. The GLOBAL:GDEPFAC (energy deposition probability for wetted solid radionuclides, which has a role in brine radiolysis), STEEL:HUMCORR (humid iron corrosion rate), and WAS_AREA:HYMAGCON (hydromagnesite conversion rate) parameters did not show much (or only very weak) correlations with releases from the repository.

5.11 FEPs Analysis

An assessment of the FEPs baseline was conducted to determine if the FEPs basis remained valid in consideration of changes introduced by the CRA-2019 PA (Kirkes 2019a). This analysis consisted of an initial FEPs screening prior to PA calculations, as well as an assessment of

whether the results of the CRA-2019 PA calculations supported the initial FEPs screening. Results of this FEPs assessment are documented in Kirkes (2019a) and summarized below.

5.11.1 Overall Results

A FEPs screening analysis began prior to performing PA calculations, but concluded subsequent to PA calculations (Kirkes 2019a). A total of 245 FEPs were screened for inclusion in CRA-2019 PA calculations; no FEPs were added or deleted since CRA-2014. Of these 245 FEPs, 164 FEPs were unchanged from CRA-2014 and 81 have been updated with new information. Of these 81 FEPs, two have had their screening decisions changed.

5.11.2 Updated Screening Decision

The FEPs analysis concluded subsequent to PA calculations, but confirmed that two additional FEPs compared to the CRA-2014 PA needed to be screened in, the FEP associated with the radiolysis of brine as a gas generation process (FEP W52) and FEP W114, *Mechanical Degradation of Panel Closures* formerly screened in has now been screened out. The radiolytic gas generation process had been implemented in the BRAGFLO code prior to undertaking CRA-2019 PA calculations based on the conclusions of Day (2019b). There was no action necessary to handle the changed screening decision for FEP W114 as a result of the salt construction of panel closures.

5.11.3 Updated Screening Arguments

Additionally, screening arguments were modified for 81 additional FEPs. Notably, the criticality FEP required assessing the results of the CRA19 analysis to confirm that the accumulation of radionuclides in the Culebra formation above the repository would not result in a nuclear critical condition (Rechard 2019). The substantially increased inventory of lead, as projected by data received in the PAIR – 2018, was discounted as a source of gas generation considered for CRA-2019 PA calculations (Kirkes 2019b).

6.0 SUMMARY

Results from the CRA-2019 PA (CRA19 analysis) are compared to those obtained in the CRA14 analysis in order to assess repository performance in terms of the current regulatory baseline. Changes incorporated into the CRA-2019 PA include repository planned changes, parameter updates, and refinements to PA implementation. New inventory information has been included and FEPs have been reassessed. Relatively impactful changes include: 1) the lack of ROMPCS emplacement between Panels 3, 4, 5, 6, and 9, modeled as the southernmost panel closure area, which allowed greater communication between the waste panel and the south rest-of-repository; 2) an increase in the inundated steel corrosion rates and the addition of brine radiolysis which resulted in an increase in hydrogen gas generation; 3) an update to the drilling rate which increased the number of drilling intrusions modeled; 4) an update to plugging pattern parameters which decreased the relative occurrence of E1 and E2 intrusions; and 5) an update to the probability that a drilling intrusion will intersect Castile brine, which increased the relative occurrence of E1 intrusions.

As a result of all changes, total normalized releases for the CRA19 analysis are increased at all probabilities compared to those from the CRA14 analysis. Releases from each release mechanism have also increased at all probabilities. Cuttings and cavings releases continue to dominate total releases at high probabilities and direct brine releases continue to dominate total releases at low probabilities. Total normalized releases continue to remain below regulatory limits. As a result, the CRA-2019 PA demonstrates that the WIPP remains in compliance with the containment requirements of 40 CFR Part 191.

This page intentionally left blank.

7.0 REFERENCES

- Bethune, J. 2019a. Analysis Package for Direct Brine Releases in the 2019 Compliance Recertification Application Performance Assessment (CRA-2019 PA). Sandia National Laboratories, Carlsbad, NM. ERMS 571370.
- Bethune, J. 2019b: Impact of Negative Flux in SECOTP2D, Memorandum to WIPP Records Center, Carlsbad, NM: Sandia National Laboratories. July, 2019. ERMS 571697.
- Brunell, S. 2019. Analysis Package for Normalized Releases in the 2019 Compliance Recertification Application Performance Assessment (CRA-2019 PA). Sandia National Laboratories, Carlsbad, NM. ERMS 571373.
- Brush, L.H., Domski, P.S., and Xiong, Y. 2012. Analysis Plan for WIPP Near-Field Geochemical Process Modeling, Rev. 1. Sandia National Laboratories, Carlsbad, NM. ERMS 556960.
- Camphouse, R. 2013. Analysis Plan for the 2014 WIPP Compliance Recertification Application Performance Assessment. Sandia National Laboratories, Carlsbad, NM: ERMS 559198.
- Camphouse, R. 2014. Impact Assessment of an Additional WIPP Shaft. Sandia National Laboratories, Carlsbad, NM: ERMS 562973.
- Clayton, D.J. 2008. Memorandum to L. Brush (Subject: Update to the Calculation of the Minimum Brine Volume for a Direct Brine Release). 2 April 2008. Sandia National Laboratories, Carlsbad, NM. ERMS 548522.
- Clayton, D.J., S. Dunagan, J.W. Garner, A.E. Ismail, T.B. Kirchner, G.R. Kirkes, M.B. Nemer. 2008. Summary Report of the 2009 Compliance Recertification Application Performance Assessment. Sandia National Laboratories, Carlsbad, NM. ERMS 548862.
- Clayton, D.J., R.C. Camphouse, J.W. Garner, A.E. Ismail, T.B. Kirchner, K.L. Kuhlman, M.B. Nemer. 2010. Summary Report of the CRA-2009 Performance Assessment Baseline Calculation. Sandia National Laboratories, Carlsbad, NM. ERMS 553039.
- Cotsworth, E. 2005. EPA Letter on Conducting the Performance Assessment Baseline Change (PABC) Verification Test. U.S. EPA, Office of Radiation and Indoor Air, Washington, D.C. ERMS 538858.
- Cotsworth, E. 2009. EPA Letter on CRA-2009 First Set of Completeness Comments. U.S. EPA, Office of Radiation and Indoor Air, Washington, D.C. ERMS 551444.
- Day, B. 2016. Operations and Experimental Area Sensitivity Study. Sandia National Laboratories, Carlsbad, NM. ERMS 565918.
- Day, B. and T. Zeitler. 2016. Panel Closure System Sensitivity Study. Sandia National Laboratories, Carlsbad, NM. ERMS 566725.
- Day, B. 2018. *Impact Analysis for BRAGFLO 6.03 Software Problem Report, SPR 18-002*. Sandia National Laboratories. Carlsbad, NM. ERMS 570325.

Day, B. 2019a. Reassessment of Need and Parameter Justification for Modeling Gas Generation due to Radiolysis of Brine and Cellulose/Plastic/Rubber in WIPP for CRA-2019. Sandia National Laboratories, Carlsbad, NM. ERMS 570873.

Day, B. 2019b. Analysis Package for Salado Flow in the 2019 Compliance Recertification Application Performance Assessment (CRA-2019 PA). Sandia National Laboratories, Carlsbad, NM. ERMS 571368.

Domski, P. 2019a. Th(IV), Np(V), and Am(III) Baseline Solubilities and Th(IV) and Am(III) Solubility Uncertainties for the CRA-2019 PA. 2019. Sandia National Laboratories, Carlsbad, NM. ERMS 571169.

Domski, P. 2019b. Uncertainty Analysis of Actinide Solubilities for CRA 2019. Sandia National Laboratories, Carlsbad, NM. ERMS 571179.

Domski, P. and C. Sisk-Scott. 2019. Prediction of Baseline Actinide Solubilities for CRA 2019 with and Updated EQ3/6 Pitzer Thermodynamic Database, DATA0.FM4. Sandia National Laboratories, Carlsbad, NM. ERMS 571178.

Herrick, C.G., M.D. Schuhen, D.M. Chapin, and D.C. Kicker. 2012. Determining the Hydrodynamic Shear Strength of Surrogate Degraded TRU Waste Materials as an Estimate for the Lower Limit of the Performance Assessment Parameter TAUFAIL. Sandia National Laboratories, Carlsbad, NM. ERMS 558479.

Herrick, C.G. 2013. Follow-up to Questions Concerning TAUFAIL Flume Testing Raised during the November 14-15, 2012 Technical Exchange Between the DOE and EPA. Memorandum to Chris Camphouse dated January 23, 2013. Sandia National Laboratories, Carlsbad, NM. ERMS 559081.

Kicker, D. 2019a. Radionuclide Inventory Screening Analysis for the 2019 Compliance Recertification Application Performance Assessment (CRA-2019 PA), Rev. 1. Sandia National Laboratories, Carlsbad, NM. ERMS 571659.

Kicker, D. 2019b. Analysis Package for Inventory EPA Units in the 2019 Compliance Recertification Application Performance Assessment (CRA-2019 PA). Sandia National Laboratories, Carlsbad, NM. ERMS 571372.

Kicker, D. 2019c. Analysis Package for Cuttings, Cavings, and Spallings in the 2019 Compliance Recertification Application Performance Assessment (CRA-2019 PA). Sandia National Laboratories, Carlsbad, NM. ERMS 571369.

Kim, S. and L. Feng. 2019. Input Parameter Report for the 2019 Compliance Recertification Application Performance Assessment (CRA-2019 PA), Rev. 1. Sandia National Laboratories, Carlsbad, NM. ERMS 571660.

Kirchner, T. 2012. AP-162 Revision 0: Analysis Plan for the Migration of the Performance Assessment Codes to the Sun Solaris Blade Server Running with Intel Processors. Sandia National Laboratories, Carlsbad, NM. ERMS 557765.

Kirchner, T., Zeitler, T., and Kirkes, R. 2012. Evaluating the Data in Order to Derive a Value for GLOBAL:PBRINE. Memorandum to Sean Dunagan dated December 11, 2012. Sandia National Laboratories, Carlsbad, NM. ERMS 558724.

Kirchner, T., A. Gilkey, and J. Long. 2014. Summary Report on the Migration of the WIPP PA Codes from VMS to Solaris, AP-162 Revision 1. Sandia National Laboratories, Carlsbad, NM. ERMS 561757.

Kirchner, T., A. Gilkey, and J. Long. 2015. Addendum to the Summary Report on the Migration of the WIPP PA Codes from VMS to Solaris, AP-162. Sandia National Laboratories, Carlsbad, NM. ERMS 564675.

Kirkes, R. 2019a. Features, Events, and Processes Assessment for the 2019 Compliance Recertification Application Performance Assessment (CRA-2019 PA). Sandia National Laboratories, Carlsbad, NM. ERMS 571366.

Kirkes, L. 2019b. Lead Inventory Impact on Gas Generation. Sandia National Laboratories, Carlsbad, NM. ERMS 571255.

Leigh, C.D., J.F. Kanney, L.H. Brush, J.W. Garner, G.R. Kirkes, T. Lowry, M.B. Nemer, J.S. Stein, E.D. Vugrin, S. Wagner, and T.B. Kirchner. 2005. 2004 Compliance Recertification Application Performance Assessment Baseline Calculation, Revision 0. Sandia National Laboratories, Carlsbad, NM. ERMS 541521.

Long, J. 2013. Execution of Performance Assessment Codes for the CRA-2014 Performance Assessment. Sandia National Laboratories, Carlsbad, NM. ERMS 560016.

Long, J. 2019. Computational Code Execution and File Management for the 2019 Compliance Recertification Application Performance Assessment (CRA-2019 PA). Sandia National Laboratories, Carlsbad, NM. ERMS 571375.

MacKinnon, R.J., and G. Freeze. 1997a. Summary of EPA-Mandated Performance Assessment Verification Test (Replicate 1) and Comparison With the Compliance Certification Application Calculations, Revision 1. Sandia National Laboratories, Carlsbad, NM. ERMS 422595.

MacKinnon, R.J., and G. Freeze. 1997b. Summary of Uncertainty and Sensitivity Analysis Results for the EPA-Mandated Performance Assessment Verification Test, Rev. 1. Sandia National Laboratories, Carlsbad, NM. ERMS 420669.

MacKinnon, R.J., and G. Freeze. 1997c. Supplemental Summary of EPA-Mandated Performance Assessment Verification Test (All Replicates) and Comparison With the Compliance Certification Application Calculations, Revision 1. Sandia National Laboratories, Carlsbad, NM. ERMS 414880.

Malama, B. 2013. Analysis Package for Direct Brine Releases: CRA-2014 Performance Assessment (CRA-2014 PA). Sandia National Laboratories, Carlsbad, NM, ERMS 560069.

Mariner, P. 2019. A Summary of Humic Colloid Parameter Values to be Implemented in the CRA-2019 Deferred Performance Assessment. Sandia National Laboratories, Albuquerque, NM. ERMS 571250.

Pasch, J. and C. Camphouse, 2011. Analysis Package for Direct Brine Releases: Panel Closure Redesign and Repository Reconfiguration Performance Assessment (PC3R PA), Revision 0. Sandia National Laboratories. Carlsbad, NM. ERMS 555249.

- Peake, Thomas. 1998. Technical Report Review of TDEM Analysis of WIPP Brine Pockets. Prepared for U. S. Environmental Protection Agency, Office of Radiation and Indoor Air, 401 M. Street, S. W., Washington, DC.
- Rechard, R. P., A. C. Peterson, J. D. Schreiber, H. J. Iuzzolino, M. S. Tierney and J. S. Sandha. 1991. Preliminary comparison with 40 CFR Part 191, Subpart B for the Waste Isolation Pilot Plant, December 1991; Volume 3: Reference Data. Sandia National Laboratories, Albuquerque, NM.
- Rechard, R. P. 2019. Improbability of Nuclear Criticality in Transuranic Waste after Compaction by Salt Creep in Bedded Salt Repository. Sandia National Laboratories, Albuquerque, NM.
- Reed, D.T., S. Okajima, L.H. Brush, and M.A. Molecke. 1993. *Radiolytically-Induced Gas Production in Plutonium-Spiked WIPP Brine, Scientific Basis for Nuclear Waste Management XVI, Materials Research Society Symposium Proceedings, Boston, MA, November 30 – December 4, 1992*. C.G. Interrante and R.T. Pabalan, eds. SAND92-7283C. ERMS 228637. Materials Research Society, Pittsburgh, PA. Vol. 294, pp. 431–438.
- Reed, D., J. Swanson, and F. Stanley. 2019. LANL/ACRSP Parameter Recommendations for the CRA-2019 Deferred Performance Assessment, Rev. 1. Los Alamos National Laboratory, Carlsbad, NM. ERMS 571296.
- Roselle, G.T. 2013. Determination of Corrosion Rates from Iron/Lead Corrosion Experiments to be used for Gas Generation Calculations. Sandia National Laboratories, Carlsbad, NM. ERMS 559077.
- Sandia National Laboratories (SNL). 1996. Summary Memo of Record, DR-3: Dynamic Closure of the North-End and Hallways, Memorandum from P. Vaughn, M. Lord, and R. MacKinnon to D.R. ERMS 230794.
- Sandia National Laboratories (SNL). 2010. Design Document and User's Manual for CCDFGF. Sandia National Laboratories, Carlsbad, NM. ERMS 554046.
- Sarathi, R. S. 2019a. Memo: Explanation of CAPMIC definition and usage in PA calculations. ERMS 570685. Sandia National Laboratories. Carlsbad, NM.
- Sarathi, R. S. 2019b. Design Document and User's Manual for PANEL Version 5.00. Sandia National Laboratories, Carlsbad, NM. ERMS 570821.
- Sarathi, R. S. 2019c. Requirements Document, Validation Plan, and Validation Document for PANEL Version 5.00. Sandia National Laboratories, Carlsbad, NM. ERMS 570820.
- Sarathi, R. 2019d. Analysis Package for Actinide Mobilization and Salado Transport in the 2019 Compliance Recertification Application Performance Assessment (CRA-2019 PA). Sandia National Laboratories, Carlsbad, NM. ERMS 571371.
- Sisk-Scott, C. 2019. Calculation of Organic-Ligand Concentrations for the WIPP CRA-2019 Deferred PA. Sandia National Laboratories, Carlsbad, NM. ERMS 571011.
- U.S. Congress. 1992. WIPP Land Withdrawal Act, Public Law 102-579, 106 Stat. 4777, 1992; as amended by Public Law 104-201, 110 Stat. 2422, 1996.

U.S. Department of Energy (DOE) 1996. Title 40 CFR Part 191 Compliance Certification Application for the Waste Isolation Pilot. U.S. Department of Energy Waste Isolation Pilot Plant, Carlsbad Area Office, Carlsbad, NM. DOE/CAO-1996-2184.

U.S. Department of Energy (DOE) 2004. Title 40 CFR Part 191 Compliance Recertification Application for the Waste Isolation Pilot Plant, , 10 vols., U.S. Department of Energy Waste Isolation Pilot Plant, Carlsbad Area Office, Carlsbad, NM. DOE/WIPP 2004-3231.

U.S. Department of Energy (DOE). 2015. Response to Environmental Protection Agency Letters Dated December 17, 2014 and February 27, 2015 Regarding the 2014 Compliance Recertification Application. U.S. Department of Energy, Waste Isolation Pilot Plant, Carlsbad Field Office. Carlsbad, NM. ERMS 563433.

U.S. Department of Energy (DOE). 2016. WIPP UPDATE: October 14, 2016, Plans Call for Controlled Withdrawal from South End of Underground.

http://www.wipp.energy.gov/Special/WIPP%20Update%2010_14_16.pdf

U.S. Department of Energy (DOE). 2017. Sandia Recommendation for Completion of Fully-Qualified RPC2 Calculations. Email from R. Patterson to P. Shoemaker dated February 7, 2017.

U.S. Department of Energy (DOE). 2018. Delaware Basin Monitoring Annual Report. DOE/WIPP-18-2308, Rev. 1.

U.S. Environmental Protection Agency (EPA). 1998. 40 CFR 194, Criteria for the Certification and Recertification of the Waste Isolation Pilot Plant's Compliance with the Disposal Regulations: Certification Decision: Final Rule, Federal Register. Vol. 63, 27354-27406.

U.S. Environmental Protection Agency (EPA). 2006. 40 CFR 194, Criteria for the Certification and Recertification of the Waste Isolation Pilot Plant's Compliance with the Disposal Regulations: Certification Decision: Final Rule, Federal Register. Vol. 71, 18010-18021.

U.S. Environmental Protection Agency (EPA). 2010. 40 CFR Part 194 Criteria for the Certification and Recertification of the Waste Isolation Pilot Plant's Compliance With the Disposal Regulations: Recertification Decision, Federal Register No. 222, Vol. 75, pp. 70584-70595, November 18, 2010.

U.S. Environmental Protection Agency (EPA). 2017a. Criteria for the Certification and Recertification of the Waste Isolation Pilot Plant's Compliance with the Disposal Regulations; Recertification Decision. July 19, 2017. Office of Radiation and Indoor Air, Docket EPA-HQ-OAR-2014-0609-0079.

U.S. Environmental Protection Agency (EPA). 2017b. Probability of Encountering Castile Brine Beneath the WIPP Waste Panels Using the TDEM Block Method. June, 2017. Office of Radiation and Indoor Air, Docket EPA-HQ-OAR-2014-0609-0047.

U.S. Environmental Protection Agency (EPA). 2017c. Technical Support Document for Section 194.24, Evaluation of the Compliance Recertification Actinide Source Term, Gas Generation, Backfill Efficacy, Water Balance and Culebra Dolomite Distribution Coefficient Values. June, 2017. Office of Radiation and Indoor Air, Docket EPA-HQ-OAR-2014-0609-0054.

U.S. Environmental Protection Agency (EPA). 2017d. Technical Support Document for Section 194.23, EPA Review of Proposed Modification to the Waste Shear Strength Parameter

TAUFAIL. July, 2017. Office of Radiation and Indoor Air, Docket EPA-HQ-OAR-2014-0609-0052.

Van Soest, G.D. 2018. Performance Assessment Inventory Report – 2018. Los Alamos National Laboratory Carlsbad Operations. Carlsbad, NM. LA-UR-18-31882.

Zeitler, T.R. 2015. Memo to Records: BRAGFLO calculations for updated northern-most ROMPCS representation. Sandia National Laboratories, Carlsbad, NM. ERMS 563875.

Zeitler, T.R. and C. Hansen. 2015a. Cumulative Distribution for STEEL:CORRMCO2. Sandia National Laboratories, Carlsbad, NM. ERMS 565005.

Zeitler, T.R. and C. Hansen. 2015b. Cumulative Distribution for STEEL:HUMCORR. Sandia National Laboratories, Carlsbad, NM. ERMS 565009.

Zeitler, T.R. and C. Hansen. 2015c. Updated Calculation of the Cumulative Distribution for STEEL:HUMCORR. Sandia National Laboratories, Carlsbad, NM. ERMS 565108.

Zeitler, T.R. and B. Day. 2016. CRA14_SEN4 Sensitivity Study, Rev. 1. Sandia National Laboratories. Carlsbad, NM. ERMS 567505.

Zeitler, T.R., B. Day, J. Bethune, R. Sarathi, J. Long. 2017. Assessment of Abandoned Panel Closures in South End of Repository and Lack of Waste Emplacement in Panel 9. Sandia National Laboratories. Carlsbad, NM. ERMS 568459.

Zeitler, T.R. and B. Day. 2017. Analysis Plan for the Assessment of Abandoned Panel Closures in South End of Repository and Lack of Waste Emplacement in Panel 9. Sandia National Laboratories. Carlsbad, NM. ERMS 568138.

Zeitler, T.R., B. Day, J. Bethune, R. Sarathi, J. Long. 2017. Assessment of Abandoned Panel Closures in South End of Repository and Lack of Waste Emplacement in Panel 9. Sandia National Laboratories. Carlsbad, NM. ERMS 568459.

Zeitler, T.R. 2018a. Cumulative Distribution for STEEL:CORRMCO2 for the CRA-2019 PA. Sandia National Laboratories. Carlsbad, NM. ERMS 570869.

Zeitler, T.R. 2018b. Bounding Calculation of the Cumulative Distribution for STEEL:HUMCORR. Sandia National Laboratories. Carlsbad, NM. ERMS 569807.

Zeitler, T.R. 2019a. Analysis Plan for the 2019 WIPP Compliance Recertification Application Performance Assessment. Sandia National Laboratories, Carlsbad, NM. ERMS 571150.

Zeitler, T.R. 2019b. Calculation of Shaft and Experimental Area Dimensions for Use in the CRA-2019 PA. Sandia National Laboratories. Carlsbad, NM. ERMS 571045.

Zeitler, T.R. 2019c. A Summary of EPA/DOE Defined Parameters to be Implemented in the CRA-2019 PA. Sandia National Laboratories. Carlsbad, NM. ERMS 570879.

Zeitler, T.R. 2019d. Analysis Package for Parameter Sampling in the 2019 Compliance Recertification Application Performance Assessment (CRA-2019 PA). Sandia National Laboratories, Carlsbad, NM. ERMS 571367.

Zeitler, T.R. 2019e. Analysis Package for the Sensitivity of Releases to Input Parameters in the 2019 Compliance Recertification Application Performance Assessment (CRA-2019 PA). Sandia National Laboratories, Carlsbad, NM. ERMS 571374.

This page intentionally left blank.

APPENDIX A. RESULTS OF CRA19_CL ANALYSIS

Details of the approach for the CRA19_CL analysis are given in AP-181 (Zeitler 2019a) and briefly described here. In short, it was of interest to examine the impact on PA calculations from reducing the time to closure for areas in the repository modeled as “open” in the CRA19 analysis. In order to do so, a separate analysis (CRA19_CL) was created with the sole difference from the CRA19 analysis being the material properties assigned to the operations (OPS), experimental (EXP), and abandoned panel closure areas. The properties of intact halite were assigned to these areas for the entire 10,000 yr simulation time covered by BRAGFLO Salado flow calculations to represent fast closure of open areas. A complete PA consisting of 3 replicates of 100 vectors each was run for the CRA19_CL analysis. Background information on the issue and results of the CRA19_CL analysis are described below.

A.1 Background

In the APCS analysis (Zeitler et al. 2017), the decision to use “open” area properties for the abandoned panel closures was shown to substantially increase estimated releases over the CRA14_SEN4 (Zeitler and Day 2016) baseline case due to increased communication between the waste panel (WP) and south rest-of-repository (SROR) areas. The increased communication was due to the substitution of an “open” area for the southernmost panel closure area in the BRAGFLO representation, which allowed for greater brine pressures and saturations in the SROR following Castile intrusions, as there was no longer a significant barrier to equilibration with the WP. The saturations resulting from the flooding of Panels 3, 4, 6, and 9 with Castile brine from the borehole in Panel 5 through the abandoned panel closure led to increased gas generation and associated brine pressures in these areas. These conditions contributed to increases in calculated direct brine releases (DBRs) and releases to/from the Culebra and increased pressures led to increased spillings releases.

In discussions between the DOE and EPA subsequent to the APCS analysis, the EPA questioned whether, due to uncertainty in the timing of closure of open areas in the repository (i.e., when the material properties of the open areas might approach the properties of intact halite), the approach to model “open” areas of the repository, including abandoned panel closure areas, as permanently “open” could potentially underpredict releases. As an example, the EPA noted that for the CRA14_SEN3 sensitivity study (Day and Zeitler 2016), in which ROMPCS, OPS, and EXP two-phase flow properties were changed to more closely resemble intact halite (e.g., decreased porosity and permeability), estimated total releases increased over the baseline CRA-2014 PA case. However, the assumption made in the APCS analysis of no panel closure emplacement in the south end of the repository, which allowed greater communication among the panels in the south, is what drove releases higher for that analysis. Therefore, an effort to reduce porosity and permeability in all open areas would also serve to return the abandoned panel closure area to having a similar role to that prior to the APCS analysis (i.e., reducing communication among the panels in the south).

Because the APCS and CRA14_SEN3 analyses were based on different baselines (CRA14_SEN4 and CRA-2014 PA, respectively), a direct comparison of releases for an “open

vs. closed” comparison had not yet been made. In order to show the impact of the assumed long-term behavior of open areas (i.e., resulting in “open” or “closed” OPS, EXP, and abandoned closure areas), the supplemental calculation (CRA19_CL analysis) was performed as part of the CRA-2019 PA.

A.2 Differences Between CRA19 and CRA19_CL Analyses

Differences between the CRA19 and CRA19_CL analyses were introduced for BRAGFLO Salado flow calculations via material properties for the OPS, EXP, and southernmost panel closure areas, each of which was considered an “open” area for CRA19 calculations and had identical properties. For the CRA19_CL analysis, intact halite (S_HALITE) material properties were assigned to the OPS_AREA, EXP_AREA, and PCS_NO materials via parameter correlations in the alg1_bf_CRA19_CL.inp ALGEBRA input file, as excerpted below:

```
!   CALCULATE PERM_X FROM PRMX_LOG AND APPLY TO PERM_Y AND PERM_Z
!   TRZ: TAKE PERMEABILITY FROM HALITE
PERM_X   = 10**PRMX_LOG[B:1]
PERM_Y   = PERM_X
PERM_Z   = PERM_X
!   TRZ: TAKE OTHER PROPERTIES FROM HALITE
COMP_RCK = COMP_RCK[B:1]
POROSITY = POROSITY[B:1]
PRESSURE = PRESSURE[B:1]
RELP_MOD = RELP_MOD[B:1]
SAT_RBRN = SAT_RBRN[B:1]
SAT_RGAS = SAT_RGAS[B:1]
CAP_MOD  = CAP_MOD[B:1]
```

Thus, the S_HALITE material sampled parameters for permeability, porosity, rock compressibility, brine far-field pore pressure, and the relative permeability model, along with the constant S_HALITE parameters for residual brine saturation, residual gas saturation, and the capillary pressure limit type model, were assigned to OPS_AREA, EXP_AREA, and PCS_NO materials for times = 0 to 10,000 years. Primarily for computational efficiency and convenience, and justified due to the limited impact on brine and gas flows in association with the extremely low intrinsic permeabilities of S_HALITE, the capillary pressure parameters of PCT_A and PCT_EXP for the OPS_AREA, EXP_AREA, and PCS_NO materials were not correlated to S_HALITE and instead maintained as zero values.

To provide a condensed overview of impacts of the material changes implemented in the CRA19_CL analysis in comparison to the CRA19 baseline (along with CRA14 for reference), all reported flow measures are presented as box plots of the integrated function average of the measure across all 300 calculated vectors, with the individual vector integrated function average measure superimposed as a scatter plot. The box plot illustrates the Q1 and Q3 quartiles and median values with whiskers spanning the range of minimum to maximum values. As usual, measures are reported for undisturbed (S1-BF), E1-intruded (S2-BF), E2-intruded (S4-BF), and E2E1-intruded (S6-BF) scenarios where S3-BF and S5-BF scenarios are omitted due to similarity with the S2-BF and S4-BF results, respectively.

A.3 Waste Area Pressures

The impact on brine pressures as a result of “closure” of the southernmost panel closure area and the OPS and EXP areas of the repository are generally consistent across all waste areas, but the observed trends are scenario specific. Figure 69 shows the increase in average brine pressure for the waste panel in both undisturbed and E2-intruded scenarios for CRA19_CL in comparison to CRA19, where the “closed” southernmost panel closure area supports a pressure increase due to the lesser ability of gas generated within the waste panel to flow into other repository regions to the north. Although the lesser ability to flow gas to the north (and ultimately accumulate the gas within the much lower void space available in the “closed” OPS and EXP areas) under CRA19_CL is a reality for all scenarios, brine pressures within the waste panel for Castile-intruded (S2-BF and S6-BF) scenarios are shown in Figure 69 to be substantially reduced in comparison to CRA19. The reduced waste panel pressures under S2-BF and S6-BF for CRA19_CL are attributed to an overall reduction in total repository brine inflows (Figure 76) from the Castile that are impeded by the “closed” southernmost panel closure area and results in reduced waste panel and south rest-of-repository brine saturations (Figure 72, Figure 73) and reduced total repository gas generation (Figure 75).

Brine pressures within the south rest-of-repository follow the same trends for CRA19_CL in comparison with CRA19 as that described above for the waste panel as shown in Figure 70. The north rest-of-repository brine pressures under CRA19_CL also follow the same trends described above (Figure 71) with the exception of S6-BF which experiences a slight increase in average pressure as compared to CRA19. This exception is attributed to the lesser ability of gas generated within the repository to flow from the north rest-of-repository into the “closed” OPS and EXP areas. It is also noted that the lesser magnitude of pressure reduction within the waste panel and south rest-of-repository is also influenced by the lesser void space for gas accumulation within the OPS and EXP under CRA19_CL where porosities have been reduced from a constant 18% value under CRA19 to a sampled parameter value between ~0.1 to ~5.2%.

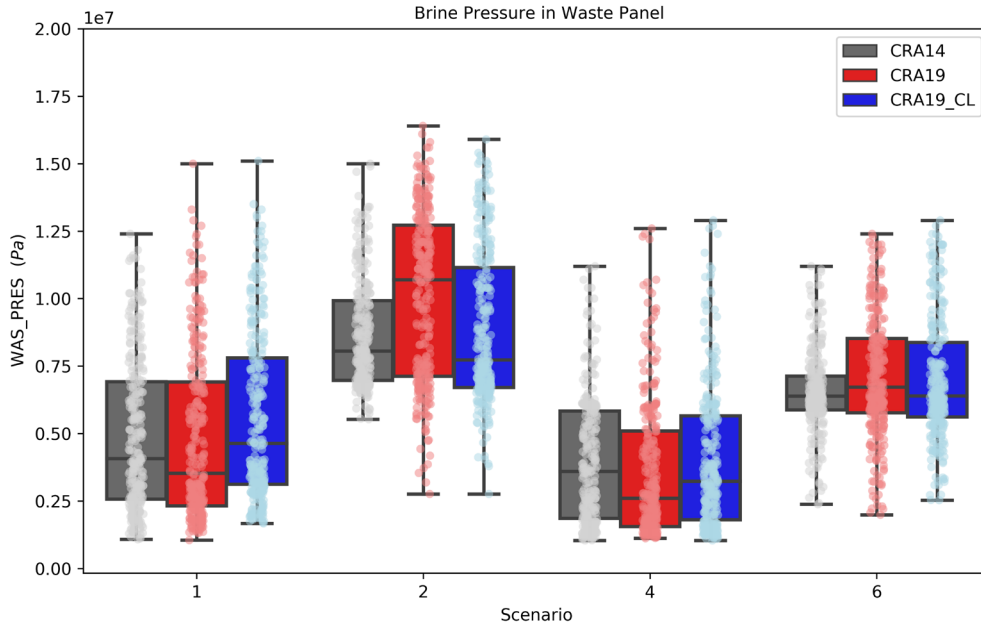


Figure 69 – Waste Panel Integrated Function Average Brine Pressures

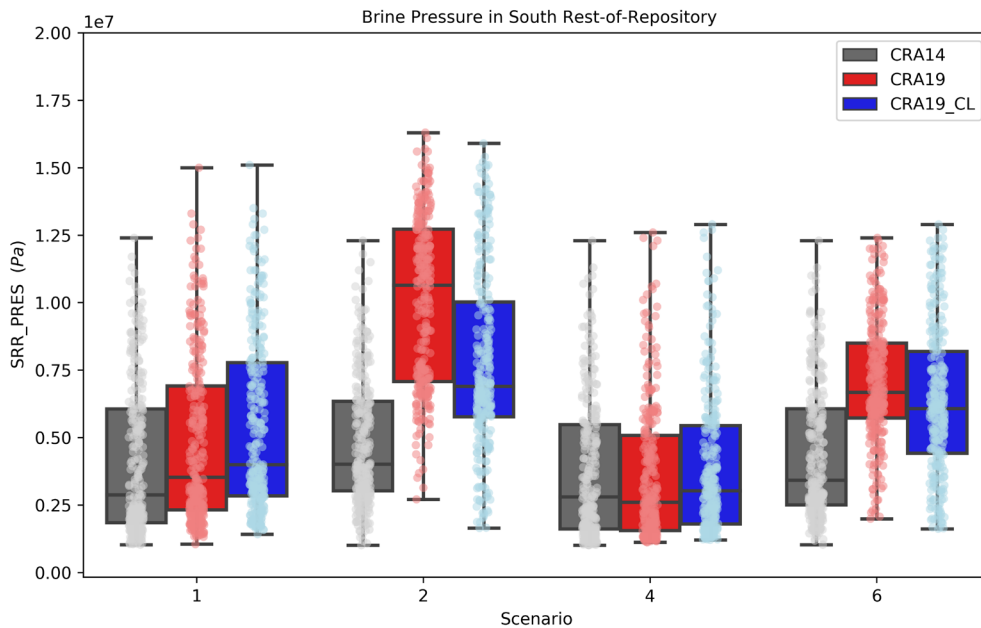


Figure 70 – South Rest-of-Repository Integrated Function Average Brine Pressures

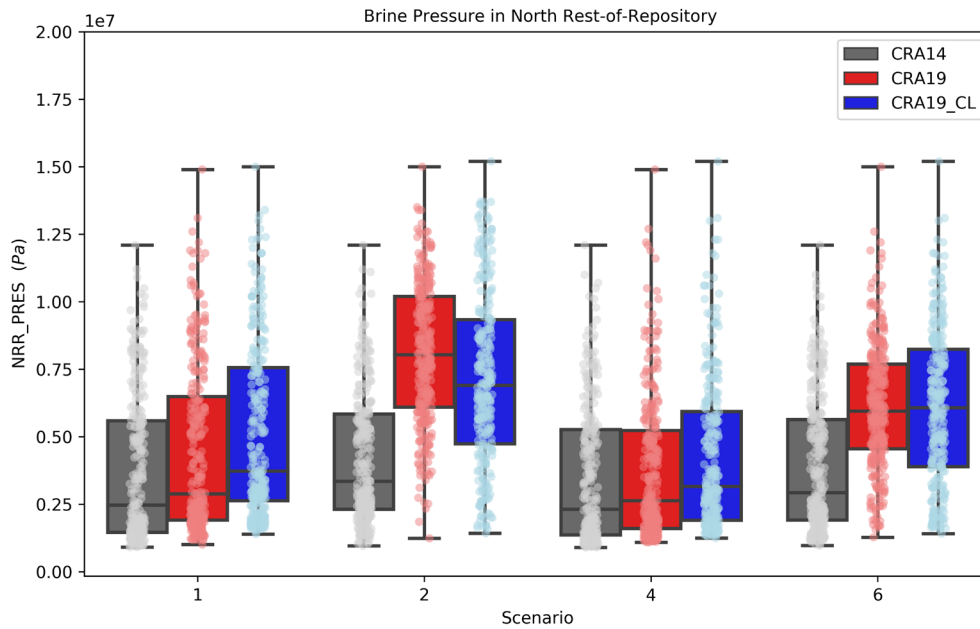


Figure 71 – North Rest-of-Repository Integrated Function Average Brine Pressures

A.4 Waste Area Saturations

Brine saturations within the waste panel and south rest-of-repository are observed to be decreased over all scenarios for CRA19_CL in comparison to CRA19 as shown in Figure 72 and Figure 73. The reduction is attributed to either higher brine pressures within these areas for the undisturbed (S1-BF) and E2-intruded (S4-BF) scenarios or the reduced inflow of brine from the hypothetical Castile brine reservoir under S2-BF and S6-BF. Brine saturations within the north rest-of-repository remain relatively low in comparison to other repository waste areas and are observed to be roughly equivalent for both CRA19_CL and CRA19 as shown in Figure 74. As noted previously, saturations are generally reduced for CRA19_CL as compared to CRA19 due to the lower quantity of brine that flows into the repository (Figure 76).

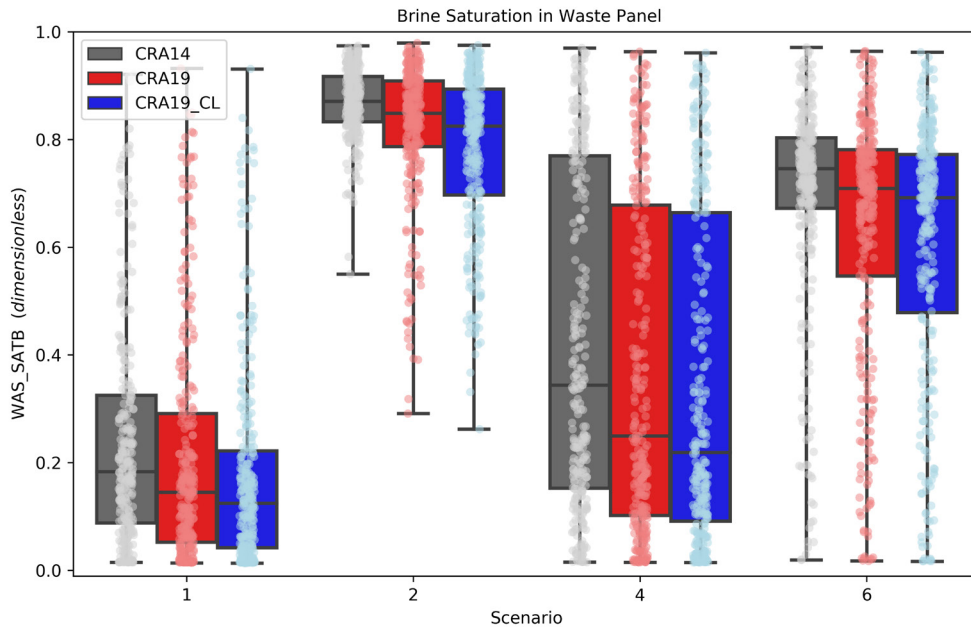


Figure 72 – Waste Panel Integrated Function Average Brine Saturations

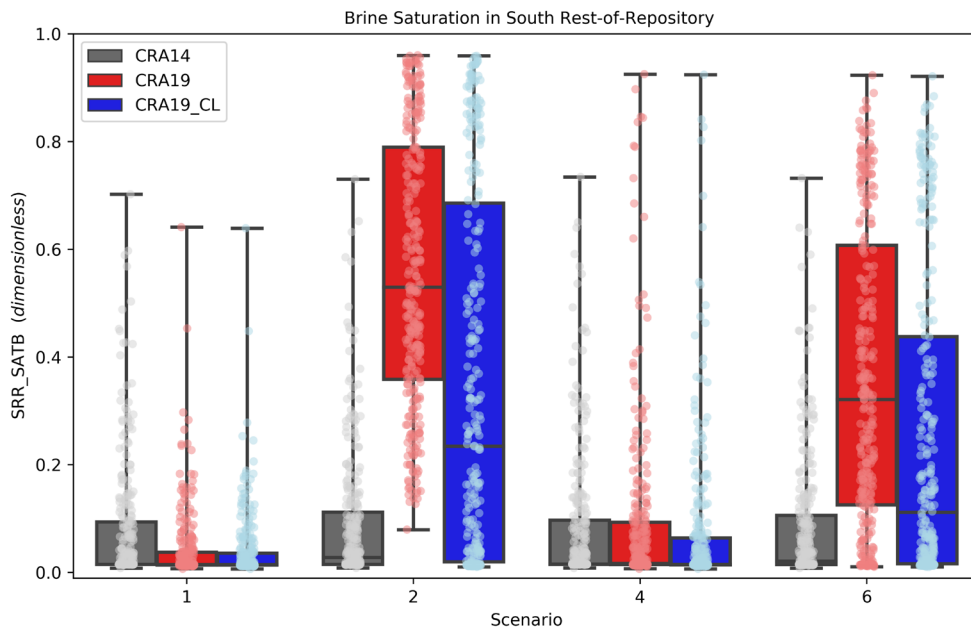


Figure 73 – South Rest-of-Repository Integrated Function Average Brine Saturations

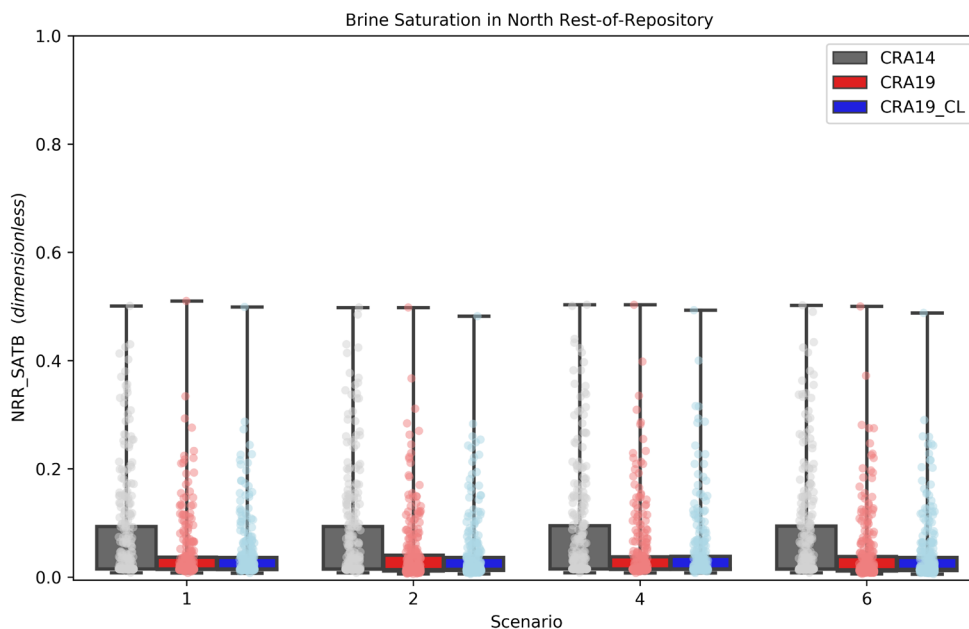


Figure 74 – North Rest-of-Repository Integrated Function Average Brine Saturations

A.5 Gas Generation and Brine and Gas Flows

Influenced by the overall repository area brine saturations, total gas generation from all sources (iron corrosion, cellulose biodegradation, and radiolysis) within the waste areas is reduced over all scenarios for CRA19_CL in comparison with CRA19 (Figure 75). As previously noted, brine flow into the repository for CRA19_CL is reduced in comparison to CRA19 as shown in Figure 76 due to either increased waste area pressures or impeded flow from the Castile across the southernmost panel closure area. Although gas generation is reduced for CRA19_CL in comparison to CRA19, the ability of the generated gas to flow northward and sequester within the OPS and EXP areas is limited and restricted by the substantially reduced void space and the low intrinsic permeabilities within the “closed” areas. As shown in Figure 77, gas flow from south to north out of the north rest-of-repository across the northernmost panel closure plane (which includes the ROMPCS and upper and lower DRZs) is severely restricted under CRA19_CL in comparison with CRA19. The impacts on repository pressure were previously discussed in Section A.3.

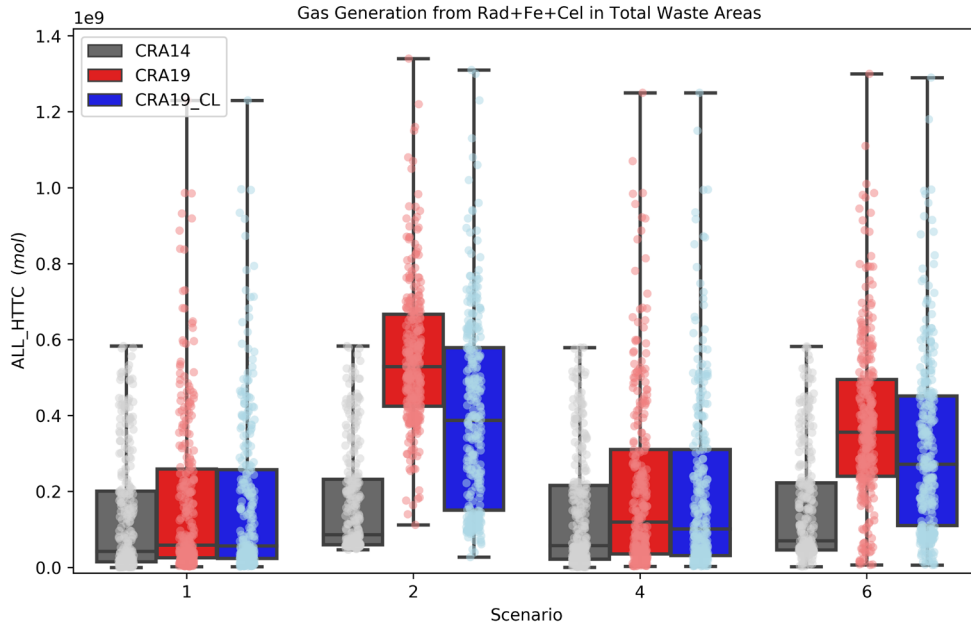


Figure 75 – Total Waste Areas Integrated Function Average Gas Generation from All Sources

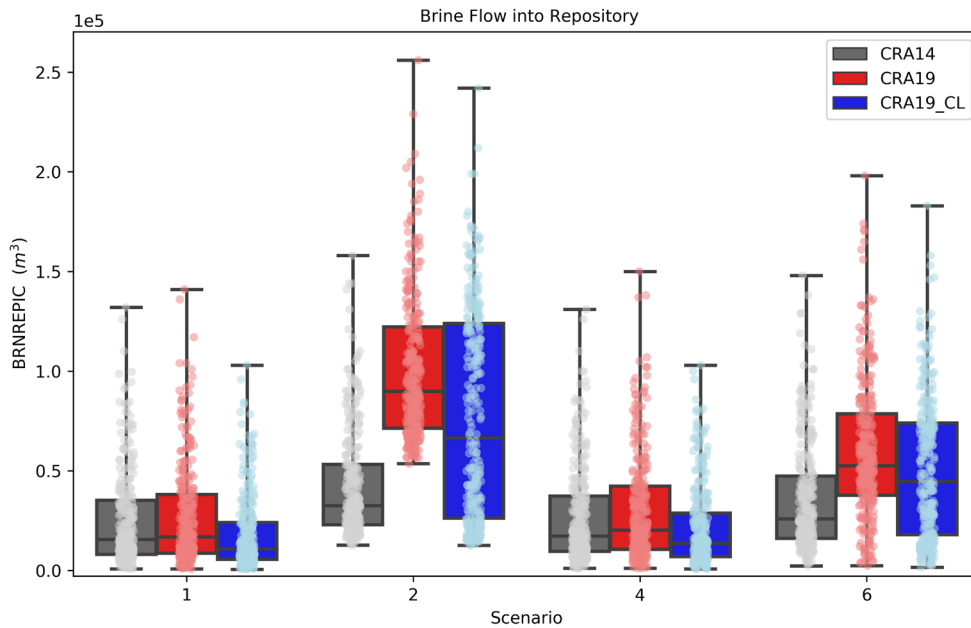


Figure 76 – Repository Waste Areas Integrated Function Average Brine Inflow

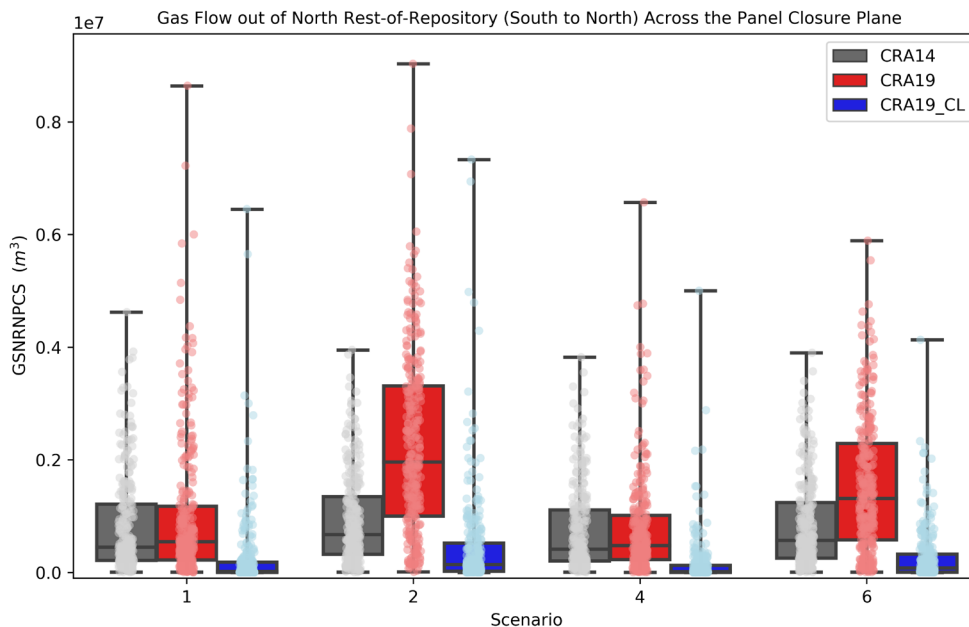


Figure 77 – North Rest-of-Repository Integrated Function Average Gas Flow (South to North) Across the Northernmost Panel Closure Plane

A.6 Normalized Releases

The impacts of changes to waste area pressures and saturations directly impact some, but not all release mechanisms. Cuttings and cavings releases are independent of waste area pressures and saturations. Spallings releases are directly dependent upon waste area pressures, but are also indirectly dependent on saturations due to the gas generation model. In general, increased saturations also lead to increased pressures due to increased output from chemical reactions. Direct brine releases are directly impacted by waste area pressures and saturations—the criteria for a DBR to occur are based on minimum pressure and saturation values. Finally, releases to the Culebra (which directly impact releases from the Culebra) are driven by brine releases up the borehole, which are impacted by the waste area pressures and saturations.

A.6.1 Cuttings and Cavings Normalized Releases

Cuttings and cavings releases are independent of waste area pressures and saturations. Figure 78 confirms that the changes made for the CRA19_CL analysis do not impact cuttings and cavings releases.

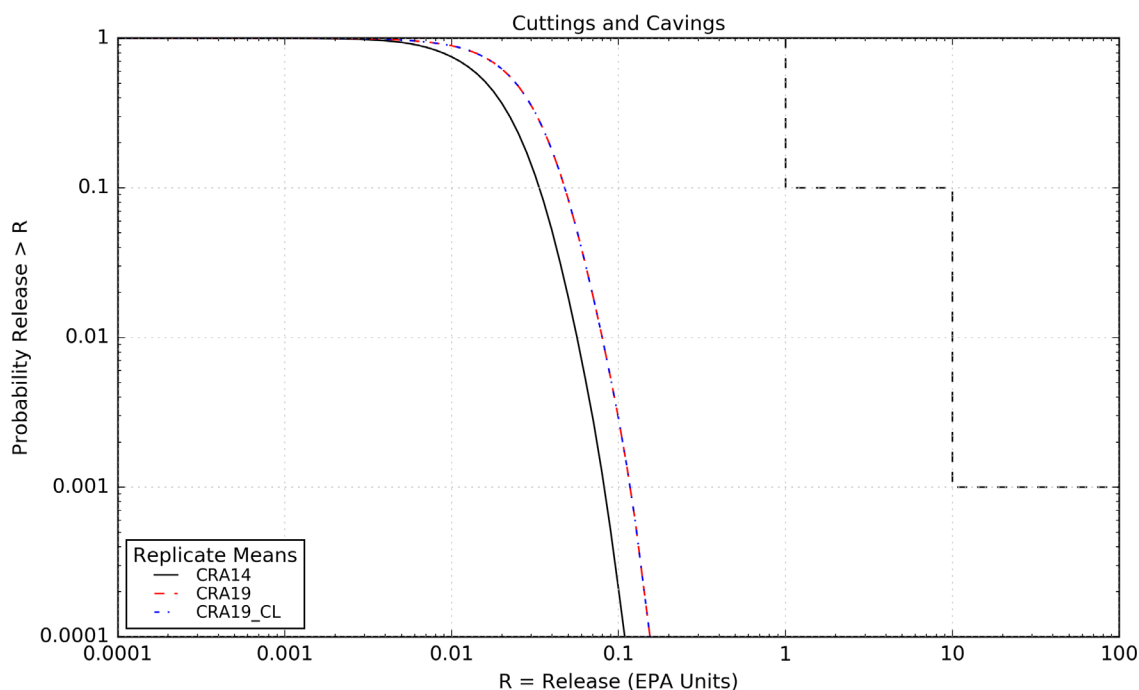


Figure 78 – Mean Cuttings and Cavings Release CCDFs Across Replicates for the CRA14, CRA19, and CRA19_CL Analyses

A.6.2 Spallings Normalized Releases

Spallings releases are directly dependent upon waste area pressures, but are also indirectly dependent on saturations due to the gas generation model. In general, increased saturations also lead to increased pressures due to increased output from chemical reactions. Figure 79 shows the comparison of spallings releases for the CRA19 and CRA19_CL analyses. CRA14 releases are also shown for reference. CRA19_CL spallings releases are observed to be lower than CRA19 spallings releases due to the larger overall decreases in pressures for Castile-intruded scenarios with only modest increases in waste area pressures for non-Castile intruded scenarios under CRA19_CL in comparison to CRA19 (Figure 69, Figure 70, Figure 71).

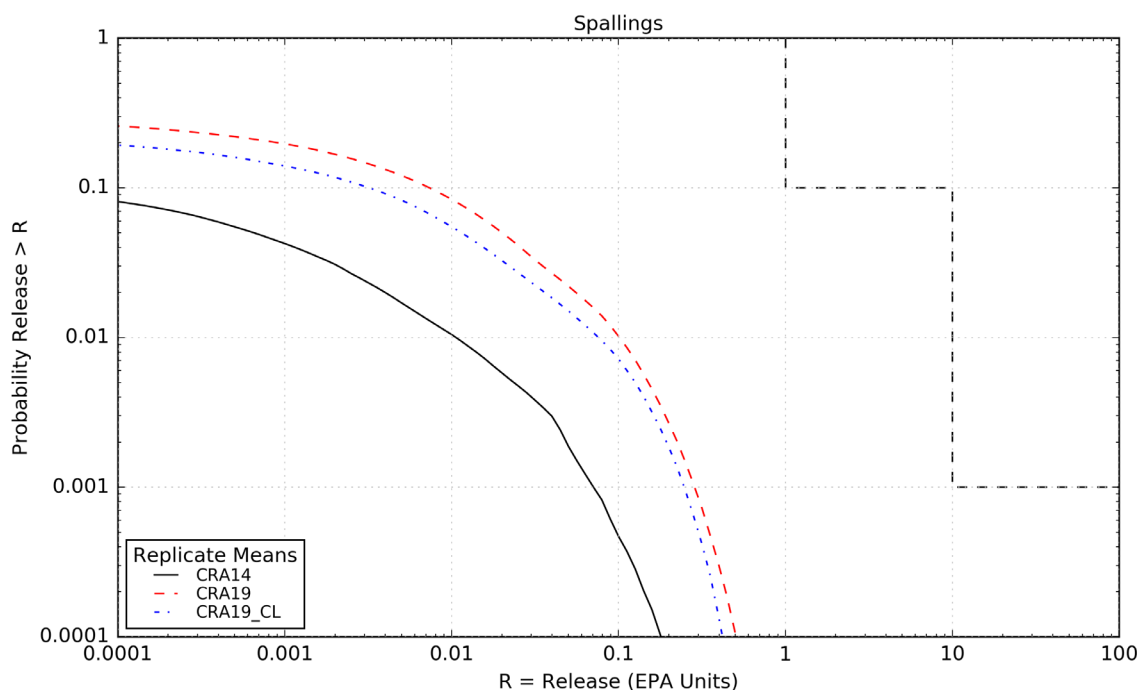


Figure 79 – Mean Spallings Release CCDFs Across Replicates for the CRA14, CRA19, and CRA19_CL Analyses

A.6.3 Normalized Direct Brine Releases

Direct brine releases are directly impacted by waste area pressures and saturations – the criteria for a DBR to occur are based on minimum pressure and saturation values. Figure 80 shows the comparison of DBRs for the CRA19 and CRA19_CL analyses. The reduction in DBRs for CRA19_CL in comparison to CRA19 is primarily attributed to the substantially lower brine saturations in the south rest-of-repository that results from the “closed” southernmost panel closure treatment in CRA19_CL that limits brine inflow from the Castile (Figure 73). The south rest-of-repository pressure and saturation changes (Figure 70, Figure 73) dominate over the slightly elevated pressures within the waste area and south rest-of-repository for undisturbed and non-Castile intruded scenarios (Figure 69, Figure 70) observed for CRA19_CL that result in less favorable conditions for DBRs.

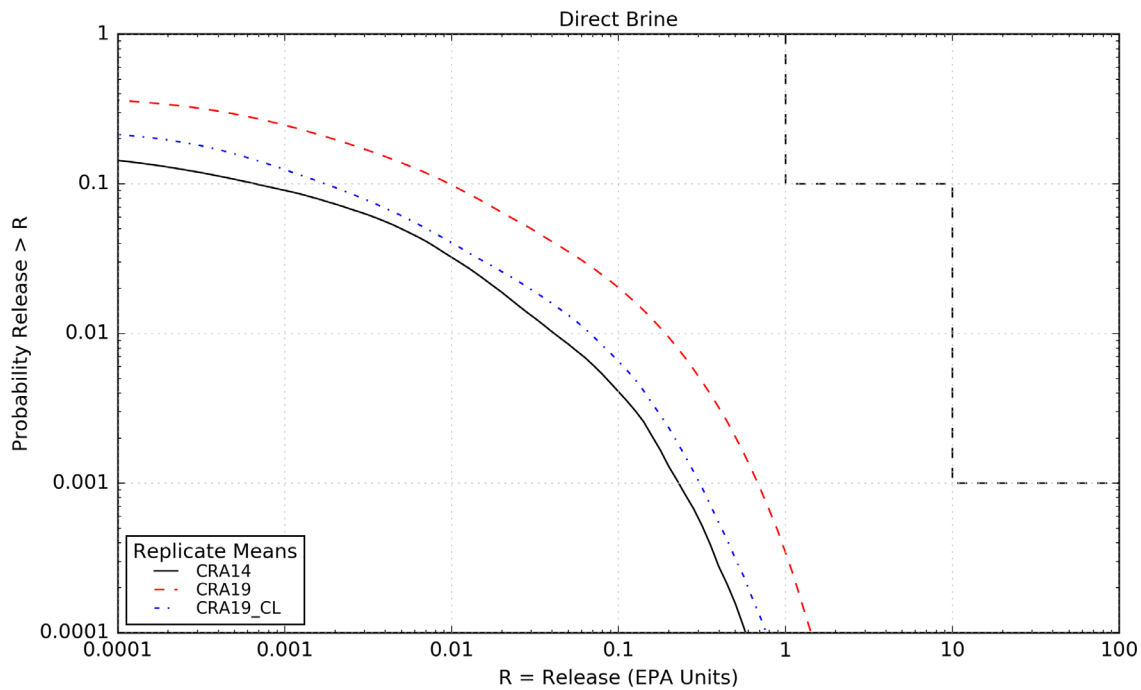


Figure 80 – Mean Direct Brine Release CCDFs Across Replicates for the CRA14, CRA19, and CRA19_CL Analyses

A.6.4 Normalized Culebra Transport Releases

Finally, releases to the Culebra (which directly impact releases from the Culebra) are driven by brine releases up the borehole, which are impacted by the waste area pressures and saturations. Figure 81 shows the comparison of releases to the Culebra for the CRA19 and CRA19_CL analyses. Figure 82 shows the comparison of releases from the Culebra for the CRA19 and CRA19_CL analyses. To and From Culebra releases for CRA19_CL are shown to be slightly reduced in comparison to CRA19 due to the lower brine pressures and saturations under Castile-intruded scenarios (Figure 69 - Figure 74) and attributed primarily to the “closed” southernmost panel closure area treatment in CRA19_CL.

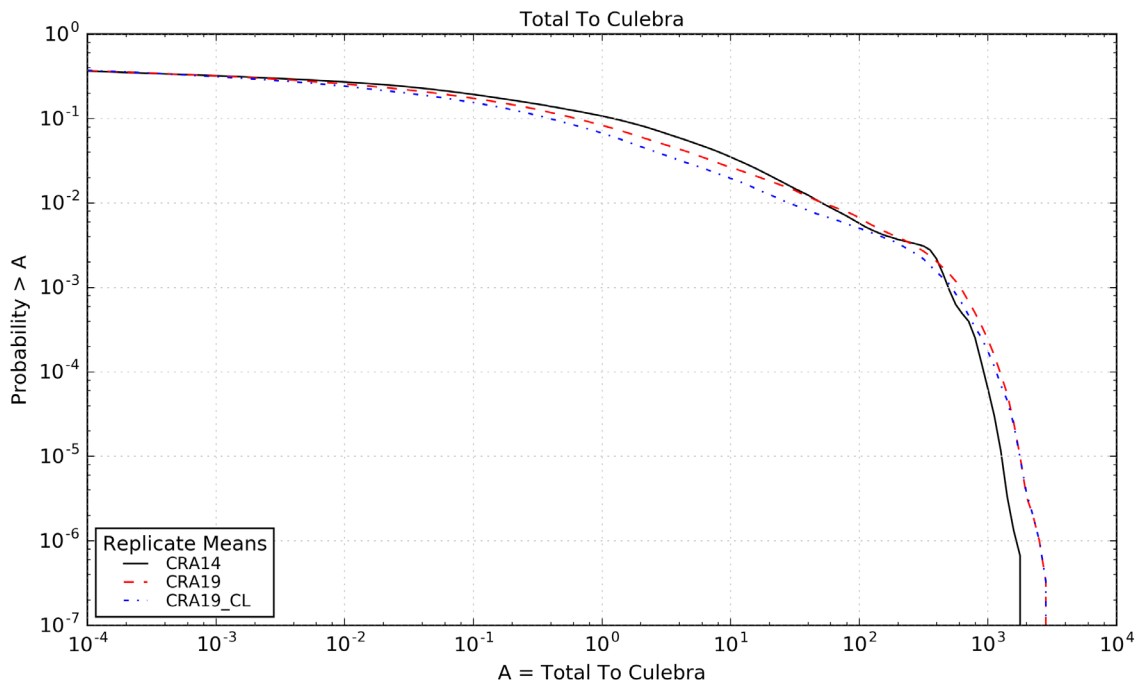


Figure 81 – Mean Release to Culebra CCDFs Across Replicates for the CRA14, CRA19, and CRA19_CL Analyses

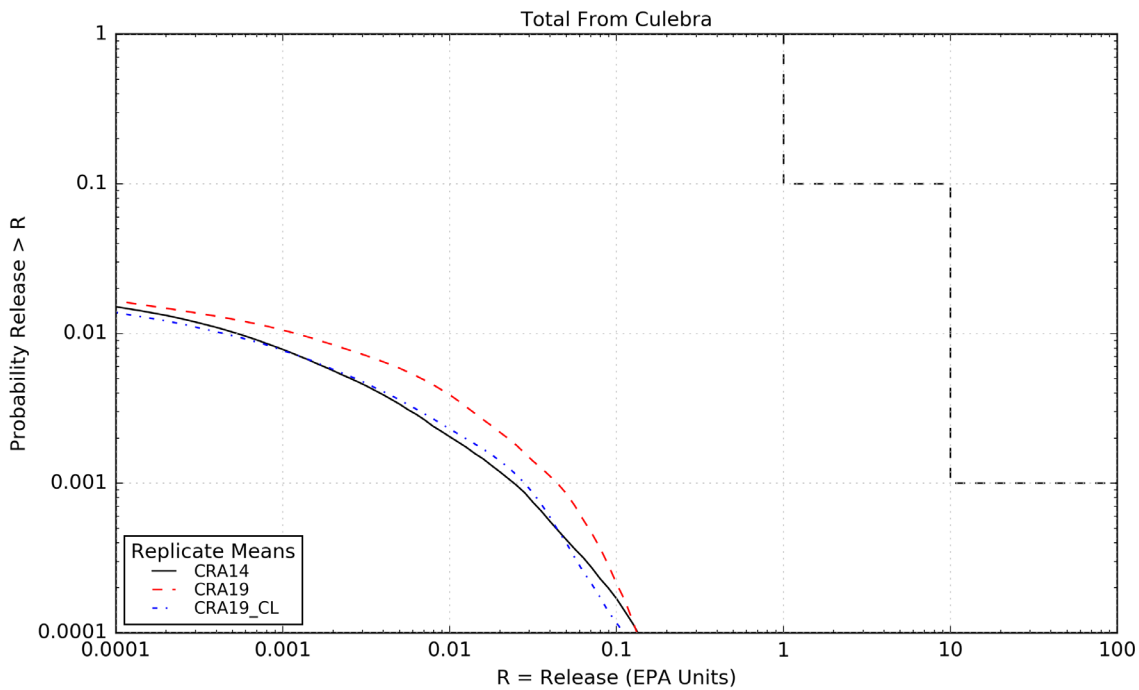


Figure 82 – Mean Release from Culebra CCDFs Across Replicates for the CRA14, CRA19, and CRA19_CL Analyses

A.6.5 Total Normalized Releases

Total releases are based on contributions from all release mechanisms. Figure 83 shows the comparison of total releases for the CRA19 and CRA19_CL analyses. Table 32 shows a comparison of calculated release values at the compliance limits for the CRA19 and CRA19_CL analyses. Total releases for CRA19_CL are observed to be decreased below the CRA19 total releases at both compliance limits.

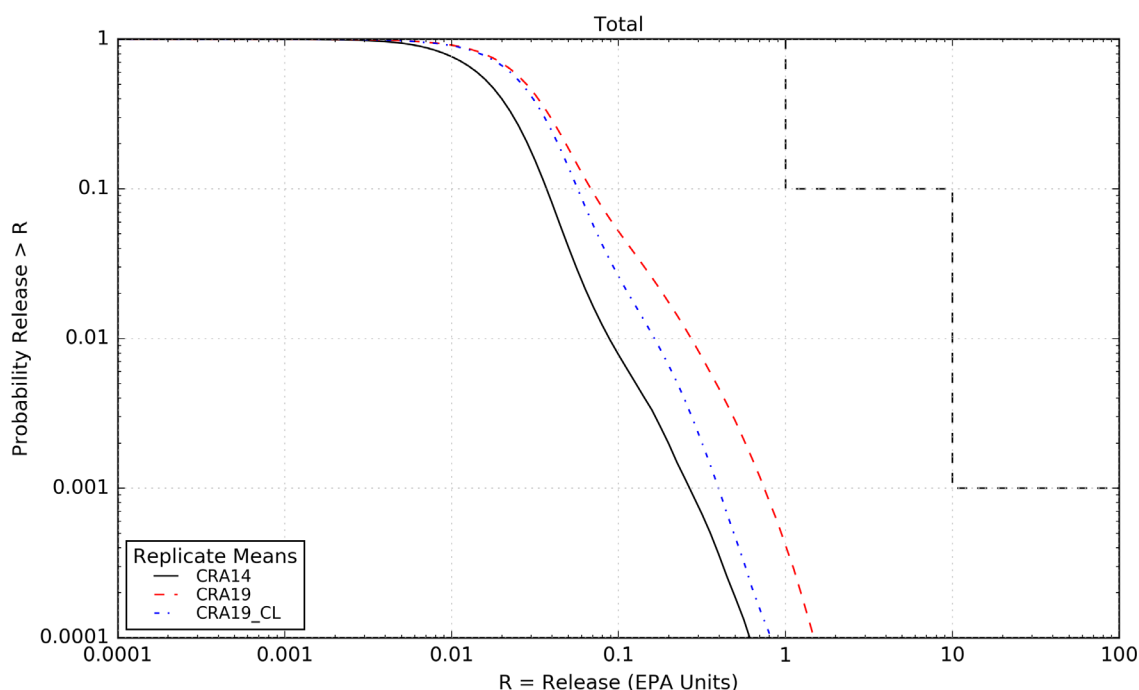


Figure 83 – Mean Total Release CCDFs Across Replicates for the CRA14, CRA19, and CRA19_CL Analyses

Table 32 – Comparison of Total Releases at Compliance Points for CRA14, CRA19 and CRA19_CL Analyses

Probability	Analysis	Mean Total Release	Lower 95% CL	Upper 95% CL	Release Limit
0.1	CRA14	0.0373	0.0355	0.0388	1
	CRA19	0.0685	0.0631	0.0745	
	CRA19_CL	0.0570	0.0539	0.0608	
0.001	CRA14	0.2677	0.2124	0.3132	10
	CRA19	0.7505	0.6301	0.8501	
	CRA19_CL	0.3974	0.3160	0.4425	

A.7 Summary

A complex interplay between waste area brine pressures and saturations drive the repository performance. **It is difficult to determine *a priori* the extent to which increased/decreased pressures and saturations over the modeled BRAGFLO scenarios will impact various release components and total releases.** The CRA19_CL supplemental evaluation was undertaken to determine the impact of the treatment of repository excavations without waste or backfill (i.e., southernmost panel closure area, OPS, EXP) under the condition that creep-closure was assumed to occur rapidly to intact Halite properties (“closed”) rather than the historically utilized properties of 18% porosity and $1\text{E-}11\text{ m}^2$ permeability. Thus, a factor of ~3 to 180 times reduction in porosity and a 10 to 13 orders-of-magnitude reduction in permeability for the southernmost panel closure, OPS, and EXP areas for CRA19_CL in comparison to CRA19, produce net repository conditions that are not bounding for any individual release mechanism and for total releases. This supplemental evaluation definitively demonstrates that treatment of abandoned panel closure and non-waste bearing excavations within the repository as “open” is an appropriately conservative representation of these areas to support performance assessments of the repository in its currently planned final closure configuration.

This page intentionally left blank.